

NAVAL POSTGRADUATE SCHOOL

Monterey, California



THESIS

**EXPLORATORY MODEL ANALYSIS OF THE SPACE BASED
INFRARED SYSTEM (SBIRS) LOW GLOBAL SCHEDULER
PROBLEM**

by

Brian L. Morgan

December 1999

Thesis Advisor:
Second Readers:

Thomas W. Lucas
Robert R. Read
Thomas D. Gottschalk

Approved for public release; distribution is unlimited.

20000309 027

REPORT DOCUMENTATION PAGE

Form Approved
OMB No. 0704-0188

Public reporting burden for this collection of information is estimated to average 1 hour per response, including the time for reviewing instruction, searching existing data sources, gathering and maintaining the data needed, and completing and reviewing the collection of information. Send comments regarding this burden estimate or any other aspect of this collection of information, including suggestions for reducing this burden, to Washington Headquarters Services, Directorate for Information Operations and Reports, 1215 Jefferson Davis Highway, Suite 1204, Arlington, VA 22202-4302, and to the Office of Management and Budget, Paperwork Reduction Project (0704-0188) Washington DC 20503.

1. AGENCY USE ONLY (Leave blank)	2. REPORT DATE December 1999	3. REPORT TYPE AND DATES COVERED Master's Thesis	
4. TITLE AND SUBTITLE EXPLORATORY MODEL ANALYSIS OF THE SPACE BASED INFRARED SYSTEM (SBIRS) LOW GLOBAL SCHEDULER PROBLEM		5. FUNDING NUMBERS	
6. AUTHOR(S) Morgan, Brian L.		8. PERFORMING ORGANIZATION REPORT NUMBER	
7. PERFORMING ORGANIZATION NAME(S) AND ADDRESS(ES) Naval Postgraduate School Monterey, CA 93943-5000			
9. SPONSORING / MONITORING AGENCY NAME(S) AND ADDRESS(ES)		10. SPONSORING / MONITORING AGENCY REPORT NUMBER	
11. SUPPLEMENTARY NOTES The views expressed in this thesis are those of the author and do not reflect the official policy or position of the Department of Defense or the U.S. Government.			
12a. DISTRIBUTION / AVAILABILITY STATEMENT Approved for public release; distribution is unlimited.		12b. DISTRIBUTION CODE	
13. ABSTRACT Proliferation of theater ballistic missile technologies to potential U.S. adversaries necessitates that the U.S. employ a defensive system to counter this threat. The system that is being developed is called the Space-Based Infrared System (SBIRS) "System of Systems." The SBIRS Low component of the SBIRS "System of Systems" will track strategic and theater ballistic missiles from launch to reentry and relay necessary cueing data to missile interceptors before the missiles reach friendly forces or countries whose safety is a vital interest to the U.S. SBIRS Low has a number of critical system requirements that for any given satellite are mutually exclusive for the length of time needed to complete the specified tasking. This limitation implies a system capacity on the total number of ballistic objects the SBIRS Low system can track at any given time. Applying exploratory model analysis, the SBIRS Low model uses the Monte Carlo method to explore large regions of the model space to identify key factors in the system and to provide insight into different tasking schemes for individual satellites. The exploratory model analysis, which consisted of 13,760,000 missiles being tracked in the analysis of the CSS-2 and M-9 missiles, yielded the following significant results: (a) defining the "best" satellite is nontrivial, (b) the SBIRS Low system was unable to initiate a booster track for an unacceptably large percentage of M-9 missiles launched near the equator, (c) if the system anticipates a long delay in revisiting a track, a stereo view should be scheduled immediately prior to the start of the delay, (d) mono viewing alone does not provide the required track accuracy, (e) track accuracy is a function of missile classification, and (f) the instantaneous track accuracy versus sensor revisit rate does not fit any well-known probability distribution.			
14. SUBJECT TERMS Ballistic Missile Defense, Exploratory Model Analysis, Space-Based Infrared Systems		15. NUMBER OF PAGES 176	
16. PRICE CODE			
17. SECURITY CLASSIFICATION OF REPORT Unclassified	18. SECURITY CLASSIFICATION OF THIS PAGE Unclassified	19. SECURITY CLASSIFICATION OF ABSTRACT Unclassified	20. LIMITATION OF ABSTRACT UL

NSN 7540-01-280-5500

Standard Form 298 (Rev. 2-89)
Prescribed by ANSI Std. Z39-18

Approved for public release; distribution is unlimited.

**EXPLORATORY MODEL ANALYSIS OF THE SPACE BASED INFRARED
SYSTEM (SBIRS) LOW GLOBAL SCHEDULER PROBLEM**

Brian L. Morgan
Lieutenant Commander, United States Navy
B.S., University of Virginia, 1989

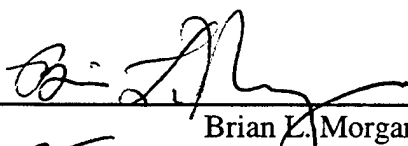
Submitted in partial fulfillment of the
requirements for the degree of

MASTER OF SCIENCE IN OPERATIONS RESEARCH

from the

NAVAL POSTGRADUATE SCHOOL
December 1999

Author:



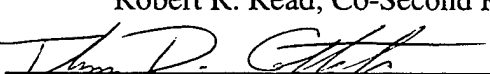
Brian L. Morgan

Approved by:

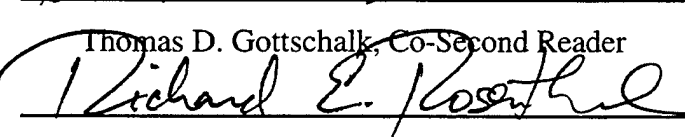


Thomas W. Lucas, Thesis Advisor


Robert R. Read, Co-Second Reader



Thomas D. Gottschalk, Co-Second Reader



Richard E. Rosenthal
Richard Rosenthal, Chairman
Department of Operations Research

ABSTRACT

Proliferation of theater ballistic missile technologies to potential U.S. adversaries necessitates that the U.S. employ a defensive system to counter this threat. The system that is being developed is called the Space-Based Infrared System (SBIRS) "System of Systems." The SBIRS Low component of the SBIRS "System of Systems" will track strategic and theater ballistic missiles from launch to reentry and relay necessary cueing data to missile interceptors before the missiles reach friendly forces or countries whose safety is a vital interest to the U.S.

SBIRS Low has a number of critical system requirements that for any given satellite are mutually exclusive for the length of time needed to complete the specified tasking. This limitation implies a system capacity on the total number of ballistic objects the SBIRS Low system can track at any given time.

Applying exploratory model analysis, the SBIRS Low model uses the Monte Carlo method to explore large regions of the model space to identify key factors in the system and to provide insight into different tasking schemes for individual satellites.

The exploratory model analysis of the CSS-2 and M-9 missiles, in which over 13 million simulated missiles were tracked, yielded the following results: (a) defining the "best" satellite is nontrivial, (b) the SBIRS Low system was unable to initiate a booster track for an unacceptably large percentage of M-9 missiles launched near the equator, (c) if the system anticipates a long delay in revisiting a track, a stereo view should be scheduled immediately prior to the start of the delay, (d) mono viewing alone does not provide the required track accuracy, (e) track accuracy is a function of missile classification, and (f) the instantaneous track accuracy versus sensor revisit rate does not fit any well-known probability distribution.

TABLE OF CONTENTS

I.	INTRODUCTION	1
	A. OVERVIEW	1
	B. BACKGROUND	3
	C. PURPOSE AND RATIONAL	5
	D. ORGANIZATION OF THESIS	6
II.	SBIRS “SYSTEM OF SYSTEMS” AND EXPLORATORY MODELING OVERVIEW	7
	A. SBIRS HIGH OPERATIONS	7
	B. SBIRS LOW OPERATIONS	8
	C. GLOBAL SCHEDULER	9
	D. SYSTEM INTEGRATION	13
	E. EXPLORATORY MODEL ANALYSIS	15
III.	SBIRS PROBLEM AND ANALYSIS GENERALITIES	19
	A. OVERALL ARCHITECTURE	19
	B. SBIRS LOW PROBLEM	22
	C. UNMODELED ASSUMPTIONS AND ISSUES	25
	D. TRACKING AND MONTE CARLO ASSUMPTIONS	29
	E. SCOPE OF ANALYSIS	32
IV.	SBIRS LOW MODEL AND ANALYSIS SPECIFICS	37
	A. BASIC MONTE CARLO STRUCTURE	37
	B. BOOST SPECIFICS	42
	C. KEPLER SPECIFICS	42
	D. SAMPLE POINTS AND PREDICT-AHEAD	48
	E. ANALYSIS SAMPLE SPACE	50

V. RESULTS	53
A. MODEL INPUT PARAMETERS	53
B. OUTPUT REPORT	55
C. ANALYSIS OF CSS-2 MISSILE DATA	56
1. Ballistic Track Initiation Failure	57
2. Synchronous Viewing	60
3. Mono Viewing	70
D. ANALYSIS OF M-9 MISSILE DATA	76
1. Ballistic Track Initiation Failure	77
2. Synchronous Viewing	78
3. Mono Viewing	84
E. COMPARISON OF CSS-2 AND M-9 MISSILE DATA	88
VI. CONCLUSION	95
APPENDIX A: MONTE CARLO METHODOLOGY	99
APPENDIX B: SBIRS LOW MODEL INPUT AND OUTPUT FILES	103
A. SBIRS LOW MODEL INPUT FILE FORMAT	103
B. SBIRS LOW MODEL OUTPUT FILE FORMAT	106
APPENDIX C: CSS-2 MISSILE DATA	109
A. BALLISTIC TRACK INITIATION FAILURE	109
B. SYNCHRONOUS STEREO VIEWING	109
C. MONO VIEWING	110
D. SEQUENTIAL MONO VIEWING	112
E. ASYNCHRONOUS VIEWING	114
F. DELAYED VIEWING	120
G. STAGGERED VIEWING	122
H. LATITUDE SHIFT	125
APPENDIX D: M-9 MISSILE DATA	127
A. BALLISTIC TRACK INITIATION FAILURE	127

B. SYNCHRONOUS STEREO VIEWING	127
C. MONO VIEWING	128
D. SEQUENTIAL MONO VIEWING	130
E. ASYNCHRONOUS VIEWING	132
F. DELAYED VIEWING	138
G. STAGGERED VIEWING	140
H. LATITUDE SHIFT	143
LIST OF REFERENCES	145
BIBLIOGRAPHY	147
INITIAL DISTRIBUTION LIST	149

LIST OF FIGURES

1. Diagram of Global Scheduler	10
2. Track File Architecture	11
3. SBIRS “System of Systems” Architecture with Communication Nodes	19
4. Ballistic Missile Launch Timeline	23
5. Ballistic Missile Launch Timeline	38
6. Orbital Elements	43
7. Eccentric Anomaly	44
8. Depiction of True Anomaly	45
9. CSS-2: Percentage Ballistic Track Initiation Failure	57
10. Probability Density Function for Chi-Squared Distribution	59
11. CSS-2: Synchronous Detection Using Sensors 1 and 2	60
12. CSS-2: Histogram of Containment Bound	62
13. CSS-2: Histogram of Containment Bound, First Five Bins Not Plotted	63
14. CSS-2: Synchronous Detection Using Sensors 1 and 3	65
15. CSS-2: Synchronous Detection Using Sensors 2 and 3	66
16. CSS-2: Mean Containment Bounds Using Synchronous Detection	67
17. Satellite Line-of-Sight and Missile's Orbital Plane	68
18. CSS-2: 95% Containment Bounds Using Synchronous Detection	69
19. CSS-2: 99% Containment Bounds Using Synchronous Detection	70
20. CSS-2: Mono Detection Using Sensor 1	71
21. CSS-2: Mono Detection Using Sensor 2	72
22. CSS-2: Mono Detection Using Sensor 3	73
23. CSS-2: Mean Containment Bounds Using Mono Detection	74
24. CSS-2: 95% Containment Bounds Using Mono Detection	75
25. CSS-2: 99% Containment Bounds Using Mono Detection	76
26. M-9: Percentage Ballistic Track Initiation Failure	77
27. Probability Density Function for Chi-Squared Distribution	78
28. M-9: Synchronous Detection Using Sensors 1 and 2	79
29. M-9: Synchronous Detection Using Sensors 1 and 3	80
30. M-9: Synchronous Detection Using Sensors 2 and 3	81
31. M-9: Mean Containment Bounds Using Synchronous Detection	82
32. M-9: 95% Containment Bounds Using Synchronous Detection	83
33. M-9: 99% Containment Bounds Using Synchronous Detection	83
34. M-9: Mono Detection Using Sensor 1	84
35. M-9: Mono Detection Using Sensor 2	85
36. M-9: Mono Detection Using Sensor 3	86
37. M-9: Mean Containment Bounds Using Mono Detection	86
38. M-9: 95% Containment Bounds Using Mono Detection	87
39. M-9: 99% Containment Bounds Using Mono Detection	88
40. CSS-2 & M-9: Mean Containment Bounds Using Synchronous Detection	89
41. CSS-2 & M-9: Mean Containment Bounds Using Mono Detection	90
42. CSS-2 & M-9: 95% Containment Bounds Using Synchronous Detection	91
43. CSS-2 & M-9: 95% Containment Bounds Using Mono Detection	91
44. CSS-2 & M-9: 99% Containment Bounds Using Synchronous Detection	92
45. CSS-2 & M-9: 99% Containment Bounds Using Mono Detection	93

LIST OF TABLES

1. Exploratory Regions	50
2. CSS-2: Ballistic Track Initiation Failure	109
3. CSS-2: Synchronous Detection Using Sensors 1 and 2	110
4. CSS-2: Synchronous Detection Using Sensors 1 and 3	110
5. CSS-2: Synchronous Detection Using Sensors 2 and 3	110
6. CSS-2: Mono Detection Using Sensor 1	111
7. CSS-2: Mono Detection Using Sensor 2	111
8. CSS-2: Mono Detection Using Sensor 3	111
9. CSS-2 Sequential Mono Viewing: Sensor 1 Handover to Sensor 2 at Time $t = 75$ seconds	112
10. CSS-2 Sequential Mono Viewing: Sensor 1 Handover to Sensor 2 at Time $t = 150$ seconds	112
11. CSS-2 Sequential Mono Viewing: Sensor 1 Handover to Sensor 3 at Time $t = 75$ seconds	113
12. CSS-2 Sequential Mono Viewing: Sensor 1 Handover to Sensor at Time $t = 150$ seconds	113
13. CSS-2 Sequential Mono Viewing: Sensor 2 Handover to Sensor 3 at Time $t = 75$ seconds	113
14. CSS-2 Sequential Mono Viewing: Sensor 2 Handover to Sensor 3 at Time $t = 150$ seconds	114
15. CSS-2 Asynchronous Viewing: Sensor 1 and Sensor 2	114
16. CSS-2 Asynchronous Viewing: Sensor 1 and Sensor 2	115
17. CSS-2 Asynchronous Viewing: Sensor 1 and Sensor 2	115
18. CSS-2 Asynchronous Viewing: Sensor 1 and Sensor 2	115
19. CSS-2 Asynchronous Viewing: Sensor 1 and Sensor 2	116
20. CSS-2 Asynchronous Viewing: Sensor 1 and Sensor 2	116
21. CSS-2 Asynchronous Viewing: Sensor 2 and Sensor 3	116
22. CSS-2 Asynchronous Viewing: Sensor 2 and Sensor 3	117
23. CSS-2 Asynchronous Viewing: Sensor 2 and Sensor 3	117
24. CSS-2 Asynchronous Viewing: Sensor 2 and Sensor 3	117
25. CSS-2 Asynchronous Viewing: Sensor 2 and Sensor 3	118
26. CSS-2 Asynchronous Viewing: Sensor 2 and Sensor 3	118
27. CSS-2 Asynchronous Viewing: Sensor 3 and Sensor 2	118
28. CSS-2 Asynchronous Viewing: Sensor 3 and Sensor 2	119
29. CSS-2 Asynchronous Viewing: Sensor 3 and Sensor 2	119
30. CSS-2 Asynchronous Viewing: Sensor 3 and Sensor 2	119
31. CSS-2 Asynchronous Viewing: Sensor 3 and Sensor 2	120
32. CSS-2 Asynchronous Viewing: Sensor 3 and Sensor 2	120
33. CSS-2 Delayed Viewing: Sensor 1 and Sensor 2	121
34. CSS-2 Delayed Viewing: Sensor 1 and Sensor 2	121
35. CSS-2 Delayed Viewing: Sensor 1 and Sensor 2	121
36. CSS-2 Delayed Viewing: Sensor 1 and Sensor 2	122
37. CSS-2 Delayed Viewing: Sensor 1 and Sensor 2	122
38. CSS-2 Delayed Viewing: Sensor 1 and Sensor 2	122
39. CSS-2 Staggered Viewing: Sensor 1 and Sensor 2	123
40. CSS-2 Staggered Viewing: Sensor 1 and Sensor 2	123
41. CSS-2 Staggered Viewing: Sensor 1 and Sensor 2	123
42. CSS-2 Staggered Viewing: Sensor 1 and Sensor 2	124

43. CSS-2 Staggered Viewing: Sensor 1 and Sensor 2	124
44. CSS-2 Staggered Viewing: Sensor 1 and Sensor 2	124
45. CSS-2 Latitude Shift to N02: Sensor 1 and Sensor 2	125
46. CSS-2 Latitude Shift to N20: Sensor 1 and Sensor 2	125
47. CSS-2 Latitude Shift to N60: Sensor 1 and Sensor 2	125
48. CSS-2 Latitude Shift to N80: Sensor 1 and Sensor 2	126
49. M-9: Ballistic Track Initiation Failure	127
50. M-9: Synchronous Detection Using Sensors 1 and 2	128
51. M-9: Synchronous Detection Using Sensors 1 and 3	128
52. M-9: Synchronous Detection Using Sensors 2 and 3	128
53. M-9: Mono Detection Using Sensor 1	129
54. M-9: Mono Detection Using Sensor 2	129
55. M-9: Mono Detection Using Sensor 3	129
56. M-9 Sequential Mono Viewing: Sensor 1 Handover to Sensor 2 at Time t = 75 seconds	130
57. M-9 Sequential Mono Viewing: Sensor 1 Handover to Sensor 2 at Time t = 150 seconds	130
58. M-9 Sequential Mono Viewing: Sensor 1 Handover to Sensor 3 at Time t = 75 seconds	131
59. M-9 Sequential Mono Viewing: Sensor 1 Handover to Sensor 3 at Time t = 150 seconds	131
60. M-9 Sequential Mono Viewing: Sensor 2 Handover to Sensor 3 at Time t = 75 seconds	131
61. M-9 Sequential Mono Viewing: Sensor 2 Handover to Sensor 3 at Time t = 150 seconds	132
62. M-9 Asynchronous Viewing: Sensor 1 and Sensor 2	132
63. M-9 Asynchronous Viewing: Sensor 1 and Sensor 2	133
64. M-9 Asynchronous Viewing: Sensor 1 and Sensor 2	133
65. M-9 Asynchronous Viewing: Sensor 1 and Sensor 2	133
66. M-9 Asynchronous Viewing: Sensor 1 and Sensor 2	134
67. M-9 Asynchronous Viewing: Sensor 1 and Sensor 2	134
68. M-9 Asynchronous Viewing: Sensor 2 and Sensor 3	134
69. M-9 Asynchronous Viewing: Sensor 2 and Sensor 3	135
70. M-9 Asynchronous Viewing: Sensor 2 and Sensor 3	135
71. M-9 Asynchronous Viewing: Sensor 2 and Sensor 3	135
72. M-9 Asynchronous Viewing: Sensor 2 and Sensor 3	136
73. M-9 Asynchronous Viewing: Sensor 2 and Sensor 3	136
74. M-9 Asynchronous Viewing: Sensor 3 and Sensor 2	136
75. M-9 Asynchronous Viewing: Sensor 3 and Sensor 2	137
76. M-9 Asynchronous Viewing: Sensor 3 and Sensor 2	137
77. M-9 Asynchronous Viewing: Sensor 3 and Sensor 2	137
78. M-9 Asynchronous Viewing: Sensor 3 and Sensor 2	138
79. M-9 Asynchronous Viewing: Sensor 3 and Sensor 2	138
80. M-9 Delayed Viewing: Sensor 1 and Sensor 2	139
81. M-9 Delayed Viewing: Sensor 1 and Sensor 2	139
82. M-9 Delayed Viewing: Sensor 1 and Sensor 2	139
83. M-9 Delayed Viewing: Sensor 1 and Sensor 2	140
84. M-9 Delayed Viewing: Sensor 1 and Sensor 2	140
85. M-9 Delayed Viewing: Sensor 1 and Sensor 2	140
86. M-9 Staggered Viewing: Sensor 1 and Sensor 2	141
87. M-9 Staggered Viewing: Sensor 1 and Sensor 2	141

88. M-9 Staggered Viewing: Sensor 1 and Sensor 2	141
89. M-9 Staggered Viewing: Sensor 1 and Sensor 2	142
90. M-9 Staggered Viewing: Sensor 1 and Sensor 2	142
91. M-9 Staggered Viewing: Sensor 1 and Sensor 2	142
92. M-9 Latitude Shift to N02: Sensor 1 and Sensor 2	143
93. M-9 Latitude Shift to N20: Sensor 1 and Sensor 2	143
94. M-9 Latitude Shift to N60: Sensor 1 and Sensor 2	143
95. M-9 Latitude Shift to N80: Sensor 1 and Sensor 2	144

GLOSSARY OF TERMS AND ACRONYMS

Clutter: any tactically insignificant set of tracking objects, e.g., noise, solar radiation, etc.

Detection: any received signal from an object whose value is above the threshold for a sensing system.

Discrimination: to make a distinction between the lethal object and all other non-lethal objects.

Divert maneuver: change in velocity of the interceptor needed for a collision to occur. If an interceptor does not have sufficient propulsive capability to accomplish the required maneuver, additional interceptor(s) must be allocated to the target to destroy it.

Dwell time: length of time that a sensor stares at an object.

Event: the occurrence of a ballistic missile launch.

False alarm: one or more signals, without “interesting” origins, that exceed the detection threshold. A random false alarm may be caused by persistent and/or structured clutter.

Generalized energy management maneuver (GEMM): a coning maneuver by an object taking place in the boost phase and is used to expend excess energy, complicate counter-targeting, and/or prevent tracking systems from reverse-tracking the missile to its launch point.

Additionally, since the maneuver affects the range of the missile, it may be used when either a depressed or lofted launch is not feasible or desirable.

In-flight target update (IFTU): a mid-course position update in estimated position of the object given to the interceptor.

Kepler orbit: the non-powered, ballistic phase of a missile's trajectory. The trajectory is elliptical with the earth located at one focii and the only force acting on the object is gravity.

Kinematic tracking: a procedure in which each sensor, using its own data, forms polynomial fits through a fixed number of detections (typically cubic fits through six detections).

Lethal object: warhead associated with a ballistic missile. A ballistic missile may have more than one lethal object contained within it.

Long wavelength infrared (LWIR): this band generally covers the wavelengths between 8 – 14 micrometers and is used by space based sensors to detect and track objects above the horizon against a cold space background.

Maneuver in the field of view (ManFOV): a compound situation consisting of sufficient divert maneuver and the target image lying within the interceptor seeker's field of view. Both of these conditions must be achieved for a successful intercept to occur.

Medium wavelength infrared (MWIR): this band generally covers the wavelengths between 3 – 8 micrometers and is used by space based sensors to detect and track objects through booster burnout against an Earth background (i.e., below the horizon against a warm background).

Missile classification: the variant of missile launched, i.e., SCUD, CSS-2, M-9, etc.

Mono track: an object whose positional data is derived from one or more successive line-of-bearing detections from a single sensor.

Non-lethal object: any object, except a warhead, which continues on a ballistic trajectory after booster burnout.

Periapsis: the point nearest the prime focus. In the context of this research, the point at which the ballistic object reaches its highest altitude.

Post-boost vehicle (PBV): nose-section of the missile that contains lethal and non-lethal objects.

Precision track: track generalized by physics-based equations of motion (e.g., Kepler motion for ballistic objects).

Resolution: smallest distance between two objects at which the system can distinguish two separate objects.

Revisit rate: scan rate for a sensor to return to an object.

Revisit scheme: sensor tasking strategy used to ensure all objects are tracked within a specified positional accuracy.

Scissors angle: the smallest angle formed by the line of sight to an object from two sensors with the object at the vertex.

Short wavelength infrared (SWIR): this band generally covers the wavelengths between 1 – 3 micrometers and is used by space based sensors to see the bright rocket plumes of boosting missiles.

Slew-settle-stare: the process in which a sensor is directed from one object to another, allowed to dampen any induced vibrations, and then "looking at" the object.

Stereo track: an object whose positional data is derived from successive intersecting line-of-bearing detections from two or more sensors.

Three-dimensional (3D) mono track: a track developed from a single sensor over several time periods. It provides range, azimuth, and elevation. To develop a 3D mono track, an active sensor or assumption of a rigid wire model is required.

Three-dimensional (3D) stereo track: a track developed from two or more line-of-sight sensors in which azimuth and elevation data is combined to derive range.

Track: a set of position coordinates and associated information that are associated with a single origin or cause. It should be noted that a track has an underlying system model, a mathematical formalism to determine properties of the underlying object based on the observed detections.

Two-dimensional (2D) mono track: a track developed from the initial conditions at booster burnout and a single line-of-sight sensor. The only trajectory data provided is azimuth and elevation.

Very long wavelength infrared (VLWIR): this band generally covers the wavelengths between 14 – 30 micrometers and is used by space based sensors to track targets against a space background.

EXECUTIVE SUMMARY

Proliferation of theater ballistic missile technologies to potential U.S. adversaries necessitates that the U.S. employ a defensive system to counter this threat. The system that is being developed is called the Space-Based Infrared System (SBIRS) "System of Systems." The SBIRS Low component of the SBIRS "System of Systems" will track strategic and theater ballistic missiles from launch to reentry and relay necessary cueing data to missile interceptors before the missiles reach friendly forces or countries whose safety is a vital interest to the U.S. The Space-Based Infrared System (SBIRS) architecture is an evolutionary step forward in the United States' forty-year program of employing space-based infrared surveillance system.

The "SBIRS System of Systems" is comprised of two separate satellite constellations, SBIRS High and SBIRS Low. SBIRS High is comprised of four satellites in geostationary earth orbit, two satellites in highly elliptical orbits, and ground assets. The first satellite launch is scheduled for 2004. The SBIRS Low will feature 25 to 30 satellites in low earth orbit (analysis in this report is done for a particular 27 satellite constellation) and will be fully operational in 2006. The SBIRS Low component will bring an entirely new capability to the warfighter—the ability to track theater and intercontinental ballistic missiles from launch to reentry and to relay necessary cueing data to missile interceptors before the missiles reach friendly forces.

The SBIRS Low system must orchestrate surveillance of the entire post-boost threat, in support of a number of system requirements such as: track maintenance, discrimination of lethal (i.e., warhead) and non-lethal objects, precise track estimates and updates for interceptors, interceptor-lethal object kill assessment, and battlefield characterizations. For any given satellite, these requirements are mutually exclusive for the length of time needed to complete the specified tasking. This limitation implies a system capacity on the total number of ballistic objects the SBIRS Low system can track.

At early stages in the analysis of a new system, the emphasis is on developing a broad understanding of the critical elements in the system and its potential applications. In such situations, there may be too much uncertainty to reliably estimate optimal solutions with the available tools. The SBIRS program is at such a stage. The SBIRS Low model was used to explore large regions of model space in an attempt to identify key factors in the system and scenarios to provide insight into the global scheduler problem, i.e., tasking of individual satellites.

The primary goal of this project is to explore various sensor tasking strategies that could be used by the SBIRS Low system, as controlled by the global scheduler, and characterize their effectiveness under different operating conditions. The tasking problem for SBIRS Low is nontrivial for the following reasons:

- a. The underlying scenario can be very dynamic with feasible sensor-to-target pairings (determined by some given criterion) changing over time.
- b. The track sensor is a limited resource, implying restrictions on the system target handling capacity.
- c. SBIRS Low has a number of system requirements that are mutually incompatible from the perspective of tasking, which results in variable demands being placed on individual sensors.
- d. A large number of target-specific tasks place time-dependent constraints on sensor assets. An example of a time-dependent task is the length of time a sensor "stares" at a target in an attempt to detect it.

Because there is so much uncertainty in the SBIRS "System of Systems," it is the ideal candidate for exploratory analysis. The exploratory modeling search strategy used in this analysis is based upon the notion that simple models must first be implemented and explored in some detail in order to gain the intuition needed for the actual system design.

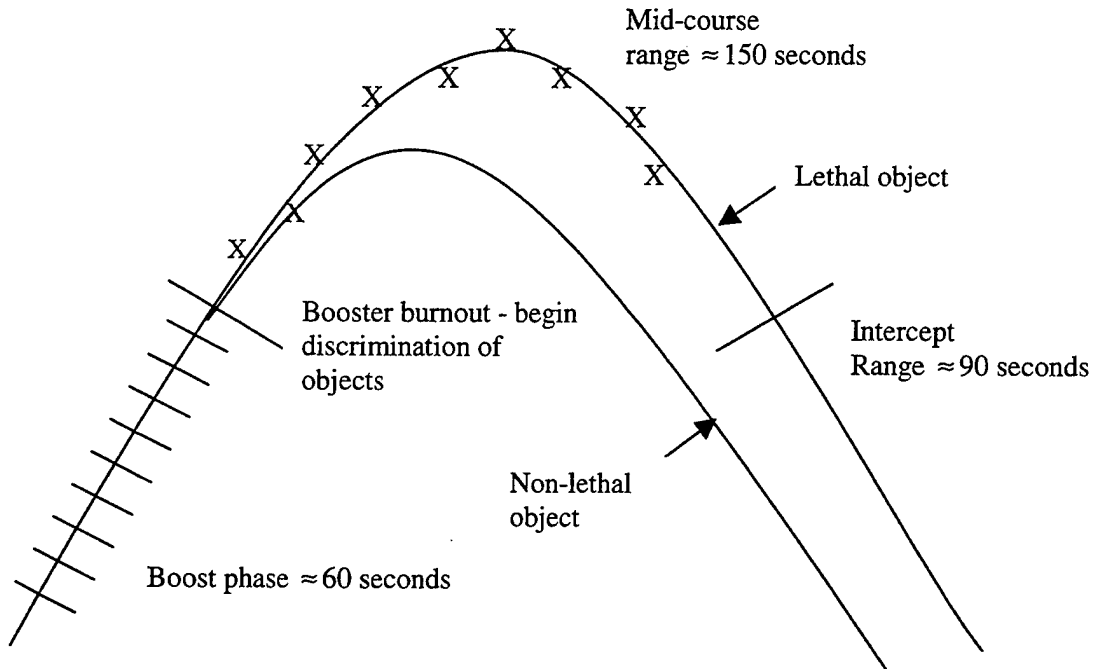
The probability of SBIRS mission success, where success is defined as destruction of the lethal object, is of the general form

$$P(\text{success}) = P(\text{acquire} \cap \text{track} \cap \text{discriminate} \cap \text{target} \cap \text{kill}).$$

With a probability of mission success that exceeds 0.99, if a track on a lethal object is lost or dropped, intercept becomes nearly impossible. Thus, there is a necessity for an in depth understanding of this complex architecture.

A typical timeline of events for a missile launch is shown in Figure 1.

Figure 1. Representative missile launch timeline.



The SBIRS Low model makes certain assumptions regarding orbital mechanics and missile detection criteria. These assumptions represent a balance between achieving a desired level of insight and the recognition that a model cannot include every contingency. Additionally, certain aspects that are critical to SBIRS Low performance are ignored because they are functionally irrelevant for this analysis. For example, the communication architecture, specific design parameters of the interceptor, and all logistic constraints associated with an interceptor battery provide no additional insight into tracking accuracy.

The SBIRS Low modeling goals are to: (1) develop of a system analysis methodology, (2) identify/explore sensitivities, (3) develop intuition, and (4) provide benchmark/reference book of track accuracies as a function of missile type, sensor revisit scheme, length of time since booster burnout (i.e., length of time in free-flight), and length of predict-ahead time.

The SBIRS Low model is a Monte Carlo computer simulation that uses “appropriate fidelity” code for actual system components and physics-based equations of motion. The chosen fidelity is a trade-off between computational speed and resources, complexity of formulas, inclusion of parameters, and desired level of insight.

The analysis consisted of examining the system tracking accuracy for two of the nine types of missiles available to the user. These missiles, the CSS-2 and M-9, were chosen because of their dynamic flight characteristics. The exploratory model analysis included over 688 simulation events and each event consisted of 20,000 individual missile launches.

Two results from the analysis are presented: (a) the failure of the system to initiate a ballistic track on a M-9 missile launched near the equator and (b) track position accuracy for a given sensor tasking strategy.

Figure 2 shows the fraction of ballistic track initiation failures as a function of ballistic track revisit rate for three different boost phase sensor revisit rates for the M-9 missile. In all three cases, an "unacceptably" large number of ballistic track initiation failures were encountered. The counts of track initiation failures for the M-9 missiles are well characterized by a Poisson distribution.

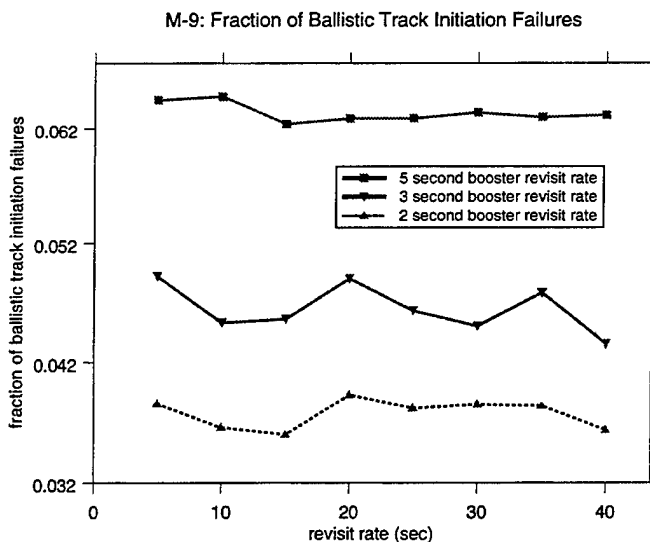


Figure 2. Line plots of the fraction of ballistic track initiation failures for a M-9 missile at eight different ballistic sensor revisit rates.

Figure 3 is representative of the analysis of the data provided by the SBIRS Low model. It shows the estimation error for three empirical containment bounds for a CSS-2 missile at time $t = 50$ seconds (after booster burnout).

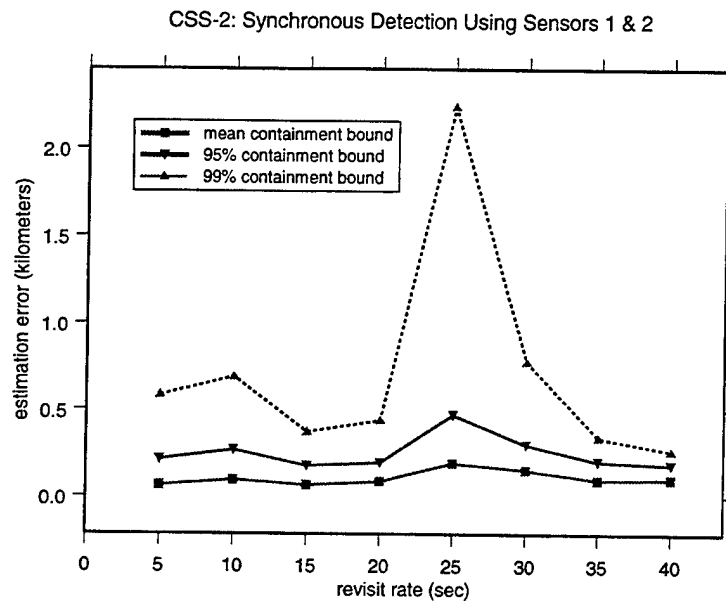


Figure 3. CSS-2: Synchronous Detection Using Sensors 1 and 2. Line plot of the revisit rate versus estimation error for a CSS-2 missile using a stereo symmetric tasking scheme for the closest and next closest satellite.

The exploratory model analysis yielded the following significant results: (a) defining the "best" satellite (based on sensor-to-target range, viewing geometry criteria, etc.) is nontrivial, (b) the SBIRS Low system was unable to initiate a booster track for an unacceptably large percentage of M-9 missiles launched near the equator, (c) if the system anticipates a long delay in revisiting a track, a simultaneous detection by two different sensors should be scheduled immediately prior to the start of the delay, (d) repeated detections by a single sensor alone does not provide the required track accuracy, (e) track accuracy is a function of the type of missile launched, and (f) the instantaneous track accuracy versus sensor revisit rate does not fit any well-known probability function.

I. INTRODUCTION

A. OVERVIEW

Throughout history, military leaders have sought to gain the high ground advantage, and by achieving this goal, commanders were able to survey large areas of the battlefield, watch enemy troop movements, and guard against surprise attacks. With the development of rocket engine technology and the atomic bomb, by the middle of the Cold War the military high ground moved to outer space.

The Space-Based Infrared System (SBIRS) architecture is an evolutionary step forward in the United States' space-based infrared surveillance system. The United States' first space-based infrared system was called Missile Defense Alarm System (MIDAS). This program was started in 1960 and the concept of using space-based infrared detectors and other technologies was proven by 1963. Additionally, in 1963, the Vela program was developed to monitor compliance with the nuclear test ban treaty.

In 1970, these two programs were consolidated into the Defense Support Program (DSP), an early warning satellite system operated by Air Force Space Command (AFSPC) and developed by the Air Force's Space and Missile Systems Center. DSP provides twenty-four hour, worldwide surveillance for missile warning and nuclear burst detection and serves as the space segment of the U.S. Integrated Tactical Warning and Attack Assessment System.

The DSP system consists of several satellites in geostationary orbit, an Overseas Ground Station (OGS) in Australia, a European Ground Station (EGS), a continental U.S. (CONUS) Ground Station (CGS), and Mobile Ground Terminals (MGTs). The infrared detector arrays on each satellite have the capability to view nearly an entire hemisphere of the earth and can detect hot plumes from boosting missiles from any location within its field of view. The data collected during these sweeps is relayed down to one of the three Air Force ground stations or MGTs around the world and then communicated to the National Command Authority or to commanders in the field.

A follow-on program to DSP is currently under development. This program is called "SBIRS System of Systems" and is comprised of two separate satellite constellations, SBIRS High and SBIRS Low. The SBIRS system is designed to perform the following four functions:

- a. Missile warning – Utilizing over 25 years of experience on DSP and state-of-the-art technology, missile warning capabilities will significantly increase, and space-based platforms will better provide missile warning information to commanders.
- b. Missile defense – This mission will be satisfied using space-based infrared platforms to track targets from initial boost phase through mid-course, and the tracking data will be relayed to interceptors.
- c. Technical intelligence – Using multiple platforms, space-based infrared sensors will provide valuable data necessary for missile characterization and phenomenology and collect information on various other military systems and operations.
- d. Battlespace characterization – Capitalizing on the advantages of space-based infrared sensors, commanders will be able to assess interceptor hit/failure and battle damage and track infrared-intense events to improve battlefield situational awareness.

[Ref. 1]

SBIRS High is scheduled for first launch in 2004 and will feature a mix of four satellites in geostationary earth orbit, two satellites in highly elliptical orbits, and ground assets. Ground assets include a CONUS based Mission Control Station (MCS), a backup MCS, a survivable MCS, overseas relay ground stations, relocatable terminals, and associated communications links. The primary objective of SBIRS High is to detect and track the boost phase of theater and intercontinental ballistic missiles and communicate trajectory parameters to the ground assets.

The SBIRS Low component will bring an entirely new capability to the warfighter—the ability to track theater and intercontinental ballistic missiles from launch to reentry and to relay necessary cueing data to missile interceptors before the missiles reach friendly forces. When fully operational in 2006, the SBIRS Low component will consist of 25 to 30 satellites in low earth orbit (analysis in this report is done for a particular 27 satellite constellation).

Each SBIRS Low satellite has two infrared sensors with which to perform its missions. One sensor, known as the acquisition sensor, will be a wide field of view scanning infrared sensor that will watch for short-wave infrared electromagnetic energy associated with missile plumes during the boost phase. Once the acquisition sensor has located a boosting missile, it begins to compute a trajectory for initialization of the ballistic track. Upon booster burnout, the initialization data for the ballistic track is transferred to the second on-board sensor. This sensor, called the track sensor, is a narrow field of view, high-precision staring sensor that is capable of detecting electromagnetic energy in multiple infrared bands. Mounted on a two-axis gimbal, the track sensor is capable of detecting post-booster burnout objects which may or may not contain various numbers of lethal objects or warheads, attitude control modules, spent booster rockets,

and decoys or penetration aids. The track sensor will track all objects through their mid-course trajectory and into their reentry phase. By this time, the on-board processing is supposed to have discriminated the lethal object(s), predicted the final ballistic trajectory of all objects, and estimated the lethal object's impact point and time of impact. This data will then be relayed to interceptor batteries where it will be used to intercept the incoming warhead(s). [Ref. 2]

Utilizing tracking data from SBIRS Low, the area defendable by a single interceptor battery increases dramatically. Whereas systems like the Patriot require that the missile be within view of its ground-based radar before it can fire, SBIRS Low will provide cueing information to interceptors while warheads are still far away from friendly forces. This additional targeting capability will allow earlier engagements and multiple interceptor attempts on incoming missiles to increase the likelihood of a successful kill.

Additionally, the entire constellation will be networked together using inter-satellite crosslinks, thus allowing each satellite to communicate with all other satellites in the constellation. This capability allows for satellite-to-satellite "handover" of target tracks. Target handover is required because the dynamic nature of the orbiting satellites and uncertainty of the launch point and time makes it extremely unlikely any one satellite will track a missile during its entire flight duration. If necessary, this type of handover will continue between satellites in the constellation until the target has been destroyed, its infrared energy can no longer be detected, or the missile impacts the surface of the earth. Additionally, SBIRS High satellites are networked, via ground relay, with SBIRS Low satellites and, if tactically prudent, can provide cueing to multiple SBIRS Low track sensors in near real-time for an extremely limited number of tracks.

B. BACKGROUND

SBIRS Low will "bridge the gap" between initial launch detection, the current capability of DSP and SBIRS High, and ground-based radar interceptors. Its primary function is to provide precise mid-course tracking and discrimination of objects for the SBIRS missile defense mission in theater conflicts and attacks against North America. The SBIRS Low system must orchestrate surveillance of the entire post-boost threat, in support of a number of system requirements such as:

- a. Track maintenance on all relevant objects until the lethal object is destroyed, the missile is judged not to be a threat and the track is dropped, or the lethal object impacts the earth.

- b. Discrimination of lethal and non-lethal objects.
- c. Precise track estimates and updates for interceptors.
- d. Interceptor-lethal object kill assessment.
- e. Battlefield characterizations. [Ref. 3]

For any given satellite, these requirements are mutually exclusive for the length of time needed to complete the specified tasking. This limitation implies a system capacity on the total number of objects the SBIRS Low system can track in the ballistic phase. With SBIRS Low, tracking, *per se*, is not an issue because the track sensor is sensitive enough to detect and discriminate objects with sufficient accuracy given most sensor-to-object geometries. The most critical issues are at the system level and these issues are tasking in highly dynamic environments and accomplishing the multiple system level requirements listed in the previous paragraph.

The component in the SBIRS Low system that is responsible for “partitioning” active entries from the track file, a listing of all objects being tracked, is called the global scheduler. The global scheduler receives tasking requirements internally, from an acquisition sensor which detects a boosting missile, or externally from sources such as a Mission Control Station. Based on the tasking requirements, the global scheduler directs the operation of track sensors via local schedulers on-board each satellite. When operating within designed capacity, the global scheduler will fulfill this tasking while maintaining the specified level of tracking accuracy for all objects. Levels of tracking accuracy include simple detection, continual object discrimination, and target quality. These criterion can be established at some given level of confidence at the time of detection and predicted ahead to provide an approximate time at which, without an update, tracking accuracy will degrade below the defined minimum acceptable level.

When the tracking accuracy for at least one track drops below the currently defined minimum acceptable level, the entire SBIRS Low system is defined to be in an overload condition. The system decision-aid will then suggest operator action necessary to relieve the overload based on utility assigned to available options. Examples of suggested operator action include no longer performing the mission of space surveillance, “dropping track” on a non-lethal object, or dropping track on a group of objects (e.g., sacrificing Pittsburgh to save Cleveland).

C. PURPOSE AND RATIONALE

The primary goal of this project is to explore feasible track revisit schemes available to the global scheduler and characterize their effectiveness under different operating conditions and conditions that result in an overload. Using exploratory model analysis, the model space can be systematically searched over a variety of assumptions and hypotheses to reveal how the system would behave if the various guesses were correct. This type of analysis produces useful results through the creation of alternative feasible model outcomes. A sensitivity analysis is subsumed in the exploratory model analysis process, which inherently provides insight into which parameters are critical by the fact that its results are not predicated on any single point.

Computer simulation and modeling plays a vital role in achieving insights which will aid in the quantification of uncertainties and determining feasible track revisit schemes for given predict ahead track position error bounds. The SBIRS Low model will provide ballistic missile launches that will be detected and tracked by the SBIRS Low satellite system and Monte Carlo simulations will be used to explore tasking and contingency operations models, target handling capacities, and system failure modes. Examples of tasking operations are using only the closest and second closest sensor from the target to track the target, using only the closest and third closest sensor from the target to track the target, or using only the second and third closest sensor from the target to track the target. In a dense tracking or sensor-deficient scenario, only one sensor may be available to track a target. These operations will each produce slightly different system behavior because:

- a. As the range from the sensor to the target increases, target positional error increases due to uncertainty in the focal plane pointing angle.
- b. Randomly assigned sensor bias errors that are varied each launch event.
- c. Differences in available tracking data, i.e., two sensors providing positional data via intersecting lines of bearing versus positional data derived from single lines of bearing taken from one sensor over some given time interval.
- d. Different contingency operations, i.e., conducting the analysis for different types of ballistic missiles (nine different missiles are currently modeled).

Based on the feasible track revisit schemes, the output can be used as input for follow-on analysis of system overload behavior.

Thus, through a high dimensional exploration of the model, this analysis will:

- a. Determine how often a track needs to be updated to remain within a prescribed positional uncertainty.
- b. Determine the distribution for positional uncertainty as a function of revisit time.
- c. Determine the tracking capacity of the system in a variety of scenarios.
- d. Determine the critical factors that result in an overload condition.

D. ORGANIZATION OF THESIS

Following this introduction, the report is divided into five additional chapters. First, the SBIRS "System of Systems" is described in additional detail. Building on this additional information, specific design and requirements of the global scheduler are examined. The final section of this chapter provides a general overview of exploratory model analysis and why this analysis is appropriate at the present stage of the SBIRS Low development.

Next, the architecture of the SBIRS Low system is further refined to include engineering complications, a definition of SBIRS mission success, and a typical timeline for a ballistic missile launch scenario. The assumptions present in the SBIRS Low model and their impact are listed in chronological order, according to the launch scenario. The chapter ends with a discussion of tracking and Monte Carlo assumptions.

Next, the specifics of the SBIRS Low model are explained. The Monte Carlo structure of the model is further detailed and a prediction on the distribution of the track accuracy is presented. An overview of orbital mechanics is presented to ensure that the reader has an understanding of the underlying astrodynamics applicable to the SBIRS Low model. The chapter concludes with a description of the analysis sample space.

Finally, the results of the exploratory model analysis are presented. The results are followed by a conclusion, which includes suggestions for additional research.

II. SBIRS “SYSTEM OF SYSTEMS” AND EXPLORATORY MODELING OVERVIEW

A. SBIRS HIGH OPERATIONS

The SBIRS “System of Systems” will provide the enhanced capabilities necessary to combat evolving theater and ballistic missile threats and help meet U.S. infrared space surveillance needs through the next several decades. The system will integrate space assets in multiple orbit configurations with a consolidated ground segment to provide more effective integration of data, improved tracking accuracy, reduced time latency, and greater detection sensitivity to maximize the operational commander’s situational awareness. The SBIRS “System of Systems” architecture will consist of four satellites located in geostationary orbit, two satellites orbiting in highly elliptical orbits, and a constellation of greater than twenty satellites in low earth orbit to provide global coverage in support of SBIRS missions.

The SBIRS High system of satellites is comprised of four satellites located in geostationary orbit and two satellites orbiting in highly elliptical orbits. These six satellites will perform the four infrared missions of missile warning, missile defense, technical intelligence, and battlespace characterization. Specifically, SBIRS High will provide global and theater infrared data and processed messages concerning launch, flight, and impact location of strategic and theater missiles and other infrared significant events to the National Command Authority and operational commanders.

The SBIRS High component will use highly flexible tasking infrared sensor technology to combat emerging threats. Each satellite will consist of a scanning infrared sensor for global coverage and a staring sensor for accurate detection and tracking of theater-level threats. This technology will allow the SBIRS High element to detect and track shorter-range missiles in the boost phase with greater accuracy. The benefit to the warfighter will be increased accuracy in determining the missile launch point and impact point predictions in support of offensive and defensive operations.

The SBIRS High ground segment architecture integrates assets from the current DSP ground segment with SBIRS unique assets to provide a highly capable, low risk system. The ground segment will consolidate three DSP operational sites and associated communications networks into a fully integrated ground segment that fuses all infrared and other data to optimize

performance for all infrared missions. The integrated ground segment will be implemented with modern, open systems processing and allow for modular hardware/software updates.

B. SBIRS LOW OPERATIONS

The SBIRS Low system of satellites will be comprised of a constellation of 25 to 30 satellites in low earth orbit. The primary function of SBIRS Low is to provide precise mid-course tracking and discrimination of objects for the SBIRS missile defense mission in theater conflicts and attacks against North America. In addition, with its low altitude putting it physically closer to the battlefield and thus allowing for higher resolution, the SBIRS Low system is well suited to support the other three SBIRS missions of missile warning, technical intelligence, and battlespace characterization.

A two-stage process characterizes the SBIRS Low sensor suite concept of operations. In the first stage, the acquisition sensor scans for very bright targets in their boost phase utilizing a fast scan, large field of view, small aperture focal plane. Then, the track sensor will stare at very dim post-boost phase targets using a technique of slew and stare with a small field of view, modest aperture focal plane. Conceptually, the track sensor's field of view is similar to looking through a soda straw. An example of the entire sensor system operation is the acquisition sensor detects the infrared signature of a booster rocket, then the acquisition sensor performs a handoff to the track sensor, which maintains a ballistic track on all post-boost vehicles. Post-boost vehicles may include the reentry vehicle (warhead), an attitude control module, spent booster rocket, and decoys. As necessary, the track sensor in one satellite will "handover" a track to another track sensor in a different satellite. This tracking information is also relayed to a ground station where the decision on target engagement procedures is made based upon the current battlespace characterization.

The interceptor batteries will receive cueing data from the SBIRS Low system. The goal is to launch as few interceptors as necessary to achieve the desired probability of kill. The interceptor battery's salvo doctrine, e.g., shoot-look-shoot, shoot-shoot-look, shoot four times, is determined by the operational commander based upon their current tactical assessment.

Because both satellites and a missile move relative to each other, different satellites will track a target based on the time of launch, location of the launch, operability of a satellite, and track revisit scheme. Communications between satellites, between a satellite and the global

scheduler, and between a satellite and a ground station is critical to ensuring tracking accuracy requirements are maintained. Three features of the SBIRS Low communications architecture are:

- a. Flood routing: relay message over set communication paths until the message repeats.
- b. Any new track data initiates communications to update all local schedulers across the system.
- c. Tasking from the ground station can be sent to specified satellites. [Ref. 4]

The key components in a general SBIRS Low tracking architecture are:

- a. Global track file: a single centralized object maintaining full system-level tracks using all available detections.
- b. Track assessor: its two specific functions are to (1) identify and remove “aged” tracks from the global track file and (2) flag requirement failures in the global track file and forward these assessments to the ground station.
- c. Global scheduler: a single module responsible for “partitioning” active entries from the track file among the system’s sensors. This component can be reprogrammed in real-time in response to dynamic battlefield circumstances.
- d. Local scheduler: replicated for each sensor/platform. This component determines the actual sequence of detection attempts and forwards the observations to the global tracker. [Ref. 5]

It is assumed that space-certified computer hardware and software will be available to meet these requirements.

C. GLOBAL SCHEDULER

In a fully autonomous mode, SBIRS Low detects and tracks all threat missiles from launch to mid-course targeting and the global scheduler determines the appropriate track revisit scheme to be employed based upon system design utility theory. The global scheduler tasking model is shown below in Figure 1.

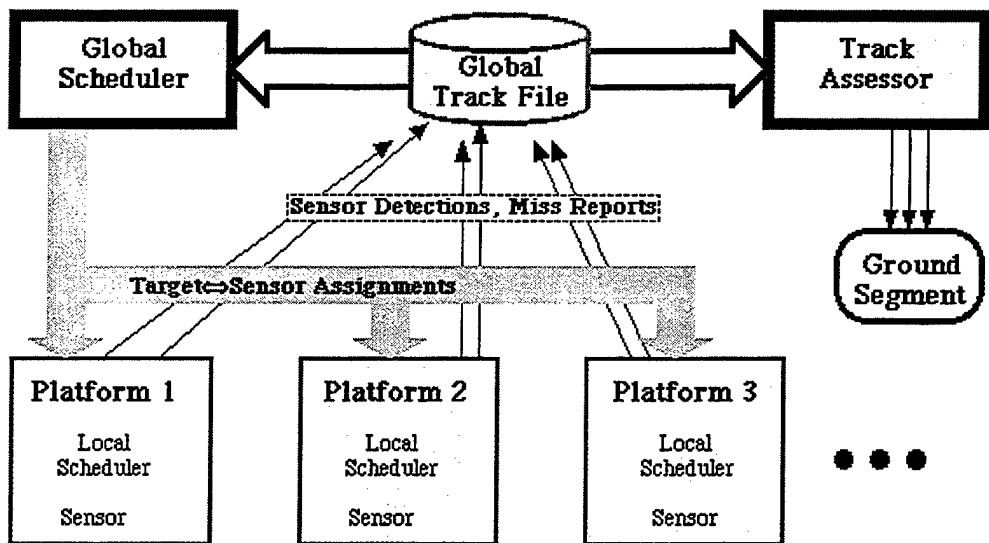


Figure 1. Diagram of Global Scheduler. Diagram of how the global scheduler interacts with the local scheduler on each satellite in response to inputs from the global track file. [Ref. 6]

The system then transmits the tactical parameter data to appropriate ground stations for use in subsequently targeting the lethal object. Operators in the ground station will assess information from SBIRS Low and other relevant sources. Based on the resulting global assessment, operators may choose to accept or override the nominal, automated decision-aided procedures. Reasons for manually overriding the automated procedures could include:

- a. The predicted impact point of a target is deemed to be insignificant (e.g., the middle of an ocean), and the associated track can be dropped.
- b. Sensor resources are needed for higher priority tasking.
- c. Override target classification.
- d. Large raid triage. In case of system overload, ground operators have final authority on tracks to be dropped (certain target spared at the expense of another). [Ref. 7]

A global scheduler is required because of battle management considerations and in general, U.S. military doctrine is characterized by centralized battle management with decentralized execution. In one SBIRS Low architecture design, a global scheduler is located on each satellite and based on the current tactical situation, the duties would be assigned to the satellite with the least tactical tasking. A command center with authority to override the global scheduler is necessarily earth-based because current technology cannot support transmitting the required volume of information to a space-based platform. For example, non-surveillance information such as target value and status, interceptor location and status, and resource

allocation decisions would have to be uplinked to a space-based scheduler in real-time. Additionally, it would be too far removed from human oversight and more vulnerable to counter-measures if it were space-based.

The global scheduler maintains two lists, a sensor list and a track list. The sensor list contains a list of all targets that a sensor detects and the target list contains a list of which sensor(s) has/have tracking responsibility for each target. The track file architecture is shown below in Figure 2.

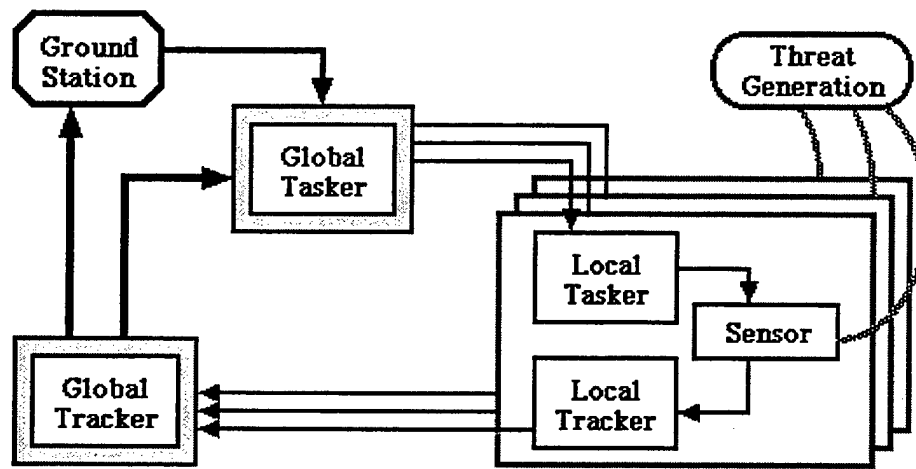


Figure 2. Track File Architecture. [Ref. 8]

The global scheduler controls the tasking of individual local schedulers. The tasking problem for SBIRS Low is nontrivial for the following reasons:

- a. The underlying scenario can be very dynamic with feasible sensor-to-target pairings (determined by some given criterion) changing over time.
- b. The track sensor is a limited resource implying restrictions on the system target handling capacity.
- c. SBIRS Low has a number of system requirements that are mutually incompatible from the perspective of tasking. The system requirements to maintain target track and/or lethal/non-lethal object discrimination and/or a target-quality track result in very different object revisit requirements for the track sensor.
- d. A large number of tasks such as sensor band switching and variable, target-specific dwell times place time-dependent constraints on sensor assets. The sensor has to sweep through some given angle to detect the next target. This motion is referred to as the slew-settle-stare process.

- e. The autonomous tasking-sensing-tracking system must interact “appropriately” with human operators in a ground station. [Ref. 9]

To satisfy the specified level of system performance, there are certain desired characteristics of the global scheduler. These characteristics include:

- a. Very simple control logic.
- b. Capability for the ground command to change target and tasking priorities in real-time.
- c. Maintain robust operations in the presence of component failures.
- d. Support all target tracking functions and ground command tasking until overloaded.
- e. Maintain feasible observation capability under all target/tasking load conditions. [Ref. 10]

The various requirements that must be scheduled by the global scheduler include:

- a. Maintain track: This level is the least stringent tracking requirement. Note, the track maybe one or more objects but system resolution or scissors angle prevents determination and the system may degrade into this condition if there is a mismatch in the total number of objects detected after a satellite-to-satellite handover.
- b. Maintain object resolution: This level is the third highest tracking accuracy requirement. It provides an accurate count of total objects but no insight into which is a lethal object. Note, in real-world operations intelligence sources may aid in assessing accuracy of object count.
- c. Maintain object discrimination: This level requires the second highest tracking accuracy requirement. At this level, the total number of objects has been determined with a high degree of confidence and the lethal objects have been determined. It is important to track all objects to preclude overlapping containment bounds. Failure to maintain nonoverlapping containment bounds could result in targeting a non-lethal object vice the lethal object.
- d. Support an intercept: This level requires the most stringent tracking accuracy. The position of the lethal object is known with sufficient precision that the interceptor will have enough maneuver in the field of view to impact the warhead.
- e. Kill assessment: In general, an accurate estimate for when the intercept should occur is available. Thus, the length of dwell time to determine whether a kill occurred is on the order of one to two seconds. Thus, kill assessment should always be able to be scheduled; however, it is a task that does not necessarily have to be accomplished.
- f. Battlespace characterization: This tasking provides battle damage assessment and tracking of infrared intense events, such as secondary explosions from a bomb attack. Battle damage assessment could be scheduled but infrared intense events would be

“random.” This tasking is important requirement but could easily be “dropped” during periods of intense missile activity.

- g. Technical intelligence gathering: This tasking, which monitors the ballistic missile program developments of potential adversaries, is most important during periods of peacetime. However, this tasking could be important in times of hostilities to determine, for example, if missile counter-measures have been modified.
- h. Space surveillance: This tasking is the lowest level of importance. This tasking is used to update the catalog of objects in space or detect new objects. This tasking may be important if space junk is predicted to come close to a satellite. [Ref. 11]

The level to which these requirements are met is based upon the current tactical assessment, available assets, and political constraints. There are no hard and fast rules on required tracking accuracy because the system wouldn't know which missile was launched and hence the system operator would not know if track discrimination were an issue. For example, the SCUD has only a single warhead so track discrimination is not applicable. However, more sophisticated theater weapons such as the SS-26 can have both a reentry vehicle and an attitude control module so track discrimination is critical. It is impossible to know in real-time which type of missile was launched, although in certain instances some could be eliminated from consideration. Even though technical intelligence sources have provided estimates of how long each type of booster burns; the system may not be able to determine the exact time of launch due to the presence of “opaque” clouds and unknown altitude of the missile launch vehicle.

The operational commander may have to revise his concept of how to accomplish these requirements. The old paradigm is that target acquisition drives system design and once a track is acquired, track maintenance is straightforward. However, the new paradigm is that requirements for reentry vehicle discrimination could be system drivers and realistic light replicas and heavy replicas impose significant line of sight and signal to noise constraints. Additionally, viewing angle constraints can exclude what would otherwise be the “best viewer”, i.e., the closest sensor. If the closest viewer is excluded, the fact that increased range decreases the signal to noise ratio and resolution of closely spaced objects decreases with increasing range may place the system in an overload condition.

D. SYSTEM INTEGRATION

The SBIRS Low system will operate at a variety of tasking levels for which it was designed, but it will also have to operate at a level of “overload.” Reasons for a system overload include too many targets, widely varying booster burn times which require an increased number

of detections to accurately initialize the ballistic trajectory algorithm, rapidness of the salvo, time of day, tracks become unresolvable, targets become too dim for further tracking, and any target motion that results in tracking ambiguities such as crossing trajectories. The SBIRS Low system will be considered to be in an overload condition when the track revisit rate for at least one track, i.e., a reentry vehicle, attitude control module, decoy, etc., cannot support some critical track performance criterion. This critical criterion might be maintain track and/or maintain track identity and/or a target-quality track solution at some given level of probability. Based upon system design, an overload condition should be predictable to allow the operator to use a deliberate decision making process to determine if manual intervention is required.

The basis for robust autonomous global scheduler operations is characterized by:

- a. Target observation data distributed throughout system (communications flood routing).
- b. No overload conditions (perform all target and tasking observations).
- c. An onboard decision-making capability that automatically responds to overload conditions by reducing the number of targets tracked per satellite, sharing targets among track capable satellites, and graceful system degradation when overload is unavoidable. [Ref. 12]

The basic process of scheduling track sensor tasking is for each target, select the earliest of the task function times to determine next tasking time. Sequence each target revisit by “nearest angle neighbor” route except when a scheduled high priority revisit would be too late compared to its required latest function tasking time. The simplified tasking criteria is based upon:

- a. Range to target, where shortest target range selects tracking satellite.
- b. Target priority, where target preference is based upon mission priority or command override.
- c. Observation function priority where preference is based upon function importance to target in track. [Ref. 13]

If target/tasking load conditions in a target rich and/or satellite poor environment result in an overload condition, graceful system degradation can be achieved by:

- a. Efficient sharing of targets/tasking between available satellites. For instance, in a time critical scenario, the second-closest sensor could be tasked, even though the closest sensor is available, because it has a shorter slew-settle-stare process. The

nominal decrease in tracking accuracy, provided by sensor 2 versus sensor 1, is offset by preventing an overload condition.

- b. Reducing targets/tasking on basis of prioritization (prioritization is automatic but Ground Command can override in real-time). An example of a task reduction is to no longer perform hit assessment.

E. EXPLORATORY MODEL ANALYSIS

When new operational concepts, doctrine, tactics, techniques, and/or procedures are developed to exploit new technologies, an experimental process is necessary to efficiently utilize the new concepts and to validate that the change actually represents an improvement in some appropriate measure of performance with some given level of confidence. To confirm the applicable hypothesis, the resulting desirability for timely, affordable testing and evaluation has put increased demands on simulation and modeling requirements. At early stages in the analysis of a new system, the emphasis is on developing a broad understanding of the critical elements in the system and its potential applications. In such situations, there may be too much uncertainty to reliably estimate optimal solutions with the available tools. The SBIRS program is at such a stage. Therefore, the SBIRS Low model will be used to explore large regions of model space in an attempt to identify key factors in the system and scenarios to provide insight into the global scheduler problem.

When insufficient knowledge or unresolvable uncertainties preclude building a surrogate for a particular system, modelers must make guesses at details and mechanisms. While the resulting model cannot be taken as a reliable image of the system to be analyzed, it does provide a computational experiment that reveals how the system would behave if the various guesses were correct. Exploratory modeling is the use of series of such computational experiments to explore the implications of varying assumptions and hypotheses and thus produces useful results through a constellation of alternative feasible model outcomes.

Exploratory modeling helps to address the following five aspects of computer modeling:

- a. Model specification: correct model structure is not known.
- b. Model estimation: adequate data is often unavailable. With military weapon systems, seldom can enemy weapon systems be acquired and fully exploited.
- c. Sensitivity analysis: complexity of models means adequate sensitivity analysis is seldom conducted.

- d. Model validation: experimental validation is impossible due to non-repeatability of human-in-the-loop experiments, uncertainties in weapon system performance, cost, and infeasibility of “live fire” events. However, exploratory analysis can be an effective tool in the process of verification and validation of the models used.
- e. Model use: any given model is probably wrong – how do we learn what the model has to tell us? Although there is considerable uncertainty in the model, with exploratory modeling uncertainty can be narrowed and partial information can provide partial answers. Also, even simple models can surprise their creators, and a model that is not validated does not mean it is not useful (can reaffirm ideas or lead to new directions and support prior knowledge or facts). [Ref. 14]

Exploratory modeling is a relatively new technique that is used to conduct a comprehensive analysis of complex or poorly understood systems. It was developed because modeling methodologies were unsuited to provide insight about the future of some forms of warfare, an uncertain event, and advances in computer technology made "high dimensionality searches" economically feasible. Thus, exploratory modeling allows the analyst to automate running many model instances to create geographical “landscapes” of possible futures, support satisfying policy design (avoid being misled by fragile optima), and support design of adaptive strategies. Each of these three aspects of exploratory modeling is discussed within the context of the SBIRS Low model in the following paragraphs.

The creation of graphical “landscapes” is the exploratory modeling environment. Accurate depiction of this environment allows analysts to navigate efficiently through the space of plausible models, model outcomes to construct lines of reasoning, and to learn about implications of both knowledge and hypotheses. [Ref. 15] By representing uncertainty/possibility with sets of alternative models, the analyst solves multiple problems that provide the following characterizations:

- a. Allows reasoning about structural uncertainty.
- b. A set of “wrong” models can bracket actual system behavior.
- c. Tolerance for incomplete models allows utilization of parameters that are known.
- d. Constraint knowledge can be represented by set boundaries.
- e. Representation of complex “challenge sets” facilitates thinking about adaptivity, responsiveness, and information agility.

The SBIRS Low model contains a large number of variables with imprecise input values. Examples of imprecise input values include:

- a. Unknown sensor availability. Sensor availability is a function of parameters such as time, type of missile launched, and enemy missile launch doctrine.
- b. Unknown sensor revisit schemes due communication delays and/or variations in slew-settle-stare requirements. Variations in "stare" requirements occur because of the time differences required for simple object detection and non-lethal versus lethal object determination.
- c. Unknown time delay, after booster burnout, for first Kepler orbit detection.

The revisit strategy for SBIRS Low model events are aggregated into a single strategy and/or as a "delay" because a high-fidelity computer model is inappropriate at this stage of the analysis. The exploratory modeling paradigm requires that the model be run over multiple dimensions, i.e., sensor availability combinations, sensor revisit schemes, and delays in beginning a ballistic track. However, the combinations are such that it is difficult to comprehensively search over more than a few dimensions. By taking representative samples of system performance at tactically critical moments in the missile's trajectory in various "dimensions," a reasonable balance of model replications and operational insight is achieved.

Exploratory modeling is using computational experiments to assist in reasoning about systems where there is significant uncertainty. An important aspect of exploratory modeling is its relationship with uncertainty. Because exploratory analysis is not predicated on any single point, it is more extensive and considers broader uncertainties such as those generally represented in combat models with many imperfectly known parameters, decisions, and measures of effectiveness. Thus, exploratory analysis can help decision-makers choose options that are robust across different scenario conditions, operational or technical preferences, and costs. The advantage of increased flexibility in decision making and knowledge of the robustness across various contingencies neutralizes risk inherent with imperfect information and an unpredictable future.

For a model to be valid, the classical model paradigm would require that all phenomena that might potentially be influential on the outcome are included and details that might prove pivotal are represented. Additionally, there will be a large number of inputs that specify initial conditions and model boundaries. From this model, a single output or course of action is provided to the analyst. If the decision-maker desires to explore unanticipated adaptive strategies, additional potentially complex modifications to the model will be required. These

changes will increase the complexity of the code and increase in the run-time and data storage requirements. Exploratory modeling provides an alternative to the classical model paradigm by:

- a. Representing knowledge as sets (ensembles, universes) or alternative possible models or scenarios (includes both parametric and structural variation).
- b. Reasoning about future possibilities (inductively) based on properties of set of plausible models inferred from a finite number of such experiments.
- c. Driving sampling strategy from goals of reasoning problem. [Ref. 16]

When developing new warfare strategies or testing new weapons systems, a sensitivity analysis is a critical stage in the computer modeling and analysis process. Sensitivity analysis shows how precise inputs must be measured or the level of fidelity required in the model to provide factual insight into the applicable system. Using traditional methods, improving the model or data alone can be inefficient and may not solve the problem. Exploratory analysis expands on sensitivity analysis and it is useful to contrast exploratory modeling to the traditional concept of sensitivity analysis.

For any traditional numerical computer program, sensitivity analysis is the process by which uncertainty in inputs is related to uncertainty in outputs. To undertake a sensitivity analysis, a parameter to be varied has to be selected. The criterion for choosing a particular parameter generally is an *a priori* belief that a change in it will result in some change in the measure of effectiveness. In a traditional model as a parameter is varied, if nonmonotonicity is encountered, the non-intuitive results may lead to a requirement for adding greater detail or better representations in the model. Again, the complexity of the model increases and the result may become more fragile as the inputs become more precise.

The advantage exploratory analysis has over the traditional approach to computer modeling is that exploratory analysis can provide greater insights into the information that explains the phenomenology being investigated and sometimes resolves troubling sensitivity results without resorting to changes in the model or data. Exploratory analysis determines the range of outputs by sampling throughout the volume of the plausible range of inputs. The accuracy of the sensitivity analysis is determined by the size of the changes in input parameters. Thus, the sensitivity analysis is predicated on the needs of the analysis and available computational resources. Utilizing this approach, changes to the SBIRS Low model may be unnecessary and the results are robust across the range of inputs.

III. SBIRS PROBLEM AND ANALYSIS GENERALITIES

A. OVERALL ARCHITECTURE

The SBIRS architecture is composed of a constellation of two satellites in highly elliptical orbits, four satellites in geostationary orbit, and greater than twenty satellites in low earth orbit, and a consolidated ground station to accomplish the four primary missions allocated to SBIRS. The SBIRS "System of Systems" is shown below in Figure 3.

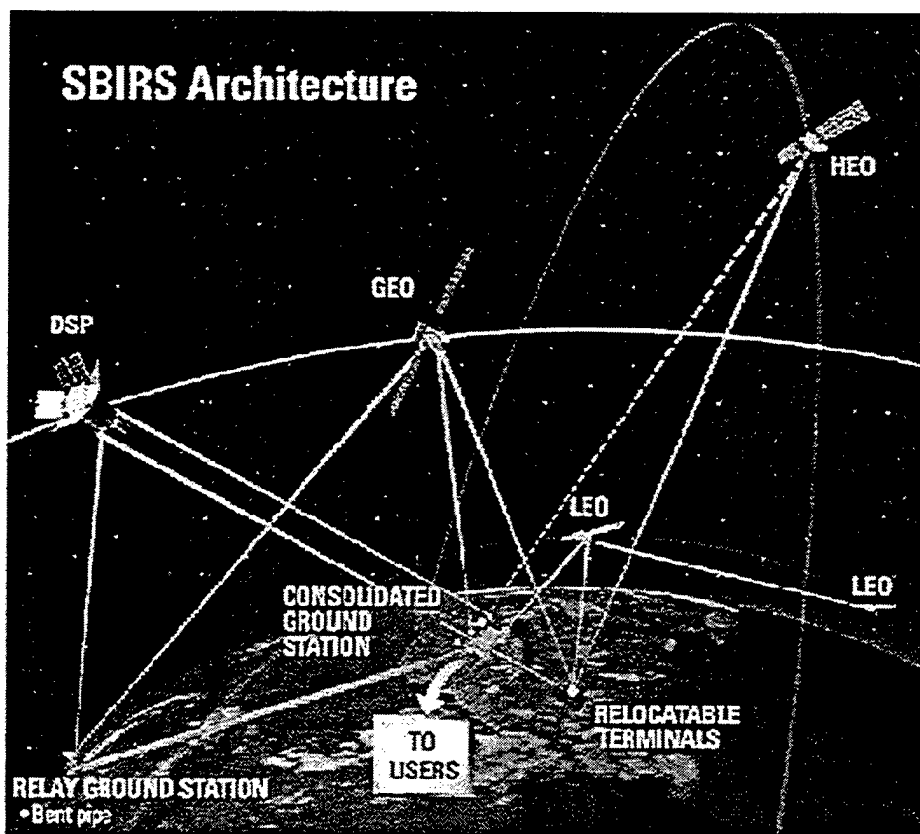


Figure 3. SBIRS "System of Systems" Architecture with Communication Nodes. [Ref. 17]

The primary goal of the SBIRS "System of Systems" architecture is to provide national missile warning and defense against tactical ballistic missiles. There is a requirement to track all objects associated with a missile launch until lethal object kill is achieved, or it is a "leaker." These objects include the lethal object(s), attitude control module, and decoys. Leakage and false alarms are the primary measures of system performance. Leakage is a far more critical measurement, with false alarms only becoming critical when considering logistic (resupply) constraints. Certainly, political ramifications of launching an interceptor at a false alarm and

operator desensitization caused by frequent false alarms are critical. However, unnecessarily launching an interceptor has little affect on the material readiness of an intercept battery while operator desensitization would result in leakage, which was previously defined as "critical."

This architecture is characterized by many "engineering complications," of which four are described in detail. Track accuracies are balanced, meaning they all degrade uniformly since they all have the same error basket. When there are too many targets, by some criteria, the auto-advisor should advise the tracking, telemetry, and control operator to drop track on a given number of targets otherwise an additional number of tracks will drop below tracking requirements. The operator can either do nothing or drop the required number of tracks. If the operator does nothing, tracks will randomly fail to meet the minimum tracking accuracy criteria.

Sensor line of sight (LOS) measurements have two primary sources of error — a random component which is ultimately determined by pixel granularity, and a bias component determined by imprecise knowledge of the position/orientation of the focal plane. This bias component can be reduced considerably by frequent recalibrations against known star positions. Typical sources of random bias are jitter and diffraction. Jitter is caused by the focal plane's gimbal assembly shaking/vibrating. Diffraction occurs as the photons, the received infrared signal, enter the assembly housing the focal plane. The diffraction occurs because as the photons enter the focal plane assembly, based on its design, they spread out according to physics-based wave theory.

The expected value of the cumulative affect of the two sources of random error and the bias error is 36 microradians. Using a representative value for the distance from a satellite to a missile, the positional uncertainty is given by

$$\text{Position}_{\text{uncertain}} = \omega_r d$$

where:

ω_r \equiv angular resolution, microradians

d \equiv distance from satellite to missile, kilometers.

Then, for example, using representative numbers

$$\text{Position}_{\text{uncertain}} = \omega_r d = (36)(4000) = 0.144 \text{ kilometers} = 144 \text{ meters.}$$

There is no navigation controller that is tasked with maintaining a shared navigation grid within the entire constellation. A common navigation grid is unnecessary because each satellite

will communicate with a global positioning satellite to update its own internal navigation system. Thus, any navigation errors are insignificantly small and will not adversely affect satellite to satellite track handovers.

The probability of SBIRS mission success, where success is defined as destruction of the lethal object, is of the general form

$$P(\text{success}) = P(\text{acquire} \cap \text{track} \cap \text{discriminate} \cap \text{target} \cap \text{kill}).$$

With very little margin of error and knowledge that if a track on a lethal object is lost or dropped, intercept becomes nearly impossible, there is a necessity for an in depth understanding of this complex architecture.

Each of these probabilities can be further subdivided into specific components where measures of performance can be assigned. Some of these components are now considered.

Three factors that affect the probability that the SBIRS Low system acquires a missile are:

- a. Geometric coverage, duty cycles. This factor is dependent on whether there are enough sensors/viewers.
- b. Sensor sensitivity, target signature, and obscurations. An example of an obscuration is cloud cover.
- c. Sensor revisit rates and single-look probability of detection. A track algorithm typically requires three hits in four scans to distinguish a valid target from random, background clutter. [Ref. 18]

Missile detection in the SBIRS Low model is partially dependent upon each of the above factors. However, target acquisition itself is a very reasonable area for exploratory data analysis, trading costs such as increased number of satellites and focal plane sensitivities versus system requirements. However, this exploratory data analysis is beyond the scope of this report since to be done right, it requires a high-resolution sensor focal plane simulation.

Once acquired in boost, there are two mechanisms for track loss due to coverage failure:

- a. The sensing constellation does not provide stereo coverage of the booster burnout point.

- b. Stereo coverage is nominally available, but one or more of the participating sensors has failed. This mechanism is not included in the SBIRS Low model.

The interceptor's probability of kill is comprised of independent events such as the probability that the interceptor's seeker head can detect the target and the probability that the interceptor has sufficient divert maneuver to hit the target. As the error basket gets larger, the probability of maneuver in the field of view decreases and the probability of leakage increases.

Because there is so much uncertainty in the SBIRS "System of Systems," it is the ideal candidate for exploratory analysis. The exploratory modeling search strategy used in this analysis is based upon the notion that simple models must first be implemented and explored in some detail in order to gain the intuition needed for the actual system design. A Monte Carlo model is used for the analysis because it provides a computationally efficient method to achieve the desired simulation accuracies.

B. SBIRS LOW PROBLEM

For the baseline SBIRS Low capability considered in this model, each SBIRS Low satellite consists of a short-wave infrared acquisition sensor and a multi-band infrared tracking sensor. One proposed design variation in the SBIRS "System of Systems" is to put the acquisition sensor on SBIRS High satellites, which then requires the SBIRS High satellite to perform a handover to a SBIRS Low satellite immediately following the determination of booster burnout. This design further complicates an already complex system by necessitating an additional handover from one system to another, which is subject to some probability of failure, and the handover is subject to some nominal time latency. Additionally, placing the acquisition sensor on SBIRS High satellites does not improve overall system survivability. Thus, this configuration is not analyzed in this project.

A typical timeline of events for a missile launch scenario analyzed by this simulation is shown in Figure 4.

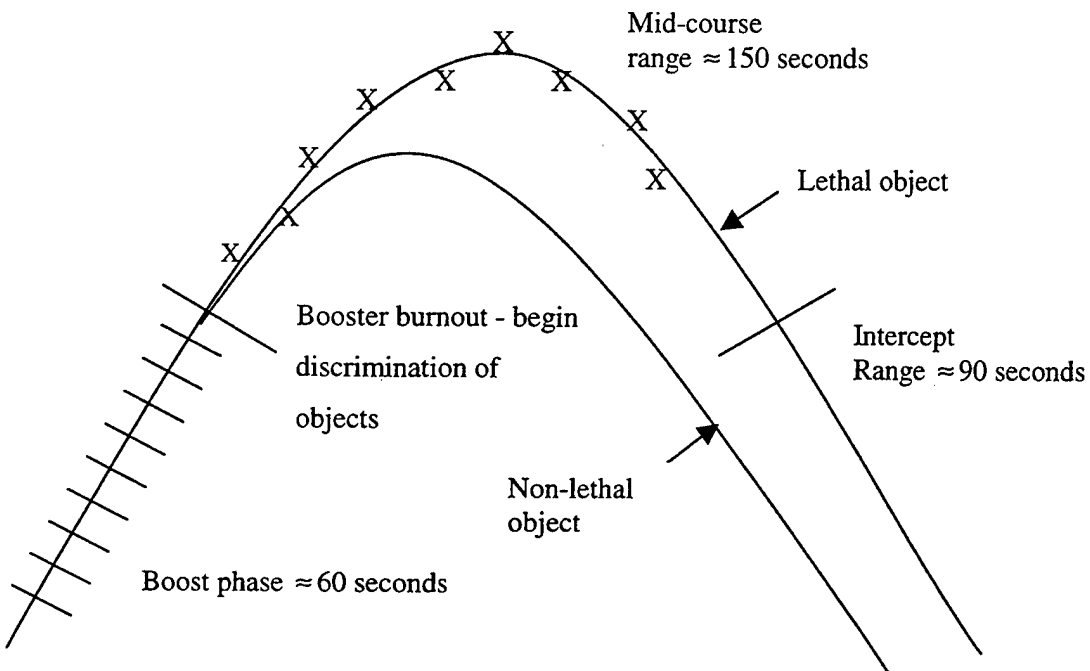


Figure 4. Ballistic Missile Launch Timeline. Timeline for ballistic missile launch scenario.

The launch is detected by the autonomous short-wave infrared sensor onboard a SBIRS Low satellite. Communication flood routing alerts all other SBIRS Low satellites to the launch and the global scheduler determines which satellites will be tasked to monitor the missile. Each satellite builds a mono track that is flood routed to all other satellites. Those satellites that are actively sensing the event fuse the mono tracking data into a three-dimensional stereo track. Precision fitting of the boost-phase trajectory continues based on the track revisit rate, nominally five seconds based on projected system capability.

Once booster burnout is detected, the global scheduler must determine the sequence of events for pointing individual track sensors. This allocation of individual sensors determines overall target handling capacity. Unfortunately, the “efficient tasking” problem is an intractable mathematical problem, especially given the fact there could be multiple, nearly simultaneous missile launches and multiple objects deployed from a single missile.

Nominally, the satellite closest to the object being tracked is the “best” sensor based upon strength of received energy (photons) and minimization of positional uncertainty caused by imprecise line-of-bearing measurement. To achieve a stereo track, the “second best” sensor is

logically the second closest satellite to the object being tracked. However, this rationale does not consider the scenario in which the scissors angle is extremely small, in the case of stereo viewing, or the scenario in which a sensor is nearly in the missile's orbital plane. Thus, the two "best" satellites could provide poor tracking data and result in track ambiguities during a handover.

There are no established rules on required tracking accuracy. The reason is that the system is unable to determine, in real-time, which missile was launched and hence cannot determine if track discrimination is applicable. For example, the SCUD missile has only a single warhead so track discrimination is not applicable. However, modern missiles may have a reentry vehicle and an attitude control module so track discrimination is critical. It can be difficult to determine which type of missile was launched, although in certain instances some could be eliminated from consideration. Even though technical intelligence sources have provided estimates on how long each type of booster burns, the system is probably unable to determine the exact time of launch due to infrared "opaque" clouds. In a real-world scenario with a scanning system, you could never know with adequate precision the height at which the booster becomes visible. If the system could determine the height at which the missile becomes visible, the time of missile launch could be estimated.

Sensor-to-object geometry is carefully modeled, and values of positional accuracy in the tails (of the applicable Gamma distribution) are likely due to "bad" geometry. As described above, the best sensor is defined as the satellite closest to the object being tracked, regardless of tracking geometry. In actual SBIRS Low operation, the determination of the best sensor is nontrivial.

The factors that affect slew-settle-stare time are:

- a. The quality of local scheduling algorithms, i.e., target intensity will be incorporated into stare times and efficient system tasking will minimize sensor slew time.
- b. Satellite phasing. The number of satellites within line of sight of any missile varies with time.
- c. The number of objects to track which is a function of the type(s) of missile(s) launched, salvo rate, salvo size, launch location, launch trajectory, available assets and time to complete a detection. The number of available assets is a function of other tasking requirements and the time to complete a detection is a function of the type(s) of missile(s) launched and possibly the task at hand (discrimination versus track versus hit assessment).

The major contributions to the expected time delay where a SBIRS Low satellite switches from tracking to targeting is any internal communications delay and the time required for the targeting sensor to schedule and move to the newly assigned target. A zero time delay in a handover occurs because each satellite knows where all tracks are located. Thus, if necessary, a satellite can “look ahead” to begin tracking a target as soon as it becomes detectable (i.e., within line of sight).

C. UNMODELED ASSUMPTIONS AND ISSUES

Classical computer modeling standards require the ultimate model to be valid for a wide range of contingencies. However, including all phenomena that might be potentially influential typically caused models to collapse under their own weight as more and more detail was added. [Ref. 19] Contemporary modeling philosophy recognizes that having a multitude of contingencies precludes modeling each and every one of them, especially in an exploratory data analysis model. Many specific aspects of system performance, for instance modeling the focal plane design, are better studied in high-resolution, cost-performance tradeoff studies. It is acknowledged that many aspects, such as the communication architecture, are critical to SBIRS Low performance, but others are functionally irrelevant. For instance, modeling an oblate earth when computing the Kepler orbit is easily accomplished, but doing so provides no additional insight into tracking accuracy at a cost of significantly increasing the computational time per event.

The unmodeled assumptions for the SBIRS Low model are presented in chronological order, according to the typical timeline for a ballistic missile launch scenario shown in Figure 4. Then, basic assumptions for U.S. and enemy tactics and proficiency are presented.

In developing the SBIRS Low model, certain simplifications of orbital mechanics were made. First, the free-flight portion of the trajectory is Kepler. This assumption states that the only force acting on the reentry vehicle, attitude control module, decoys, and spent booster rockets is gravity. Second, the earth is spherical and has no atmosphere. Modeling the earth as a sphere eliminates perturbations of the gravitational field due to the real nonspherical shape of the earth. The lack of atmosphere allows factors such as winds, temperature, atmospheric density, and drag to be ignored. However, opaque clouds are modeled to a user-defined altitude, below which the SBIRS Low system cannot detect a missile. The version of the computer code used in this analysis does not model “solar outages,” i.e., obscuration of a missile by the sun being in the

background. However, “hooks” are included in the code for eventual modeling of this phenomenon.

Once the satellites are in orbit, they cannot be repositioned in response to an anticipated threat. Mechanical failures do not occur, which eliminates the requirement to take corrective action such as realignment of the constellation, reprogramming of a satellite, and launching replacement satellites. Additionally, the position error of a satellite is insignificantly small. Each satellite maintains its own navigation solution and receives updates from global positioning satellites. Additionally, random bias errors are trivially small since calibration is essentially continuously performed using stars.

Each missile is launched with identical boost-phase performance and Kepler orbit flight characteristic, and all trajectories are elliptical with the focus at the center of the earth. Tracking accuracy will vary slightly run to run due to the random effects of the various sources of error.

Missile classification, in general, will not be possible due to uncertainty in missile launch time. This lack of classification makes tracking requirements difficult to quantify since certain missiles contain only a warhead while others contain a warhead, decoys, and/or an attitude control model. Thus, in certain but unknown instances, track discrimination is extremely critical while in other instances it is irrelevant.

Discrimination or the lack thereof, between objects contained in the post-boost vehicle does not affect track accuracy. Discrimination between lethal objects, the reentry vehicle, and non-lethal objects, light replicas, heavy replicas, attitude control module, and spent booster rocket, is “only” critical when determining which object to target.

It is also assumed that there is perfect track correlation between sensors. For instance, as one sensor is no longer able to track an object (reentry vehicle, attitude control module, or spent booster rocket), the sensor that receives the “handover” “sees” the same tactical picture and objects remain discriminated. Although track correlation ambiguities are likely (and require nontrivial solutions), by making this assumption a “best case” answer is determined. Additionally, a track “handover” occurs instantaneously and in general, all communications occur

instantaneously and are not subject to failures, errors, being missed, misinterpretation, or being "lost."

Detection is based upon line of sight and heuristics (based on tangent height from the earth), not a probability of detection based on factors such as signal to noise ratio, minimum scissors angle, minimum dwell time, or higher priority tasking taking precedence. Note, the SBIRS Low model does not model time factors such as:

- a. The length of time a sensor must stare at an object to detect it.
- b. The length of time a sensor must stare at an object to perform lethal/non-lethal object determination.
- c. The length of time to complete the slew-settle-stare process.

In a dense target environment, the assignment problem, associating observations with tracks, use of tracking gates only begins to solve the problem. Additional logic is required when an observation falls within the gates of multiple target tracks or when multiple observations fall within the gates of a target track. Additionally, one sensor may "handover" a single track, but when the new sensor looks for this track, it is conceivable, based on sensor-to-target geometry, that the new sensor sees an additional track not detectable by the first sensor. Tracking ambiguities could, for example, occur during a "handover" from one track sensor to another, a handover from one acquisition sensor to another, or if SBIRS High is used to cue a SBIRS Low track sensor. However, they will not occur in the SBIRS Low model because all events are run where a single missile is in-flight at any given time. This modeling assumption will result in the SBIRS Low model providing a "best case" estimate.

Specific design parameters of the interceptor are ignored since actual interceptor-missile engagements are not analyzed in the SBIRS Low model. For additional studies, assume the interceptor design is well balanced. In general, the probability of maneuver in the field of view is comprised of the divert maneuver capability of the interceptor and detection capability of the focal plane. Analysis could be complicated by the fact that divert capability is limited by a circular contour while detection is limited by the square contour of the focal plane assembly. However, the interceptor design is balanced by assumption,

$$\frac{\Delta V}{V} \approx \frac{FOV}{2},$$

where:

ΔV \equiv divert maneuver capability, m/sec

V \equiv nominal closing speed of an interceptor relative to its target lethal object, m/sec

FOV \equiv interceptor seeker/sensor field of view, radians.

Then, the probability density of tracking errors can be projected on any two dimensional surface like the interceptor focal plane assembly as a Rayleigh distribution. [Ref. 19]

All logistic constraints are ignored. Although an unlimited supply of interceptors would allow a battery commander to shoot any arbitrary number of interceptors at a missile to achieve the desired probability of kill, tracking and global scheduler overload is not directly affected by the number of available interceptors.

The U.S. will honor all applicable treaty limitations. This assumption has no affect on system tracking accuracy but is applicable to certain actions that could be used if the system was in an overload condition.

Attrition of the enemy's missile launching capability is not possible due to system mobility and deception tactics used by the enemy, and a large quantity of transport erector launchers and missiles allows the enemy to be unconstrained by logistic limitations.

Certain additional assumptions must be made regarding enemy capabilities and political and military doctrine. First, enemy ballistic missiles do not have terminal guidance. If terminal guidance is used, the calculations for predicted position probabilities cannot be utilized to schedule sensor revisits and determining marginal tracking requirements to support intercept and impact points is not possible. Thus, if a missile has terminal guidance, the model and actual SBIRS Low operation cannot support this eventuality with any predetermined accuracy. However, the missile may perform a generalized energy management maneuver prior to booster burnout.

The enemy may violate treaty limitations imposed on missile performance characteristics. This assumption does not currently affect the results provided by the model since the booster phase is being modeled by a kinematic algorithm, track discrimination factors such as multiple objects along a single line of sight are ignored, and track detection factors such as signal-to-noise

ratio are ignored. Thus, this assumption currently only affects the rate at which an overload condition is reached and resolved.

The enemy is a rational actor who will employ deception tactics to disguise launch facilities, vehicles, and missile launches and will attempt to attack military and politically sensitive targets. The enemy is also competent so that threat missile performance is within design parameters and the enemy is capable of properly employing the missile.

The enemy cannot directly target the interceptor or SBIRS Low satellites, but the enemy is capable of targeting sea-based and shore-based SBIRS assets and associated communication links. This assumption has no effect on the performance of the simulation, but would effect the outcomes determined by higher-resolution models.

D. TRACKING AND MONTE CARLO ASSUMPTIONS

A ballistic missile trajectory is composed of three parts: the powered flight portion, the free-flight portion, and the re-entry portion. The powered flight portion lasts from launch to booster burnout, and based on the assumptions described in the previous section, the free-flight and re-entry portion comprise the remaining time of flight.

Three types of powered flight trajectory models are rigid wire, flexible wire, and stereo kinematic. The rigid wire model assumes that target altitude and down-range travel only depend on time since launch. This model is the most restrictive in that it assumes every booster rocket of a given class follows the same trajectory. The flexible wire model assumes altitude and down-range travel is a function of time since launch and a constant, which may change during the trajectory. This constant changes the shape of the trajectory. The stereo kinematic model is a cubic polynomial fit of successive detections by the acquisition sensor. This model has the most number of degrees of freedom for a closed-form solution and hence offers a “worst-case”, in terms of accuracy, solution. However, as the model makes no assumptions on underlying booster dynamics, it is completely general. This model is used as the default in the analysis because it offers a lower bound on booster phase tracking accuracy and hence will require the greatest number of detections to provide an acceptable initialization of the Kepler trajectory algorithm.

The cubic polynomial fits in the first step are computed using a fixed number of detections, typically through six detections. The time derivative of the position, velocity,

acceleration, and jerk vector is a velocity, acceleration, jerk, and zero vector and a noise term vector which only affects jerk. Note, jerk is the derivative of acceleration with respect to time. Thus, the equation is given by

$$\frac{d}{dt} \begin{pmatrix} x \\ v \\ a \\ j \\ 0 \end{pmatrix} = \begin{pmatrix} v \\ a \\ j \\ 0 \\ 0 \end{pmatrix} + \begin{pmatrix} 0 \\ 0 \\ 0 \\ q \\ 0 \end{pmatrix} \text{ and}$$

$$x(t) = x_o + v_o t + \frac{1}{2} a_o t^2 + \frac{1}{6} j_o t^3.$$

There are two primary components of the velocity error associated with booster tracking: state estimation errors in boost phase tracking and additional uncertainties in boost-to-ballistic propagation due to unknown burnout time. The accuracy of determining the boost phase motion is important for initial computation of the Kepler motion. It affects computational accuracy and hence the frequency and number of detections required to achieve the desired ballistic track accuracy. In general, the exact time of booster burnout cannot be determined, but with a five second revisit rate and three satellites tasked to track the missile, the expected accuracy can be computed.

First, the following four assumptions are made:

- a. The booster is equally likely to burn out during any given 5 second interval and its time of burnout is independent of sensor operation.
- b. The sensors act independently.
- c. The sensors are randomly assigned to track the missile, but once the order is established, it does not change.
- d. The time to detect the missile is instantaneous.

Without loss of generality, assume sensor 1 looks at time $t = 0$, and then sensor 2 and sensor 3 have detections within the next t seconds. Then,

$$Y = \min[U_2, U_3]$$

where:

U_2 ≡ time at which sensor 2 detects the missile

U_3 ≡ time at which sensor 3 detects the missile.

With t defined to be the length, in seconds, of the revisit rate (5 seconds in this example), then

$$\Pr[Y < y] = \Pr[\text{at least one } U_2, U_3 < y]$$

$$\Pr[Y < y] = 1 - \Pr[U_2, U_3 > y]$$

$$\Pr[Y < y] = 1 - [U_2 > y][U_3 > y]$$

because sensor 2 and sensor 3 operate independently.

Since U_2 and U_3 are distributed uniformly over the interval t ,

$$\Pr[Y < y] = 1 - \left[1 - \frac{y}{t}\right]^2.$$

Thus, the cumulative distribution function is given as

$$F_y(y) = 1 - \left[1 - \frac{y}{t}\right]^2 \text{ for } y \in [0, t].$$

After differentiating the cumulative distribution, the probability density function is written

$$f_y(y) = -2\left[1 - \frac{y}{t}\right]^1 \left(-\frac{1}{t}\right) = \frac{2}{t} \left[1 - \frac{y}{t}\right].$$

With $t = 5$,

$$f_y(y) = \frac{2}{5} - \frac{2y}{25}.$$

To compute the expected value of the length of uncertainty, the following equation is used

$$\begin{aligned} \int_0^t y f_y(y) dy &= \int_0^5 y \left(\frac{2}{5} - \frac{2y}{25}\right) dy \\ \int_0^5 \left(\frac{2y}{5} - \frac{2y^2}{25}\right) dy &= \left. \frac{y^2}{5} - \frac{2y^3}{75} \right|_0^5 = \frac{25}{5} - \frac{250}{75} = \frac{5}{3} \text{ seconds.} \end{aligned}$$

The cumulative distribution function can be generalized to any number of sensors with any given revisit rate, and is given by

$$F_y(y) = 1 - \left[1 - \frac{y}{t} \right]^{s-1} \text{ for } y \in [0, t]$$

where:

$s \equiv$ number of sensors

$t \equiv$ revisit rate.

The (averaged) quality of the estimated three-dimensional target state, both at the time of the last detection and at the time of the Kepler initiation, is controlled by a number of factors, including:

- a. The assumed random and bias components of the line-of-sight error for individual detections. The random error is assumed to be normally distributed with a mean value of zero and standard deviation of 30 microradians. The bias is an unknown additive constant that is present due to errors in pointing the focal plane. This error is also assumed to be normally distributed, but with a mean value of zero and standard deviation of 20 microradians.
- b. The order of the interpolating polynomials for the mono fits.
- c. The number of detections (i.e., the time window) used in the mono fits.
- d. Track quality at time of predict-ahead.

The missile may perform a generalized energy management maneuver prior to beginning its ballistic trajectory. This event is currently not coded into any missile profile, however, the kinematic tracking algorithm will track the missile during this maneuver.

E. SCOPE OF ANALYSIS

The scope of this analysis is to identify and assess feasible, tactically prudent track revisit schemes for SBIRS Low operations using Monte Carlo computer simulation and exploratory data analysis. The problem of analysis using exploratory modeling can be conceptualized as the problem of how to select the limited number of experiments that can be practically run to best inform the question of interest. The design of the exploratory analysis is based upon timeline constraints dictated by the typical missile launch scenario shown in Figure 4 and conducting a reasonable number of model events without sacrificing details of analysis.

The primary concern is the development of a methodology and a specific implementation that is designed, from the outset, to address some of the important open questions in SBIRS Low

operations. The SBIRS Low model can be characterized as a scalable, high-performance compute engine and a flexible overall system design allowing use of "minimum acceptable fidelity" components for some studies or higher fidelity components as needed for other studies. The chosen fidelity is a trade-off between computational speed and resources, complexity of formulas, inclusion of parameters, and desired level of insight. The sampling strategy utilized is Monte Carlo because it provides the desired high degree of accuracy and the computational resources are available. A discussion of Monte Carlo methods is contained in Appendix A.

The use of 20,000 Monte Carlo simulation runs per event was chosen to reduce the standard error of the instantaneous position accuracy at time $t = 50$ seconds to an order of five meters. Suppose that $\eta_1, \eta_2, \dots, \eta_n$ are independent observations from the same parent distribution. Then an unbiased estimator of the mean of this parent distribution is

$$\bar{\eta} = \frac{\eta_1 + \eta_2 + \eta_3 + \dots + \eta_n}{n}$$

and it has estimated standard error

$$\sigma_n = \frac{\sigma}{\sqrt{n}}.$$

This computational technique provides an accurate estimation of the distribution's "tail" behavior.

For a Gamma distribution, the expected value and variance is given by

$$E[X] = \mu = \alpha\beta \text{ and } V(X) = \sigma^2 = \alpha\beta^2.$$

From which the standard deviation follows:

$$\sigma = \sqrt{\sigma^2} = \beta\sqrt{\alpha}.$$

Thus, the estimated standard error is written

$$\sigma_\eta = \frac{\beta\sqrt{\alpha}}{\sqrt{n}}.$$

Using instantaneous positional accuracy values at time $t = 50$ seconds from a CSS-2 launch in which sensor 1 and sensor 2 have a 5 second revisit rate, a representative scenario is given by

$$\sigma_{\eta} = \frac{\beta\sqrt{\alpha}}{\sqrt{n}} = \frac{(0.1498)(\sqrt{0.4965})}{\sqrt{20000}} = \frac{0.1056}{141.42} = 0.0007464 \text{ kilometers} = 0.7464 \text{ meters}.$$

Note, this is the precision of the Monte Carlo calculation itself, not a “real world” measurement of the precision of the SBIRS Low system.

The SBIRS Low modeling goals are identification of the metrics, identify/explore sensitivities, develop intuition, and provide benchmark/reference book of track accuracies as a function of missile type, sensor revisit scheme, length of time since booster burnout (i.e., length of time in ballistic orbit), and length of predict-ahead time.

The instantaneous or any arbitrary predict-ahead time position error is modeled as a generalized gamma distribution where

$$f(x; \alpha, \beta) = \begin{cases} \frac{1}{\beta^\alpha \Gamma(\alpha)} x^{\alpha-1} e^{-\frac{x}{\beta}} & \text{for } x \geq 0 \\ 0 & \text{otherwise} \end{cases}$$

where $\alpha > 0, \beta > 0$.

The gamma distribution was chosen because it is the parent distribution of the chi-squared distribution. Each component of the position error was created from a normal distribution and by construction of the formulation, the errors are independent. The result of squaring then summing “n” independent standard normal random variables is a chi-squared distribution with n-degrees of freedom. Thus, the ratio of the absolute value of the position error divided by the variance of the position error is distributed χ^2 with three degrees of freedom. The result of dividing by the variance is to normalize the random variable. This equation is given by

$$\frac{|\bar{x}_{predict} - \bar{x}_{truth}|}{\sigma_{predict}^2} = \frac{\delta_x^2 + \delta_y^2 + \delta_z^2}{\sigma_{predict}^2} \sim \chi^2_{[3]}.$$

This relationship can also be expressed as

$$\vec{\delta}^T P^{-1} \vec{\delta} \sim \chi^2_{[3]}$$

where:

$$P \equiv \text{variance/covariance matrix} = \begin{bmatrix} \sigma_x^2 & \sigma_{xy} & \sigma_{xz} \\ \sigma_{xy} & \sigma_y^2 & \sigma_{yz} \\ \sigma_{xz} & \sigma_{yz} & \sigma_z^2 \end{bmatrix} = \begin{bmatrix} \sigma_x^2 & \rho_{x,y}\sigma_x\sigma_y & \rho_{x,z}\sigma_x\sigma_z \\ \rho_{x,y}\sigma_x\sigma_y & \sigma_y^2 & \rho_{y,z}\sigma_y\sigma_z \\ \rho_{x,z}\sigma_x\sigma_z & \rho_{y,z}\sigma_y\sigma_z & \sigma_z^2 \end{bmatrix}$$

and $\rho \equiv$ correlation coefficient.

The parameters α and β are estimated using the method of moments technique that is given by the following equations

$$\hat{\alpha} = \frac{\bar{x}^2}{\left(\frac{1}{n}\right)\sum x_i^2 - \bar{x}^2}$$

$$\hat{\beta} = \frac{\left(\frac{1}{n}\right)\sum x_i^2 - \bar{x}^2}{\bar{x}}$$

where:

$$\bar{x} = \sum_{bins} (bin)(count)$$

$$\left(\frac{1}{n}\right)\sum x_i^2 = \sum_{bins} (bin)(count)^2$$

and

bin \equiv mean value of each position error bin (x-axis value)

count \equiv proportion of position errors in the given histogram bin (y-axis value).

By modeling the data as a generalized Gamma distribution, the expected value and variance of this distribution can be compared to the mean and variance of a χ^2 with v degrees of freedom, which is given by v and $2v$, respectively. Hence, the normalized theoretical mean and variance are 3 and 6, respectively. This modeling technique will allow comparison between theoretical and actual simulation results.

THIS PAGE INTENTIONALLY LEFT BLANK

IV. SBIRS LOW MODEL AND ANALYSIS SPECIFICS

A. BASIC MONTE CARLO STRUCTURE

A "model event" is a computer simulation of the SBIRS Low tracking system's response to an individual threat missile launch. It consists of:

- a. "Flying" the simulated booster and resulting ballistic objects.
- b. Generation of simulated detection sets based on SBIRS Low observations of the physics-based booster rockets and subsequent ballistic tracks.
- c. Computation of an estimated track position based on the random data.
- d. Evaluation of track performance metrics (e.g., difference between estimated and true positions).

A "Monte Carlo analysis" is simply the generation of a large number of pseudo random model events and the evaluation of empirical probability distributions (e.g., histograms) from the performance metrics of individual events.

A model event is specified for a given satellite constellation, acquisition and track sensor revisit scheme, and missile type. For all model events, the satellite constellation consisted of a total of 27 satellites, three satellites in nine different orbits, and the acquisition sensor, which detects the plume from the missile's booster motor, had a track revisit rate of five seconds. The revisit rate for each track sensor, which detects ballistic objects, was varied according to a notional pattern and consisted of

- a. Delaying the time after booster burnout the sensor first attempted to detect the ballistic object, and/or
- b. Varying the number of satellites used to track the ballistic object, and/or
- c. Specifying whether the closest, next closest, or third closest satellite was utilized.

Each run consisted of a specified number of single missile launches distributed at random, according to a uniform distribution with respect to the surface area, within a specified latitude/longitude box. The number of runs per event, 20,000, was determined based on a desire for the estimated standard error to be on the order of five meters. See Chapter 3, section E for the applicable calculations.

The timeline for a representative missile launch is shown below in Figure 5, which is identical to Figure 4.

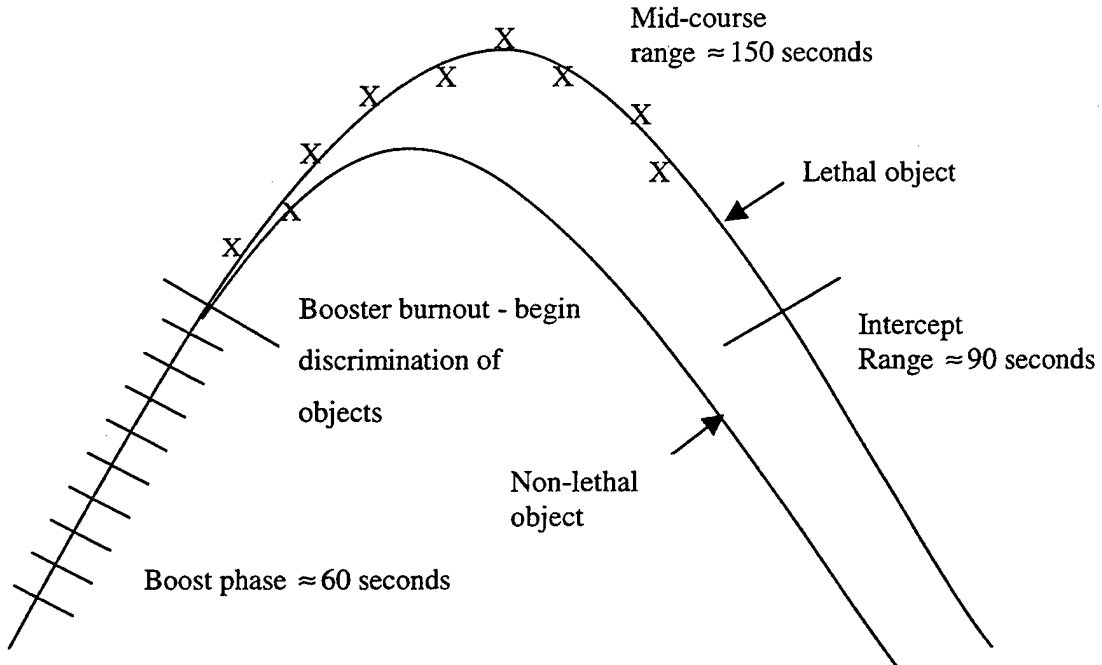


Figure 5. Ballistic Missile Launch Timeline. Nominal SBIRS Low system operational timeline.

A random launch time is generated within the launch window. The primary effect of randomizing the launch time is to vary the phasing of the SBIRS Low constellation. This randomization helps to ensure inferential validity of the analysis.

All available satellites, typically three, collect the boost phase tracking data. The two-dimensional boost phase data is collected from each satellite every Δt seconds and fused to the track's three-dimensional earth-centered inertial reference frame state matrix (position and velocity vectors) at burnout.

Once booster burnout is sensed, the acquisition sensor performs a track handover to the track sensor. A post-boost burnout handover from the acquisition sensor to the track sensor is the preferred option because a reliable trajectory model for predictions exists only for ballistic targets and the ballistic initiation prescription provides an unbiased estimate of the Kepler trajectory from the available sensor data. If the handover were attempted prior to this perceived burnout, the target state estimation errors can only get worse, with an associated increase in the overall track loss probability.

The most significant factor in track loss probability is the precision of the velocity estimate for Kepler initiation. In this regard, the track loss probabilities (for differing fields of view) are highly correlated with the precision of the associated velocity estimate provided by the boost phase tracking system.

The ballistic phase analysis is characterized by iterating through the following three steps until the missile impacts the earth.

1. Positional data on the ballistic object is collected from the specified sensors based on the track revisit scheme.
2. The Kepler track parameters are fitted according to least squares estimation.
3. Positional accuracy and their statistical distribution are calculated for various predict-ahead times.

For example, at times $t = 50, 100$, and 150 seconds after booster burnout, the current Kepler track fit is formed. The instantaneous, 50 second predict-ahead, and 100 second predict-ahead tracking accuracies are then computed and a Gamma distribution is fit to the probability of a given relative positional uncertainty. In determining relative spherical error, the absolute value of the difference between the detected and actual location divided by the variance of the prediction is computed.

This equation is given by

$$\frac{|\bar{x}_{predict} - \bar{x}_{truth}|}{\sigma_{predict}^2} = \frac{\delta_x^2 + \delta_y^2 + \delta_z^2}{\sigma_{predict}^2}.$$

Note that this error is a "real" error and does not require Gaussian assumptions. By avoiding the requirement to make Gaussian assumptions, the critical tail region is more accurately determined. However, if the assumption of combining independent Gaussian random variables is made, then the relative spherical error is distributed as chi-squared with three degrees of freedom.

Tracking uncertainties are induced into the system by assigning errors to all sensors. The error, ϵ , is given as

$$\epsilon_{ijk} = \epsilon_{r_{ijk}} + \epsilon_{b_{ij}}$$

where:

ϵ \equiv total error

$\epsilon_{r_{ijk}}$ \equiv random error $\sim N(0,30^2)$

$\epsilon_{b_{ij}}$ \equiv bias error $\sim N(0,20^2)$

$i \equiv i^{\text{th}} \text{ sensor} = 1, \dots, 27$

$j \equiv j^{\text{th}} \text{ event} = 1, \dots, 20000$

$k \equiv k^{\text{th}} \text{ detection.}$

The bias error remains constant for each sensor during a missile's entire time of flight and is then recomputed for the next event, but the random error is varied for each sensor after every detection.

The ballistic phase tracker may use a tracking scheme of mono sensing only, stereo sensing only, or a combination of both. The stereo sensing rapidly provides accurate determination of the orbital elements because azimuth and elevation information from each satellite is combined to form range. In the case of mono sensing only, the determination of the orbital elements requires significantly more detections, and hence time, because the tracker must derive range over multiple detections. Additionally, tracking predict-ahead accuracy is greatly degraded.

The goals for any generic tracker are interpretation of sensor data and identification and characterization of targets of interest. These goals are achieved by balancing two system-level trade-offs, (1) false reports versus missed (true) reports, and (2) timeliness versus confidence. The tracker must interpret sensor data and accurately identify and ignore the clutter while associating interesting detections into tracks.

The tracking problem, associating detections into tracks, is not rigorously solvable due to a number of unavoidable difficulties such as extraneous detections (false alarms), inadequate/unknown system models ("stochastics"), and association ambiguities for multiple objects. Additionally, the number of tracks seen by one sensor may not match the total number of tracks seen by another. This difficulty is especially challenging to resolve in the case of a "handover" from one satellite to another. In real world SBIRS Low operation, discrimination

failures would be costly. This "first step" analysis sidesteps the real tracking issue by considering only (randomized) single target launches.

There are varied methods for modeling trackers such as kinematic versus precision and deterministic versus stochastic. They are implemented by either batch or recursive computations. Batch implementation is characterized by single fits to multiple detection sets and in mathematical terms, this type of tracking is known as least squares. Hence, the entire data is refit upon arrival of each new observation. The advantages of this method are robustness and it is a "proven" technology. The disadvantages are CPU-costly and does not easily handle model errors. Recursive implementation is characterized by continual re-fits as new detections are made and in mathematical terms, one of several types like this is known as Kalman filtering. Thus, the tracker will iterate an update of the current estimate from a single new measurement. The advantages of this method are it is fast and naturally accommodates model errors. The disadvantage is that it generally has poorer convergence characteristics compared to least squares.

A system model that represents the trade-off between detections and an acceptable false alarm rate is problematic because:

- a. A poor system model accepts junk.
- b. An overly rigid system model accepts nothing.
- c. An unconstrained model accepts everything.
- d. A model with the ideal ratio of probability of detection to probability of false alarm may require a long time window.

Optimal association problems require large CPU costs, however, the larger problem is that poor/incorrect behavior for incomplete data, such as missed detections or "new objects," can cause substantive errors. There is no one single answer to the tracking problem and specifics must be matched to overall system requirements. Thus, pure mathematics must be tempered by heuristics and operator intuition, and since no single method works everywhere, full-scale system simulations are essential.

B. BOOST SPECIFICS

The trajectory of each type of missile is modeled as a physics-based parametric fit to observed trajectories, using data from relevant intelligence sources.

The rotation of the earth must be accounted for when aiming a ballistic missile. This aiming point does not coincide with the target at the time the missile is launched. Rather, it is a point at the same latitude as the target but east of it an amount equal to the number of degrees the Earth will turn during the total time the missile is in flight. This problem is solved by a straightforward iterative procedure that is repeated until the computed value of total time of flight agrees with the estimated value. [Ref. 20]

Given the simulated model trajectory, individual boost phase detections are generated in the SBIRS Low model using a simple model with:

- a. A constant revisit rate per sensor,
- b. Simple geometric "cuts" to determine target visibility (no signal-to-noise ratio determinations).

The target viewing times of individual boost sensors are staggered randomly, but once this relationship is established, it does not change for the duration of the event.

Given the boost data, the booster state at burnout is estimated using the general kinematic estimation procedure outlined in Section C. The alternative of "tracking" using a model based on the underlying data generation model tends to give unrealistically small state estimation errors and was not used in the final analyses described in this paper.

C. KEPLER SPECIFICS

Five independent quantities called "orbital elements" are sufficient to completely describe the size, shape, and orientation of a ballistic orbit. A sixth element is required to pinpoint the position of the satellite along the orbit at a particular time. The set of five orbital elements is shown in Figure 6.

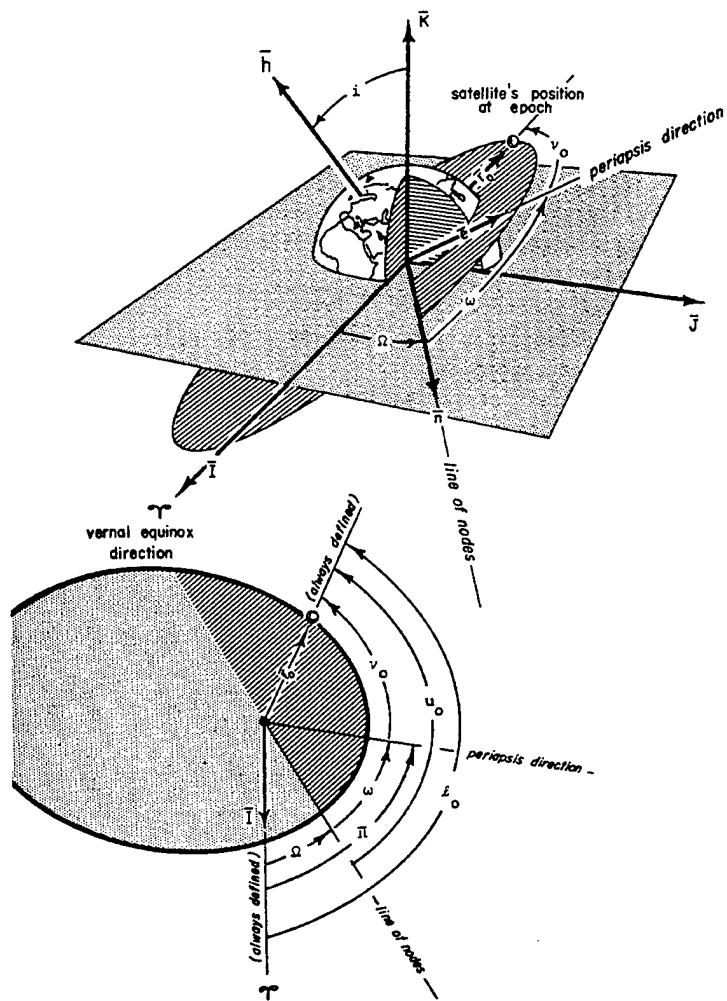


Figure 6. Orbital Elements. [Ref. 21]

Five of the orbital elements are defined as follows:

- Semi-major axis (a): a constant defining the size of the conic orbit.
- Eccentricity (e): a constant defining the shape of the conic orbit.
- Inclination (I): the angle formed between the **K** unit vector and the angular momentum vector, **h**.
- Longitude of the ascending node (Ω): the angle, in radians, in the fundamental plane, between the **I** unit vector and the point where the satellite crosses through the fundamental plane in a northerly direction (ascending node) measured counterclockwise when viewed from the north side of the fundamental plane.

e. Argument of periapsis (ω): the angle, in radians, in the plane of the satellite's orbit, between the ascending node and the periapsis point, measured in the direction of the satellite's motion. In the standard Kepler set (circular orbits), this parameter is undefined and set to zero.

The sixth orbital element is mean anomaly at time $t_0 = 0$, the time of booster burnout.

Mean anomaly is defined as

$$M = E - e \sin(E).$$

According to Kepler,

$$\frac{dM}{dt} = \text{constant}$$

so that M is the natural "time measure" for Kepler orbits.

The angle E , called the eccentric anomaly, is shown in Figure 7

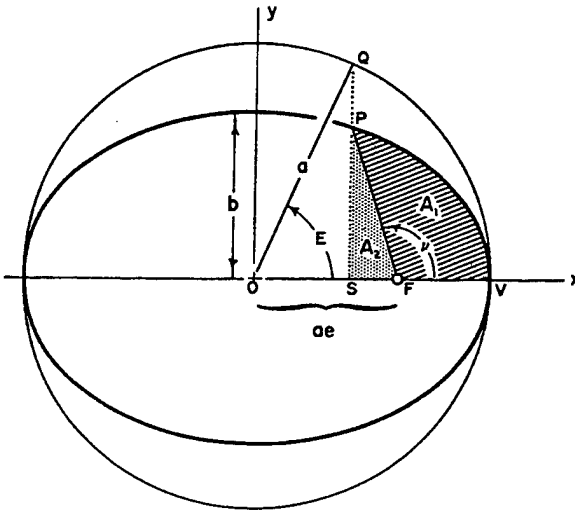


Figure 7. Eccentric Anomaly. Eccentric anomaly, E . [Ref. 22]

where:

$a \equiv$ radius of circle, centered at O, that has been circumscribed about the ellipse (path of Kepler orbit)

$F \equiv$ focal point of the ellipse, which is the center of the earth for this analysis

$OV \equiv$ line extending along the major axis of the ellipse, denoted as the x-axis.

The eccentric anomaly is related to true anomaly, v , shown in Figure 8, by

$$\cos(E) = \frac{e + \cos(v)}{1 + e \cos(v)}.$$

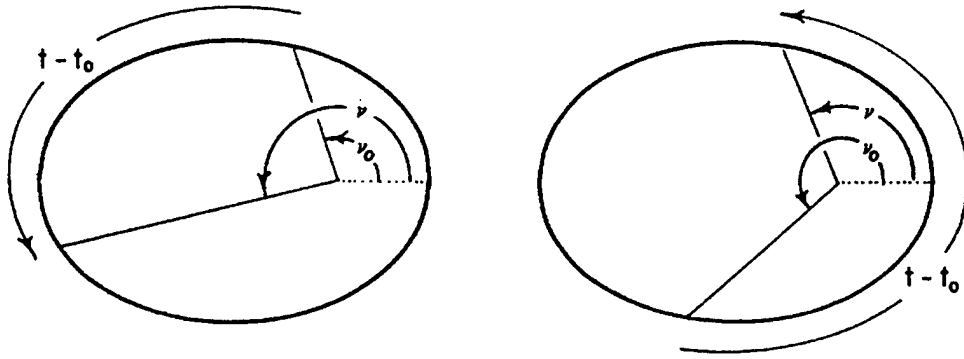


Figure 8. Depiction of True Anomaly. Depiction of true anomaly, v . [Ref. 23]

To transition from the powered flight model to the Kepler orbit model, the boost-phase tracker data initializes the non-linear least squares algorithm used by the ballistic-phase tracker. The algorithm used in the ballistic-phase tracker is the Levenberg-Marquardt method, which is an extension of Newton's algorithm. [Ref. 24] The Levenberg-Marquardt method varies smoothly between the extremes of the inverse Hessian method and the steepest descent method. The latter is used far from the minimum, switching continuously to the former as the minimum is approached. It should be noted that this method enjoys the property of global convergence, i.e., the algorithm converges to a point of zero gradient regardless of the starting point. However, the initial starting point must be "reasonably" close to the solution to achieve the appropriate solution.

The non-linear least squares model is defined as

$$\vec{Y} = \vec{Y}(\bar{\Theta}, t)$$

where:

$\bar{\Theta}$ \equiv M-element parameter vector

\vec{Y} \equiv N-element vector of all data

t \equiv indexing variable (time, bin number, etc.).

Implementation of the standard linearized least squares is given by

$$\delta\bar{\Theta} = \left(\sum_j A_j \right)^{-1} \left(\sum_j \bar{B}_j \right) \equiv A^{-1} \bar{B}$$

where:

$\delta\bar{\Theta}$ \equiv correction step from linearized approximation

A_j \equiv linearized matrices for final estimated parameter value
 B_j \equiv matrices of observed data minus predicted values
 j \equiv index of data (sum over full data set).

The Marquardt modification is given by modifying the matrix A as

$$\delta\bar{\Theta} = M(\lambda)^{-1} \bar{B}$$

$$M_{ij} \equiv A_{ij} (1 + \lambda \delta_{ij})$$

where:

λ \equiv Marquardt convergence factor. λ is nonnegative and scales the step size.

For small λ ,

$$\delta\bar{\Theta} \approx \delta\bar{\Theta}_{LS}$$

For large λ ,

$$\delta\bar{\Theta} \approx \frac{1}{\lambda} \bar{V}_e \chi^2 \approx \text{small gradient step}$$

To assess the goodness of fit, a score function that is to be minimized is defined as

$$S_{TOTAL} = \sum_{j=1}^N S_j \sim \chi^2_{[N]}$$

where:

N \equiv number of data values - number of estimated parameters.

With the implementation outlined above, the Marquardt algorithm is initialized by choosing λ small (e.g., $\lambda = 10^{-4}$) and making initial guess $\bar{\Theta}_0$. The method is performed using the following iterative steps (an explanation of the method is given following the algorithm):

1. Compute

$$\delta\bar{\Theta}_j = M(\lambda)^{-1} \delta\bar{B}$$

$$\bar{\Theta}_{trial} = \bar{\Theta}_j + \delta\bar{\Theta}_j$$

$$S_{new} = S(\bar{\Theta}_{trial})$$

2. If $S_{new} < S_{old} = S(\bar{\Theta}_j)$

Accept step: $\bar{\Theta}_{j+1} = \bar{\Theta}_{trial}$

$$\text{Reduce scale: } \lambda \rightarrow \frac{\lambda}{R} \quad (R \geq 10)$$

Go to (1) for next step.

3. If $S_{\text{new}} > S_{\text{old}}$ then repeat

$$\begin{aligned}\lambda &\rightarrow \lambda R \\ \delta\bar{\Theta}_j &= M(\lambda)^{-1} \delta\bar{B} \\ \Theta_{\text{trial}} &= \bar{\Theta}_j + \delta\bar{\Theta}_j\end{aligned}$$

$$\text{Until } S_{\text{new}} = S(\bar{\Theta}_{\text{trial}}) < S_{\text{old}}$$

$$\bar{\Theta}_{j+1} = \bar{\Theta}_{\text{trial}}$$

Go to (1) for next step.

End of algorithm.

In step 1, the first equation determines the direction in which the parameter vector "moves" and the second equation updates the parameter vector based on the step size. The third equation applies the updated parameter vector to the score function.

Step 2 is executed if the value of the new score function is less than the old function (i.e., represents an improvement). The trial parameter vector updates the previous vector and the convergence factor is reduced. By reducing the convergence factor, the next step size is smaller since the algorithm is closer to its termination criteria.

Step 3 is executed if the value of the new score function is greater than the old function (i.e., does not represent an improvement). The first three equations represent the algorithm attempting to find a descent direction by taking increasing step sizes. Once a descent direction is found, the parameter vector is updated and the algorithm is repeated.

The algorithm is terminated when some appropriate stopping condition (i.e., level of accuracy) is met.

Applying the above general procedures to computing the Kepler state matrix, the non-linear least squares is fit using:

$$\text{minimize: } \chi^2_{[j]} = \sum_j \bar{D}_j^T P_j^{-1} \bar{D}_j$$

where:

$$D_j = [Observation - Prediction]_{jth \text{ datum}} = Z_j - Z_{pred}(\bar{p})$$

$$j = 1, 2, \dots, N_{data}.$$

The first datum is the handover from the boost-phase tracker which is given by

$$\bar{D}_1 = (\bar{x}, \bar{v}; P_{xv}).$$

Subsequent data points are two-dimensional line-of-sight detections provided by each ballistic-phase tracker that either remain mono detections or are fused to become stereo detections. The arithmetic to solve each minimization problem is straightforward but tedious.

The above procedure is not the most general; Kalman filters would allow "model noise," but model noise is not important for non-maneuvering ballistic tracks.

D. SAMPLE POINTS AND PREDICT-AHEAD

The global scheduler must ensure that the appropriate level of tracking accuracy is maintained throughout the missile's time of flight. For example, the system must be able to discriminate objects, e.g., a re-entry from an attitude control module, not just track each individually. This level of tracking is highly scenario dependent where different tasks are time-dependent, and is another facet of the difficult to quantify efficient tasking problem.

The data is sampled at time $t = 50, 100$, and 200 seconds (after booster burnout) because these times represent critical points in the timeline of the representative ballistic trajectory. By time $t = 50$ seconds, the system should have discriminated the non-lethal objects from the lethal objects, if applicable. Although the simulation models detections as instantaneous occurrences, object discrimination in actual system operation may take a dwell time considerably longer than 10 seconds. Thus, by time $t = 50$ seconds, the system would have several opportunities to dwell on multiple objects. By time $t = 100$ seconds, the system should have discriminated the lethal objects and be tracking the lethal objects with sufficient accuracy to target them with interceptors. By time $t = 200$ seconds, interceptors should be airborne.

At each of these three times, four quantities are computed. First, predict-ahead positional accuracy is computed for instantaneous, 50 seconds, and 100 seconds. For the 50 and 100 second predict-ahead quantities, these predictions assume that the system receives no additional updates on the given ballistic track during the predict-ahead period. Four empirical containment bounds, 80%, 90%, 95%, and 99%, are computed at the three data sampling times. These four bounds were chosen because they represent analogous, commonly used confidence intervals.

Second, histograms are then created at the specified sampling time(s). Two parameters, N_{Bins} and X_{Max} , are used to match the granularity of the histogram bins to plausible estimation error variations. For all events N_{Bins} was set at 80 and for all events except "Mono" and "Sequential Mono" (described in Section E), the parameter X_{Max} was set at 8 kilometers. For the "Mono" and "Sequential Mono" events, X_{Max} was set at 32 kilometers.

Third, an empirical cumulative distribution function is determined from the histogram in the straightforward manner—simply sum up histogram bin contents below each histogram bin edge.

Fourth, the empirical histograms are fit to a Gamma distribution parameterized as

$$P\{x; \alpha, \lambda\} = \begin{cases} \frac{\lambda e^{-\lambda x} (\lambda x)^{\alpha-1}}{\Gamma(\alpha)} & x \geq 0 \\ 0 & \text{otherwise} \end{cases}$$

$$\text{where } \alpha, \lambda > 0 \text{ and } \mu = \frac{\alpha}{\lambda} \text{ and } \sigma^2 = \frac{\alpha}{\lambda^2}.$$

This parameterization is equivalent to that given in Chapter 3 with $\beta = \frac{1}{\lambda}$ and the containment bound levels used for predicting positional accuracy are also used in predicting the two Gamma distribution parameters. See Chapter 3, Section E., for the method of moments technique for estimating α and β . The containment bound levels are calculated by counting events, that is, a 95% containment bound is calculated by finding $r_{0.95}$ such that

$$\frac{N(r < r_{0.95})}{N_{total}} \approx 0.95$$

where $r_{0.95}$ is the range corresponding to the 95th percent order statistic.

E. ANALYSIS SAMPLE SPACE

The analysis consisted of the exploratory region shown in Table 1 and analyzing the system's tracking accuracy of the CSS-2 and M-9 missiles. These missiles were chosen because their dynamic flight characteristics at booster burnout combined with the uncertainty of the time of booster burnout represent a worst-case scenario in the initialization of a ballistic track.

Exploratory Regions

Type of Event	Description
Mono	Event viewed by only one sensor.
Sequential Mono	Event viewed by one sensor for first 75 or 150 seconds then performs handover to another sensor. Handover combinations were sensor 1 to sensor 2, sensor 1 to sensor 3, and sensor 2 to sensor 3.
Synchronous	Event viewed by two sensors with simultaneous revisit rates
Asynchronous	Event viewed by two sensors with different revisit rates
Delayed	Event viewed by two sensors with synchronous revisit rates but delay viewing ballistic track after booster burnout.
Staggered	Combination of the synchronous and delayed events
Latitude Shift	Synchronous revisit rates using sensor 1 and sensor 2 for randomly chosen latitude between N02 to N05, N22 to N25, N62 to N65, and N82 to N85.

Table 1. Exploratory Regions. SBIRS Low model sample space.

In each case, the revisit rate is varied between 5 and 40 seconds in 5 second increments. Where applicable, the delay in beginning the Kepler track was varied between 5 and 30 seconds in 5 second increments. The latitude for all events was randomly chosen between N42 to N45, except for the "Latitude Shift" events.

The range of revisit rates was chosen because it provides the desired insight into the trade-off between a large number of detections over a small time period versus a small number of detections over a large time period. The 5 second increment increase per event represents a balance between accuracy of extrapolation between revisit rates and conducting a reasonable number of model events. The default latitude range from which launches originated was selected because it is a mid-range latitude from which most threat missiles would be launched. The

longitude range was held constant, between E52 and E56, for all model runs because positional accuracy is not a function of longitude (with regard to using an earth-centered inertial reference frame to specify the position of each satellite in the constellation) since launch times are randomized over an entire day.

THIS PAGE INTENTIONALLY LEFT BLANK

V. RESULTS

A. MODEL INPUT PARAMETERS

The SBIRS Low model input parameters are contained in an ASCII text file. The input file is divided into four sections: (1) CONTROL, (2) BOOSTER, (3) BALLISTIC, and (4) OUTPUT. An overview of an input file is discussed in this section and specific parameter names, valid entries, and miscellaneous file-specific requirements are listed in the sample input file described in Appendix B, section A.

The control parameters specify the SBIRS Low configuration and the number of Monte Carlo simulated events to be included in the run. For all runs, the satellite constellation was defined as nine rings with three satellites per ring and the number of events per run was 20,000. As described in Chapter 3, section E, this number of events results in the estimated standard error of the instantaneous position accuracy being on the order of 5 meters.

The booster phase parameters specify the trajectory profile, launch mode, launch and target position, and sensor viewing availability for the missile to be launched. Individual launches were generated using a simple, efficient interpolation of appropriate boost phase data (see Chapter 3, section D). The launch mode was "random" for all events, which results in a random target position (impact point). There are nine different missile classifications available to the user and they are described below. The CSS-2 and M-9 missiles were the only missiles used in the exploratory model analysis because of their dynamic flight characteristics at booster burnout.

- a. CSS2: Follow-on version of the first operational Chinese ballistic missile, the liquid-fuelled CSS-1 which was reverse-engineered from two Russian R-2 (SS-3) intermediate range ballistic missiles delivered in 1958. The CSS-2 can deliver a 3 megaton nuclear warhead over a distance of 2800 km. Saudi Arabia purchased 36 CSS-2s with conventional warheads in 1988, where they are maintained and operated by Chinese personnel. The CSS-2 gives Saudi Arabia the longest-range theater ballistic missile capability in the Arabian Gulf region, and enables them to target cities as far apart as Moscow, Algiers, and Rome. China currently deploys 40 CSS-2s at six field garrisons and launch complexes.
- b. M9: A Chinese intermediate-range, road mobile, solid propellant missile that began development in 1984. It has a range of 600 km, a single 500 kg high-explosive warhead, and a circular error probability of approximately 300 m. There are approximately 300 missiles in service in China.

- c. SCUD: This missile forms the basis of Iraq's missile program. It purchased this missile from the Soviet Union in 1974. The SCUD-B has a liquid-fuel booster rocket, a single warhead, and a range of approximately 300 km.
- d. ALAB: Al Abbas. A modified SCUD missile in which the size of the warhead has been decreased to provide space for additional propellant. The missile had the warhead reduced to 300 kg and a further increase in liquid fuel capacity to give a range of 900 km. The circular error probability is reported to be no more than 3 km. Iraqi technicians were reported to have concluded that an upgraded version of the Al Hussein with improved motor performance and higher energy liquid fuel would give greater range with a larger payload than could be achieved with the Al Abbas.
- e. ALHU: Al Hussein. A modified SCUD-B missile with a range of more than 500 km. Analysis of the Al Husseins fired during the Gulf War revealed that its 600 – 650 km range had been achieved by reducing the warhead weight to around 500 kg to allow an increase in fuel capacity. The circular error probability of the Al Hussein is poor, with reports generally estimating it to be between 1 and 3.2 km.
- f. ND: Nodong 1. A North Korean SCUD-based missile with a range of 1000 km and a payload of 1000 kg based on deductions from intelligence photographs of the missile's size and fuel capacity. Like the SCUD-B and SCUD-C, the Nodong 1 is road mobile and transported and launched by a Korean-produced copy of the Russian MAZ 543P transport erector launch vehicle. Using a three-gyroscope inertial guidance package similar to that of the SCUD-B, the Nodong 1 is believed to have a circular error probability of approximately 700 meters.
- g. SS26: A Russian missile that is a follow-on variant to the SCUD-B. It is a short-range, road mobile, single-stage solid propellant missile. It has a single 700 kg high-explosive warhead, a range of 400 km, and circular error probability of approximately 10 m. Additionally, it may contain tactical decoys.
- h. GENR: A notional missile, developed as an analyst tool, with a booster burn time of 100 seconds.
- i. UNK1: Argentinean Condor 1 (acronym is historical accident). The Condor 1 was manufactured in Argentina in the late 1970s. The Condor 1 is a single-stage, solid-fuel sounding rocket with a range of 100 km and a 400 kg warhead. [Ref. 25]

The ballistic phase parameters specify the parameters and frequency of ballistic track sensing. The sensors were ordered by range-to-target and this ordering was recomputed, based on a user-defined value, every 60 seconds. For the entire analysis, the maximum number of available satellites was defined to be three, but at any given time the maximum number of satellites that were used to detect an object was two. Additionally, the notional uncertainty of the time of booster burnout is defined. This value is used in estimating the initial state covariance matrix of the ballistic object.

The output control section specifies the quantities that are computed and reported during program execution. For all events, 80%, 90%, 95%, and 99% track containment bounds were computed at times $t = 50, 100$, and 200 seconds after booster burnout because these three times represent critical points in the timeline of the representative ballistic trajectory. At each of these three times, the containment bounds represent the instantaneous, 50 second predict ahead, and 100 second predict ahead accuracy. Additionally, histogram data and cumulative distribution for the fitted gamma distribution data are outputted to separate files.

B. OUTPUT REPORT

The SBIRS Low model provides the user with up to three separate output files. The most important file is the one that contains the output report. This report is divided into four sections where the first three sections summarize the user-defined inputs. The output report is an ASCII text file and an overview of an output file is discussed in this section. A detailed description of a sample output file is given in Appendix B, section B. The other two files contain histogram data on the track containment level and an empirical gamma cumulative distribution function fit to the histogram data.

The output file is divided into four sections: (1) Run Control Boost Component Summary, (2) Run Control Ballistic Component Summary, (3) Run Control Output Selection Summary, and (4) Run Control Results. The description below corresponds to the output file shown in Appendix B, section B.

The Run Control Boost Component Summary is described below.

In this event, the chosen missile is an M-9 whose booster stage is modeled as a flexible wire. The launch time window is given as 0.00 to 7200.00 seconds, which equates to one day (making positional accuracy independent of launch longitude). With a random launch mode, the actual launch points vary within a region defined by N52.00 to N56.00 and E042.00 to E045.00, which represents a region in Russia east of Moscow. The two closest sensors will build the boost phase track with a revisit time of every 5 seconds.

The Run Control Ballistic Component Summary is described below.

After booster burnout, time is reset to zero. Ballistic tracking data will be used from the three closest sensors, although additional sensors may be within line of sight of the missile. Sensors are numbered from the closest sensor-to-missile distance, to the next closest sensor-to-missile distance, etc. Thus, for sensor 1, the closest sensor, from time zero to 100 seconds, the sensor will revisit the missile every ten seconds. At 100 seconds, the revisit time is changed to every thirty seconds until time equals 300 seconds. From time equals 300 until the missile impacts its target position, the sensor revisits

every fifty seconds. Entries for sensor 2 are exactly analogous to sensor 1 and the entries for sensor 3 are analogous to sensor 1 except the sensor does not begin tracking the missile until fifty seconds after booster burnout. The Sensor Order Viewing Window is the frequency, in seconds, in which the distance from the missile to all sensors in the missile's line of sight is recomputed. Once the order is determined, it remains unchanged until the distances are recomputed.

The Run Control Output Selection Summary is described below.

These parameters generate position predictions at time equals 50 seconds, 150 seconds, and 250 seconds. For each of these times, position predictions, assuming no additional updates, are made for the current position, time equals 50 seconds into the future, and 100 seconds into the future. For the current position, the distance specified is the mean track error distance. By specifying a containment level (percentage), the output computes the distance that contains this given percentage of missiles. Additionally, at each of these three times, a gamma distribution is fit to the empirical track estimation error data.

The Run_Control Results is described below.

The first set of data reports various machine processing times and initial error in initializing the Kepler trajectory. The number of event attempts should always match the number of successful events. One reason for an unsuccessful event is large errors in the boost phase tracking which result in imprecise initialization of the Kepler trajectory. In actual system operation, the track sensor would be unable to locate the post-boost vehicle.

A total of three State/Prediction Statistics are generated for tracking error and the fitted gamma distribution. The Delta X entry represents the mean track error and the estimated standard error of this value. The entries in the columns to the right, for each containment level, are the distance, in units of kilometers, that contain the corresponding percentage of missiles. The statistical values describe the fitted gamma distribution, parameterized as shown in Chapter 4, section D.

If "Insufficient Results" is displayed, the most likely reason is that the missile has impacted the earth prior to the time of the applicable computation. For example, if a missile has a ballistic flight duration of 240 seconds, the model cannot calculate a predicted position for time 250 seconds.

C. ANALYSIS OF CSS-2 MISSILE DATA

The SBIRS Low model was used to conduct an exploratory analysis of system tracking performance of a CSS-2 missile. For each of the seven types of events described in Chapter 4, the simulation provides tracking data at the specified times for the desired predict-ahead times, estimation of parameters for the gamma distribution, a histogram, and an empirical cumulative distribution function. The results are reported in the following three sub-sections. Additionally, in section E, the results are compared to those from the M-9.

In the first sub-section, an analysis of the ballistic track initiation failures is made for the Latitude Shift event where the launch latitude is bounded by N02 and N05. In the second and third sub-sections respectively, an analysis of mean estimation error distances for all Synchronous and Mono Viewing events is made. In all three sections, data is reported for instantaneous positional accuracy at time $t = 50$ seconds (after booster burnout) because by this time, the SBIRS Low system should be transitioning from object discrimination to targeting of the lethal object, a critical point in the missile's timeline.

The results for the remaining events are listed in Appendix C.

1. Ballistic Track Initiation Failure

Figure 9 was generated using the launch latitude randomly selected between the latitudes of N02 and N05.

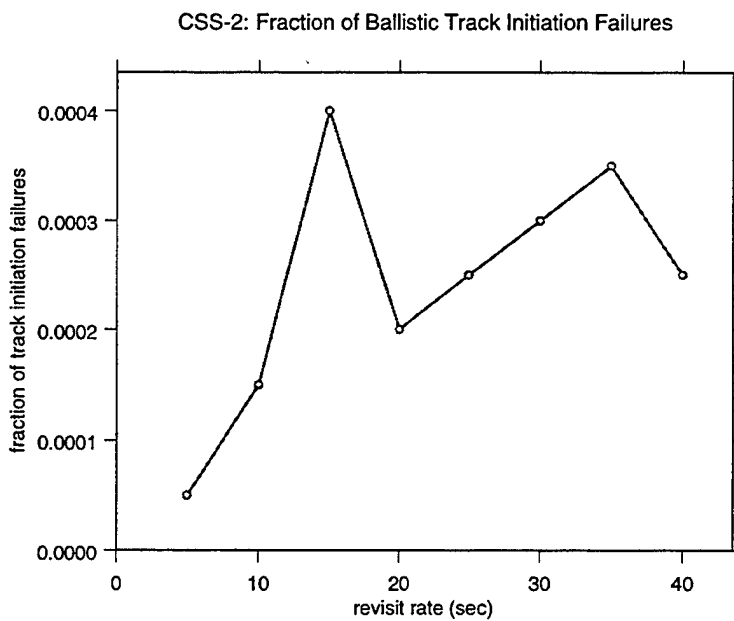


Figure 9. CSS-2: Percentage Ballistic Track Initiation Failure. Line plot of the fraction of ballistic track initiation failures for a CSS-2 missile at eight different ballistic sensor revisit rates.

Figure 9 shows the fraction of ballistic track initiation failure for each of the eight ballistic sensor revisit rates, from 5 to 40 seconds in 5 second increments. In each case, the booster sensor revisit rate was five seconds. The interpretation of Figure 9 is that for the given ballistic sensor revisit scheme, generally described as with no delay after booster burnout is

detected the two closest ballistic sensors use synchronous viewing to track the ballistic object, the fraction of ballistic track initiation failures is "acceptable."

The number of ballistic track initiation failures is independent of the track revisit rate because for each ballistic track revisit rate, sensors 1 and 2 immediately initiate a detection attempt as soon as the booster burnout event is determined to have occurred. The success or failure of the detection attempt by sensors 1 and 2 is a Bernoulli trial. Each trial is independent because of the random launch time, which results in a random phasing of satellites, random launch location, and the success or failure of one event has no bearing on the subsequent event. With the number of failures between one and eight per 20,000 attempts, the model for these counts is taken to be the Poisson distribution.

The probability mass function of the Poisson distribution for a random variable x is given by

$$p(x; \lambda) = \frac{e^{-\lambda} \lambda^x}{x!}, \quad x = 0, 1, 2, \dots$$

for some $\lambda > 0$, where λ is the rate.

Using Bayesian statistics to determine a two-sided 95% credibility interval on λ , the noninformative prior is given by

$$p(\lambda) \propto \lambda^{\frac{1}{2}}.$$

Using this noninformative prior, the posterior distribution of λ is

$$p(\lambda | x) = c \lambda^{n\bar{x} - \frac{1}{2}} \exp(-n\lambda), \quad \lambda > 0$$

where:

$$c = n^{-(n\bar{x} + \frac{1}{2})} [\Gamma(n\bar{x} + \frac{1}{2})]^{-1} \text{ and}$$

$x \equiv$ vector of observations (number of failures).

From the posterior distribution of λ , $n\lambda$ is distributed as $\frac{1}{2}\chi^2$ with $2n\bar{x} + 1$ degrees of freedom. [Ref. 26]

From the data shown in Figure 9, using the maximum likelihood estimation technique with $n = 8$, $\bar{x} = 4.875$ and $\hat{\lambda} = 4.875$. Thus, $2n\hat{\lambda}$ is distributed $\chi^2_{[79]}$ as shown in Figure 10.

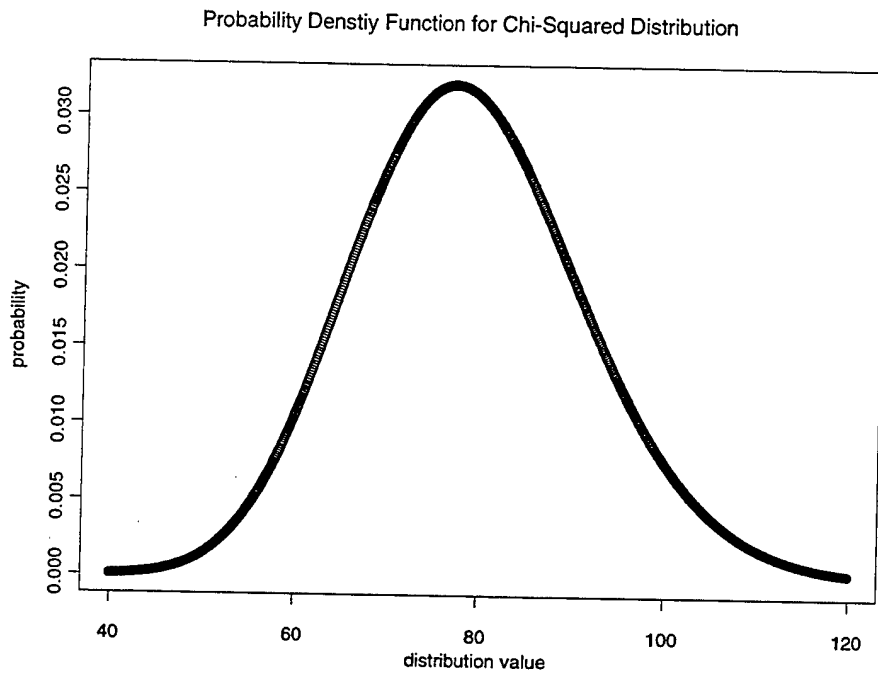


Figure 10. Probability Density Function for Chi-Squared Distribution. Chi-squared distribution of $2n\lambda$ with 79 degrees of freedom.

Given the distribution on $2n\lambda$, the two-sided 95% credible interval for $\hat{\lambda}$ is (3.519, 6.592). A one-sample Kolmogorov-Smirnov goodness of fit test, with the null hypothesis being the true cumulative distribution function is the Poisson distribution with $\lambda = 4.875$ and the alternate hypothesis being the true cumulative distribution function is not the Poisson distribution with $\lambda = 4.875$, resulted in a failure to reject the null hypothesis with a p-value of 0.7461. Although the Poisson distribution is discrete, these counts are extremely rare and it did not seem too inappropriate to use the Kolmogorov-Smirnov goodness of fit test.

The reasons for a ballistic track initiation failure are the satellite phasing and the tangent height of the opaque clouds, which is a maximum at the equator. The rings of the constellation are 40 degrees apart (since the satellites are in polar orbits) and the distance between adjacent rings, due to angular separation, is a maximum at the equator. Combining the increased distance between satellites and constraints on satellites within line-of-sight of the missile, an extremely small percentage of missile launch events are not tracked with sufficient accuracy to initiate a ballistic track.

The existence of coverage gaps near the equator is a known phenomenon and is currently an "accepted" risk based on previous trade-off analyses. Various trade-off analyses considered the cost of increasing the number of satellites in the constellation, implications of placing the satellites in higher orbits, and analysis of the likely implications of an actual missile launch from near the equator.

Because the percentage failure is acceptable for the default booster and variable ballistic track revisit rates, no additional simulation events were conducted at faster booster sensor revisit rates.

2. Synchronous Viewing

At time $t = 50$ seconds, Figure 11 shows synchronous viewing using the closest and second closest sensors.

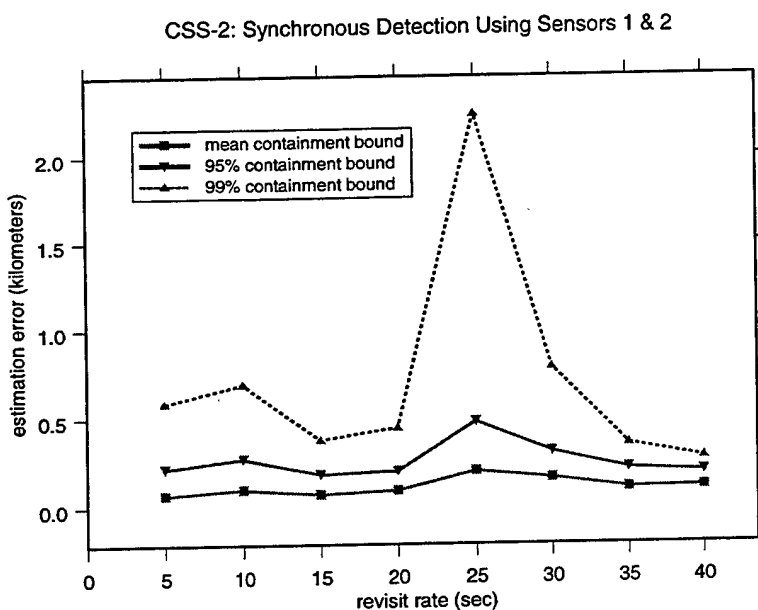


Figure 11. CSS-2: Synchronous Detection Using Sensors 1 and 2. Line plot of the revisit rate versus estimation error for a CSS-2 missile using a stereo symmetric tasking scheme for the closest and next closest satellite.

Figure 11 shows the estimation error for each of the eight ballistic sensor revisit rates, from 5 to 40 seconds, in 5 second increments. The y-axis scale is estimation error, in units of kilometers, and the lower the value, the more accurate the missile is being tracked.

The estimation error for the mean containment bound is nearly constant over the range of revisit rates and is at an "acceptable" accuracy. The large increase in estimation error at a revisit rate of 25 seconds is due to the fact that the simulation computes its tracking statistics prior to making a detection. Thus, given a detection occurs at time $t = 25$ seconds, the track's positional error is extrapolated an additional 25 seconds prior to the computation of tracking statistics. By comparison, given a detection occurs at time $t = 40$ seconds (using a revisit rate of either 10, 20, or 40 seconds), the track's positional error is extrapolated only ten seconds. If statistics are computed at time $t = 50$ seconds, the length of time of the extrapolation is a maximum when the revisit rate is 25 seconds. This behavior, an increase in estimation error as the length of time of the extrapolation increases, is common to all revisit schemes analyzed.

There is only a modest increase in the estimation error when going from the 95% confidence bound to the 99% confidence bound, except at a revisit rate of 25 seconds. The rationale for the large increase at 25 seconds explained in the previous paragraph is germane.

The SBIRS Low model indicated that a gamma distribution may not fit the estimation error data. A detailed statistical analysis was made on the empirical track estimation error for the above sensor tasking strategy with a five second revisit rate.

Generally, the matter was resolved by increasing the number of histogram bins to 400 (to better describe the continuous distribution), the bin data was scaled to represent a proper probability density, and the value for the gamma distribution parameters $\hat{\alpha}$ and $\hat{\beta}$ was derived using the method of moments shown in Chapter 3, section E. The resulting estimates were in acceptable range, $\hat{\alpha} = 0.2951$ and $\hat{\beta} = 0.2195$, but the shape parameter is smaller than one. Such a value is not compatible with the physical interpretation of the problem. Using these values, the chi-squared goodness of fit value was 104.9333 based on five degrees of freedom and the p-value was infinitesimal.

Additionally, the chi-squared goodness of fit statistic for composite hypotheses is specified as

$$\chi^2_{[3]} = \sum_{\text{all cells}} \frac{(\text{observed} - \text{estimated expected})^2}{\text{estimated expected}}.$$

Applying the statistic to all cells with a bin count greater than or equal to five, otherwise cells were grouped, resulted in strongly rejecting the hypothesis that the distribution was gamma with the above values of α and β .

The statistical analysis shifted to using the method of maximum likelihood to estimate the values of α and β because the estimation error did not fit a gamma distribution with the parameter values calculated using the method of moments. Using the Newton-Raphson method in the iterative numerical analysis, $\hat{\alpha} = 1.162$ and $\hat{\beta} = 0.0558$. Although the estimate for α is greater than one, the chi-squared goodness of fit value was 2181.8 and the p-value was infinitesimal. These results are no better than before. Clearly, the distribution of the estimation error data is not gamma.

The histogram plot of the observed data is displayed in Figure 12. Note, because of the y-axis scale, the data appears to be unimodal and plausibly fitted to a gamma distribution.

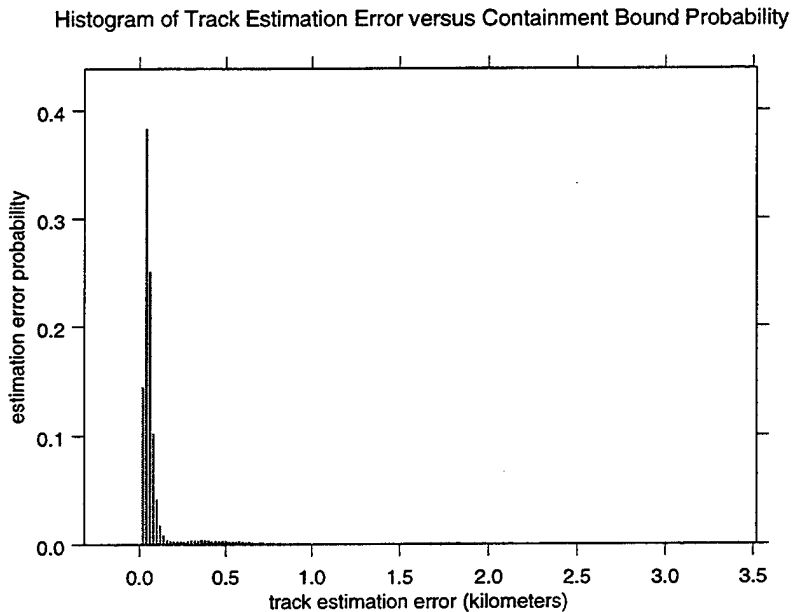


Figure 12. CSS-2: Histogram of Containment Bound. Histogram of track estimation error probability using 400 bins.

Figure 13 shows the same data except the first five bins are not plotted.

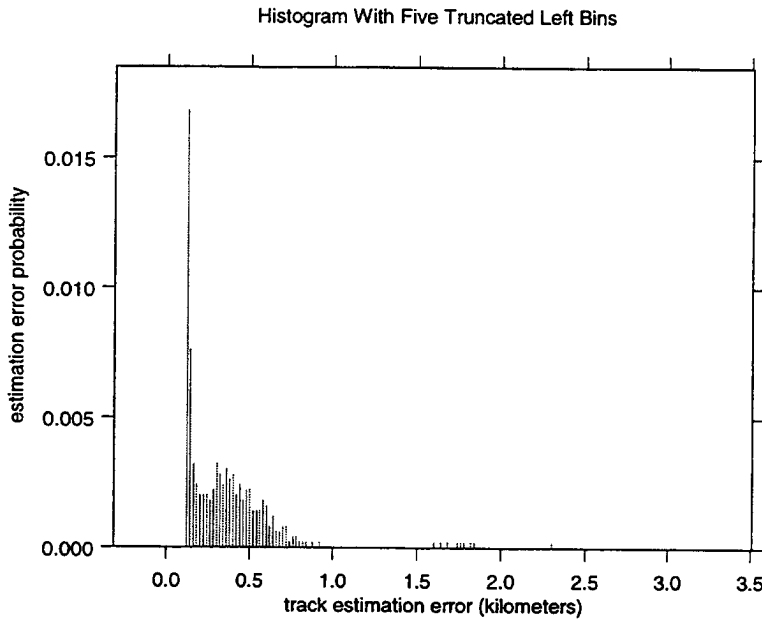


Figure 13. CSS-2: Histogram of Containment Bound, First Five Bins Not Plotted. Histogram of track estimation error probability, with the first five bins not plotted, using 400 bins.

By not plotting the first five bins, the bimodal shape of the track estimation error is readily apparent at approximately 0.3 kilometers where the estimation error percentage increases. The histogram data between 1.6 and 1.8 and at 2.3 kilometers also contributes to a failure to fit the data to a gamma distribution. The reason for the bimodal shape is that a small but significant percentage of events encounter nearly co-linear scissors angle, i.e., the "best" sensors are not necessarily the two closest sensors. This bimodal shape is evaluated to be present in all model events based on the inability of the SBIRS Low model to adequately fit a gamma distribution to each event. The statistical interpretation of the bimodal shape is that it is the superposition of two gamma distributions (each with a different shape parameter), one the result of "acceptable" viewing geometry and the other the result of "unacceptable" viewing geometry.

Contrary to what was anticipated, it was concluded that the observed data couldn't be modeled as a gamma distribution. Additionally, no comparison could be made between the observed data and the chi-squared distribution since the observations could not even be modeled as the more general gamma distribution. Similar analysis resulted in failure to fit the data to the following distributions: exponential, Weibull, lognormal, normal, or Rayleigh. Thus, the emphasis on generating a catalogue of empirical distributions. A variety of tracking geometries are suspected as the cause of this instability.

The 400-bin histogram data were also used to calculate the variance and standard deviation of the 95% and 99% containment bounds. Each of the 20,000 observations at time $t = 50$ seconds (after booster burnout) represent independent identically distributed random variables with common probability density $f(\bullet)$ and cumulative distribution function $F(\bullet)$. Let ξ_p be the unique solution in x of $F(x) = p$ for some $0 < p < 1$. (ξ_p is the p th quantile.) Let p_n be such that np_n is an integer and $n|p_n - p|$ is bounded. Finally, let $Y_{np_n}^{(n)}$ denote the (np_n) th order statistic for a random sample of size n . Then $Y_{np_n}^{(n)}$ is asymptotically distributed as a normal distribution with mean ξ_p and variance given by

$$\text{var} = \frac{p(1-p)}{n[f(\xi_p)]^2}. \quad [\text{Ref. 27}]$$

From the histogram data, at the 99th percentile,

$$f(\xi) = \frac{\text{bin height}}{\text{bin width}} = \frac{0.0018}{0.02} = 0.09.$$

Thus, with $p = 0.01$ and $n = 20,000$,

$$\text{var} = \frac{(0.01)(0.99)}{(20,000)(0.09)^2} = 0.0000611 \text{ and}$$

$$\text{standard deviation} = \sqrt{\text{var}} = \sqrt{0.0000611} = 0.007817 \text{ kilometers.}$$

Similarly for the 95th percentile, the variance is 0.0002375 and the standard deviation is 0.01541 kilometers. The data from all other revisit schemes will yield similar results.

The analysis with 200 histogram bins was objectively worse and the bimodal shape was less noticeable.

Figure 14 shows synchronous viewing using the closest and third closest sensors.

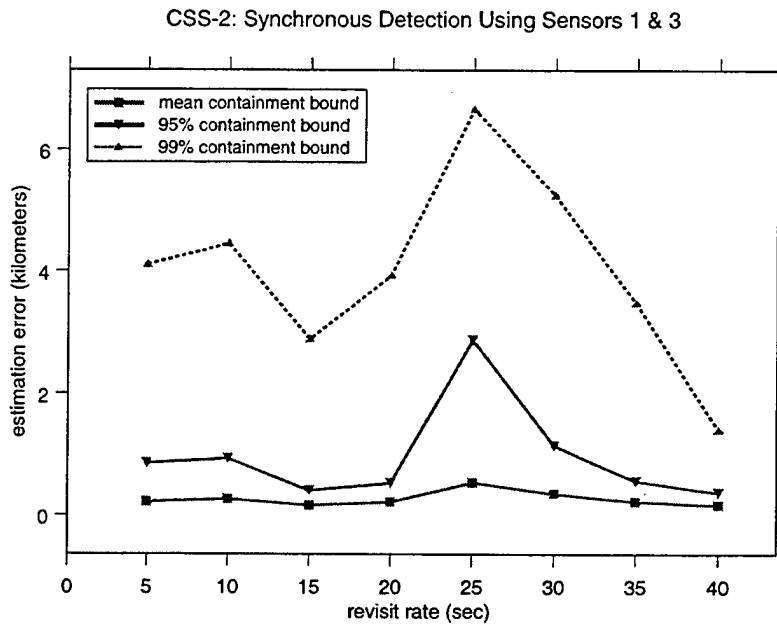


Figure 14. CSS-2: Synchronous Detection Using Sensors 1 and 3. Line plot of the revisit rate versus estimation error for a CSS-2 missile using a stereo symmetric tasking scheme for the closest and third closest satellite.

The estimation error for the mean containment bound is nearly constant over the range of revisit rates and is an "acceptable" accuracy. The large increase in the estimation error at a revisit rate of 25 seconds is due to the fact that the simulation computes its tracking statistics prior to making a detection. The estimation error for the 95% and 99% containment bounds are smaller for a revisit rate of 15 seconds, compared to 10 seconds, because the delay until the statistics are computed (at 50 seconds) is only 5 seconds compared to 10 seconds. There is a large increase in the estimation error when going from the 95% confidence bound to the 99% confidence bound, especially at a revisit rate of 25 seconds. Based on this result, the probability density function may rise quicker than a normal distribution, but the tails are significantly longer. The cause of this increase is most likely associated with the increase in the sensor-to-object distance for sensor 3 compared to sensor 2 since the presence of longer tails is not present in the sensor 1 and 2 tasking scheme.

Figure 15 synchronous viewing using the second and third closest sensors.

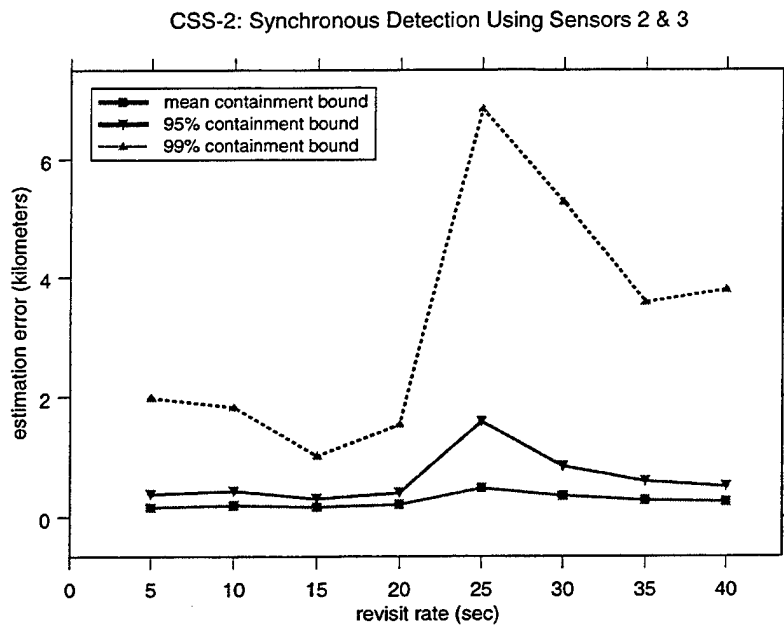


Figure 15. CSS-2: Synchronous Detection Using Sensors 2 and 3. Line plot of the revisit rate versus estimation error for a CSS-2 missile using a stereo symmetric tasking scheme for the second and third closest satellite.

The estimation error for the mean containment bound is nearly constant over the range of revisit rates and is an "acceptable" accuracy. Again, the large increase at a revisit rate of 25 seconds is due to the fact that the simulation computes its tracking statistics prior to making a detection. There is a large increase in the estimation error when going from the 95% containment bound to the 99% containment bound, especially at a revisit rate of 25 seconds. The cause of this increase is most likely associated with the increase in the sensor-to-object distance for sensor 2 compared to sensor 1.

Figure 16 shows the mean containment bound for each of three sensor combinations.

CSS-2: Mean Containment Bound Using Synchronous Viewing

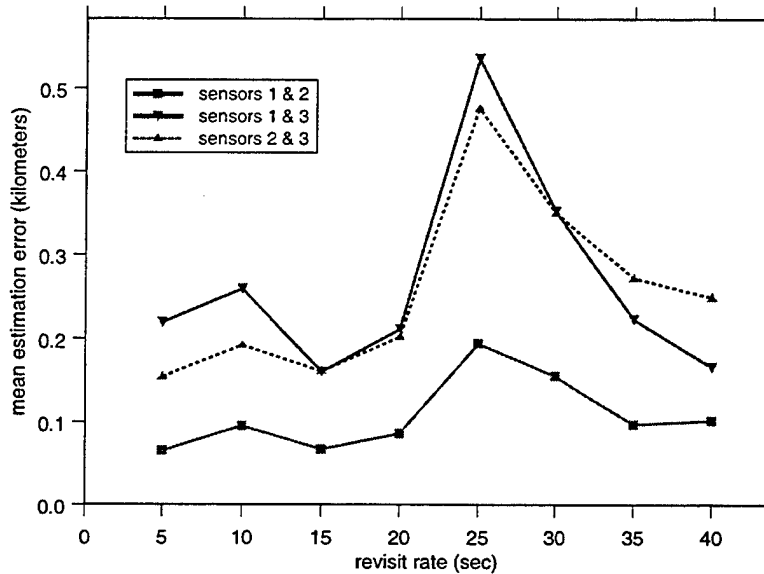


Figure 16. CSS-2: Mean Containment Bounds Using Synchronous Detection. Line plot of the revisit rate versus mean estimation error for a CSS-2 missile comparing the tracking performance of the three synchronous viewing tasking schemes.

From Figure 16, the configuration of sensors 1 and 2 provides the most accurate tracking over the entire range of revisit rates. For revisit times less than 30 seconds, the combination of sensors 2 and 3 provides a smaller mean estimation error than the combination of sensors 1 and 3. This result is counter-intuitive since the effect of azimuth and elevation errors increases with range. Also, the random phasing of the satellite constellation should ensure each sensor combination encounters a representative sample of possible tracking geometries (scissors angle).

The cause of this behavior is due, in part, to the fact that the most likely satellite to be in or adjacent to the orbital plane of the missile is the closest satellite. The angle θ is defined as the angle formed by the vector normal to the plane of the ballistic object's orbit and the line-of-sight of the sensor. Thus,

$$\theta = \hat{l} \bullet \hat{n}$$

where:

\hat{l} \equiv sensor line-of-sight

\hat{n} \equiv normal vector to the plane of the ballistic object's orbit.

Figure 17 is a plot of $\cos(\theta)$ versus detection count for a representative ballistic track revisit scheme (10,000 events) using sensors 1, 2, and 3.

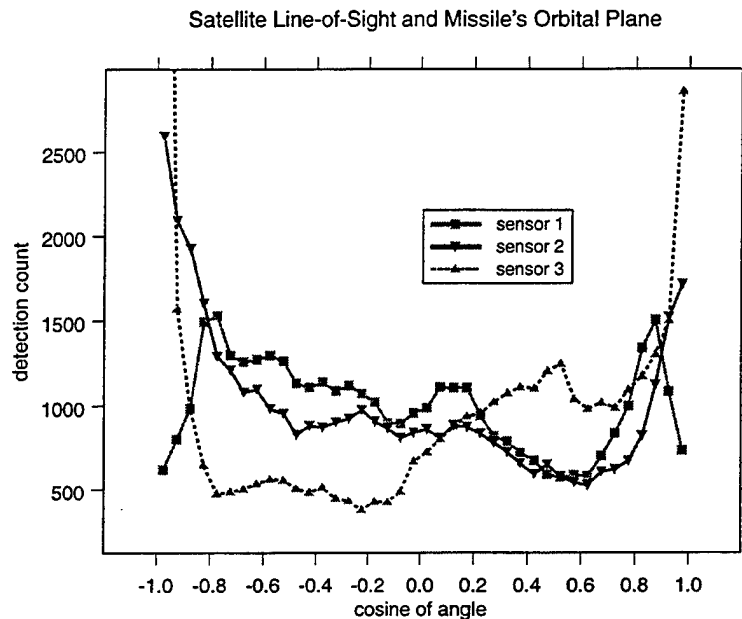


Figure 17. Satellite Line-of-Sight and Missile's Orbital Plane. Plot of $\cos(\theta)$, grouped in bins with width 0.05, versus detection count.

Values in which the absolute value of $\cos(\theta)$ is “small” represents the satellite being nearly in the plane of the ballistic object’s orbit and values in which $\cos(\theta)$ are “large” represent a satellite’s line-of-sight being nearly perpendicular to the plane of the ballistic object’s orbit. The plot shows that sensor 1 has the highest number of occurrences of being in the plane of the ballistic object’s orbit. If a satellite is nearly in the orbital plane of the missile, positional data provided by that satellite is severely degraded. Additional research is necessary to fully quantify this phenomenon and underscores the notion that the definition of the best satellite is nontrivial.

Figure 18 shows the 95% containment bounds for each of the three sensor combinations.

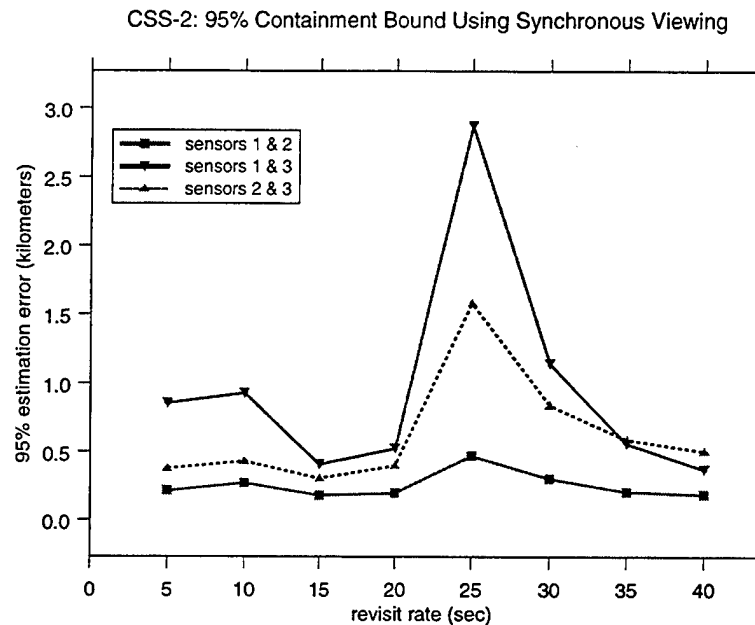


Figure 18. CSS-2: 95% Containment Bounds Using Synchronous Detection. Line plot of the revisit rate versus 95% estimation error for a CSS-2 missile compares the tracking performance of the three synchronous viewing tasking schemes.

For nearly the entire range of revisit rates, the sensor combination of sensors 2 and 3 provides a smaller 95% containment bound than the combination of sensors 1 and 3. The analysis provided for Figure 16 is germane to Figure 18.

Figure 19 shows the 99% containment bounds for each of the three sensor combinations.

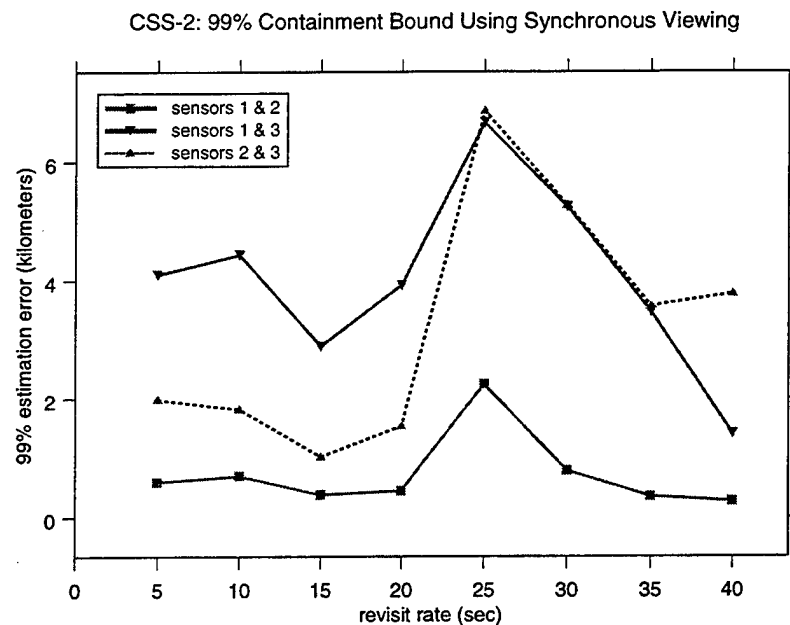


Figure 19. CSS-2: 99% Containment Bounds Using Synchronous Detection Line plot of the revisit rate versus 99% estimation error for a CSS-2 missile compares the tracking performance of the three synchronous viewing tasking schemes.

For nearly the entire range of revisit rates, the sensor combination of sensors 2 and 3 provides a smaller 99% containment bound than the combination of sensors 1 and 3. The analysis provided for Figure 16 is germane to Figure 19.

3. Mono Viewing

At time $t = 50$ seconds, Figure 20 shows mono viewing using the closest sensor.

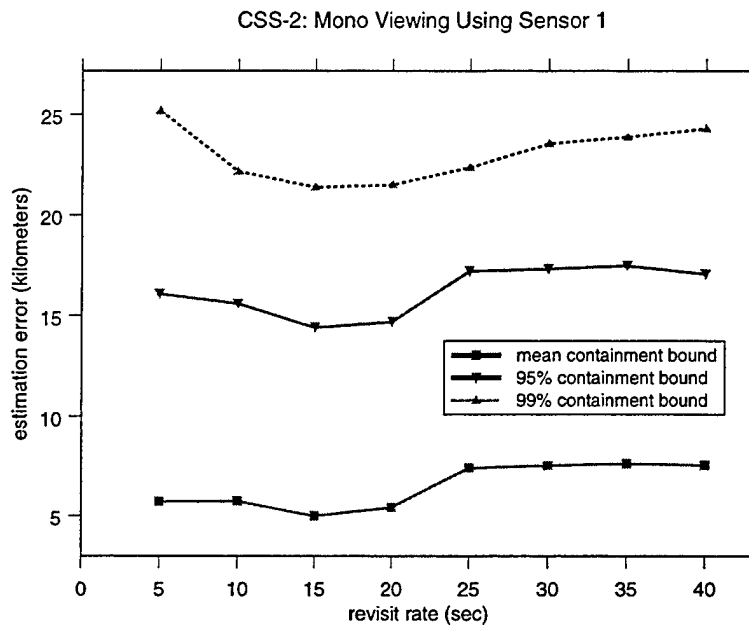


Figure 20. CSS-2: Mono Detection Using Sensor 1. Line plot of the revisit rate versus estimation error for a CSS-2 missile using a mono tasking scheme for the closest satellite.

The estimation error for the mean containment bound is variable over the range of revisit rates and the accuracy is "unacceptable." There is a large percentage increase, approximately 300%, in the estimation error when going from the mean containment bound to a 95% containment bound. The percent increase in going from the mean containment bound to a 99% containment bound is approximately 400%.

Using the procedures described in the previous sub-section, a detailed statistical analysis was made on the mean containment bound data for a five second revisit rate. Again, the observed data does not fit a gamma distribution, based on the chi-squared goodness of fit test and p-value, or the following distributions: exponential, Weibull, lognormal, normal, or Rayleigh. Also, the histogram had a bimodal shape.

Figure 21 shows mono viewing using the second closest sensor.

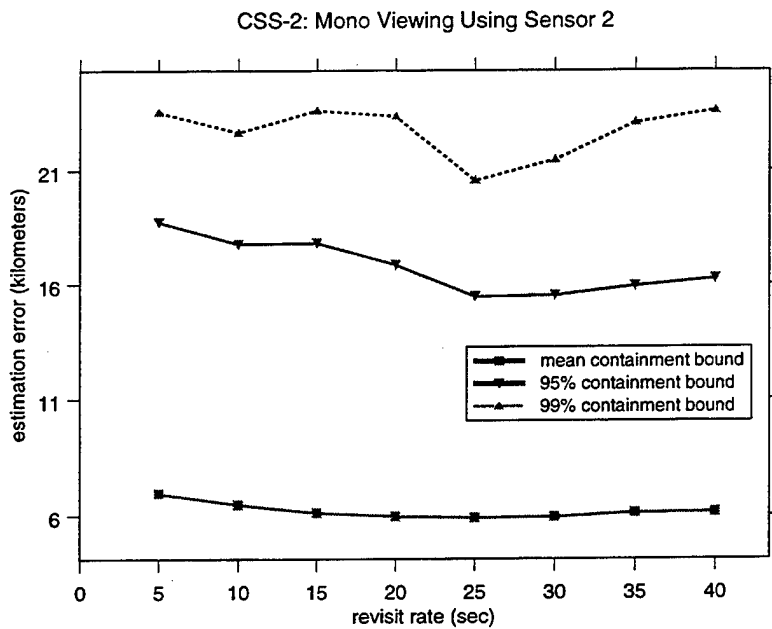


Figure 21. CSS-2: Mono Detection Using Sensor 2. Line plot of the revisit rate versus estimation error for a CSS-2 missile using a mono tasking scheme for the second closest satellite.

The estimation error for the mean containment bound radius is essentially constant over the range of revisit rates and the accuracy is "unacceptable." The percentage increase in the estimation error when going from the mean containment bound to the 95% containment bound and when going to the 99% containment bound is similar to that shown in Figure 20.

Figure 22 shows mono viewing using the third closest sensor.

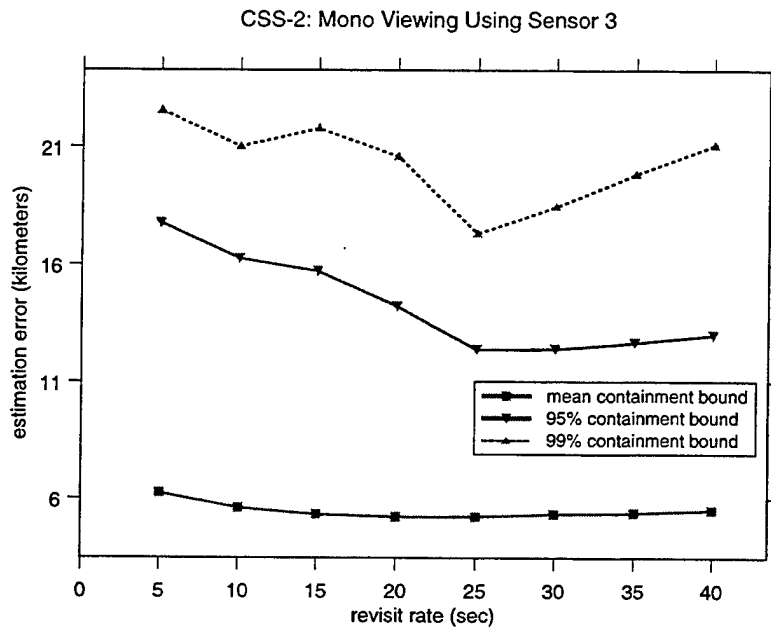


Figure 22. CSS-2: Mono Detection Using Sensor 3. Line plot of the revisit rate versus estimation error for a CSS-2 missile using a mono tasking scheme for the third closest satellite.

The estimation error for the mean containment bound is essentially constant over the range of revisit rates and the accuracy is "unacceptable." The percentage increase in the estimation error when going from the mean containment bound to the 95% containment bound and when going to the 99% containment bound is slightly smaller than that shown in Figure 21.

Figure 23 shows the mean containment bound for each of the three sensor combinations.

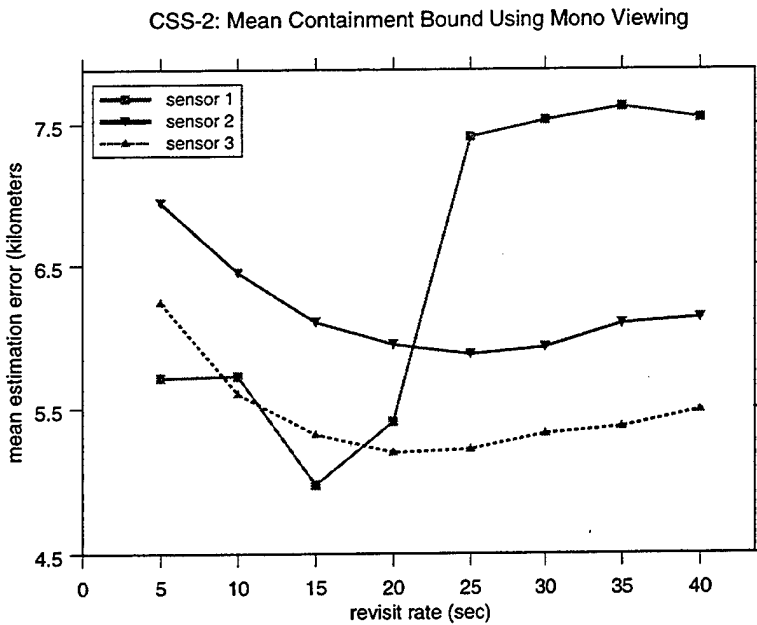


Figure 23. CSS-2: Mean Containment Bounds Using Mono Detection. Line plot of the revisit rate versus mean estimation error for a CSS-2 missile comparing the tracking performance of the three mono viewing tasking schemes.

From Figure 23, tracking accuracy is similarly shaped for sensors 2 and 3. However, the tracking accuracy for sensor 1 varies considerably, and for revisit rates greater than approximately 22 seconds, it provides the worst performance. This result is counter-intuitive since the affect of sensor bias error increases with range. The analysis provided for Figure 16 and shown in Figure 17 is germane.

Figure 24 shows the 95% containment bound for each of the three sensor combinations.

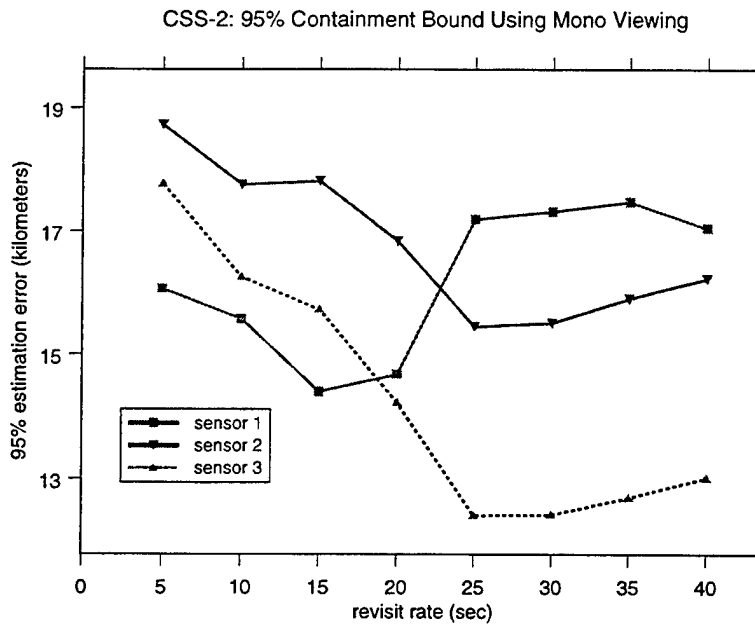


Figure 24. CSS-2: 95% Containment Bounds Using Mono Detection. Line plot of the revisit rate versus 95% estimation error for a CSS-2 missile comparing the tracking performance of the three mono viewing tasking schemes.

From Figure 24, tracking accuracy is similarly shaped for sensors 2 and 3, although sensor 3 provides significantly better performance when the revisit rate is greater than 25 seconds. The tracking accuracy for sensor 1 varies considerably, and for revisit rates greater than approximately 25 seconds, its tracking accuracy provides the worst performance. The rationale explained in the previous paragraph is germane.

Figure 25 shows the 99% containment bound for each of the three sensor combinations.

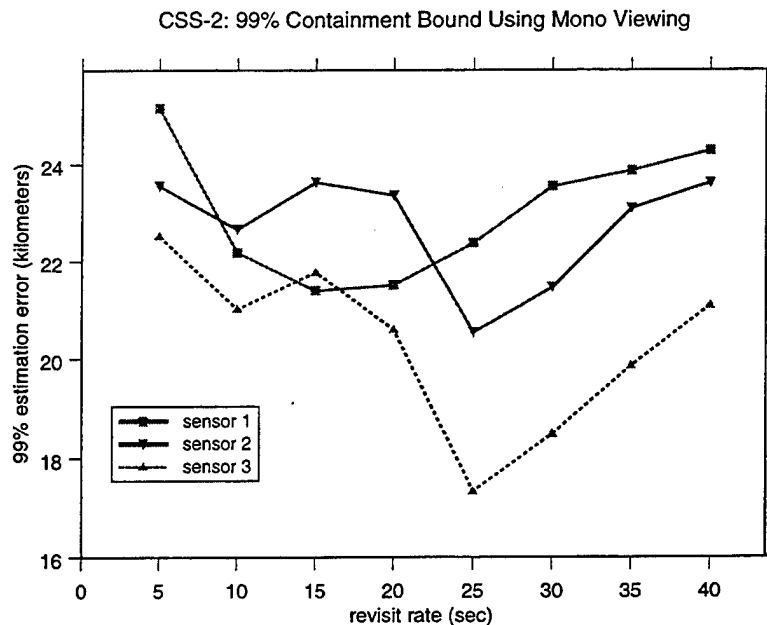


Figure 25. CSS-2: 99% Containment Bounds Using Mono Detection. Line plot of the revisit rate versus 99% estimation error for a CSS-2 missile comparing the tracking performance of the three mono viewing tasking schemes.

From Figure 25, tracking accuracy is similarly shaped for sensors 2 and 3, where sensor 3 provides the best tracking accuracy when the revisit rate is greater than approximately 16 seconds. The tracking accuracy for all sensors varies considerably, and for revisit rates greater than approximately 23 seconds, sensor 1 provides the worst performance. Again, this result is counter-intuitive since the affect of sensor bias error increases with range. The rationale explained for Figure 23 is germane.

D. ANALYSIS OF M-9 MISSILE DATA

The SBIRS Low model was used to conduct an exploratory analysis of system tracking performance of a M-9 missile. For each of the seven types of events described in Chapter 4, the simulation provides tracking data at the specified times for the desired predict-ahead times, estimation of parameters for the gamma distribution, a histogram, and an empirical cumulative distribution function. The results are reported in the following three sub-sections. Additionally, in section E, the results are compared to those from the CSS-2.

In the first sub-section, an analysis of the ballistic track initiation failures is made for the Latitude Shift event where the launch latitude is bounded by N02 and N05. In the second and

third sub-sections respectively, an analysis of mean estimation error distances for all Synchronous and Mono Viewing events is made. In all three sections, data is reported for instantaneous positional accuracy at time $t = 50$ seconds (after booster burnout) because by this time, the SBIRS Low system should be transitioning from object discrimination to targeting of the lethal object, a critical point in the missile's timeline.

The results for the remaining events are listed in Appendix D.

1. Ballistic Track Initiation Failure

With the launch latitude randomly selected between N02 and N05, Figure 26 was generated.

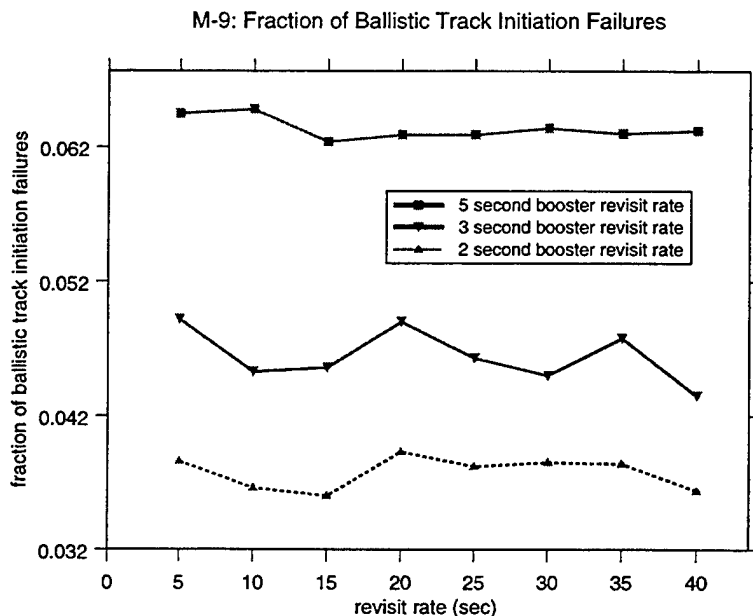


Figure 26. M-9: Percentage Ballistic Track Initiation Failure. Line plots of the fraction of ballistic track initiation failures for a M-9 missile at eight different ballistic sensor revisit rates.

Because of the unacceptably large fraction of ballistic track initiation failures with a booster revisit rate of five seconds, two additional events were run where the revisit rate was increased to every three seconds and then every two seconds. In all three cases, an "unacceptably" large number of ballistic track initiation failures were encountered.

Using the procedures shown in section C, sub-section 1, the data for each of the three booster revisit rates is fit to a Poisson distribution with rate λ . Given a 5 second booster track revisit rate the maximum likelihood estimate for $\hat{\lambda}$ is 1267.25 and the 95% credible interval for

$\hat{\lambda}$ is (1242.76, 1292.19). The Kolmogorov-Smirnov goodness of fit test resulted in failure to reject the null hypothesis with a p-value of 0.3439. The distribution for $2n\hat{\lambda}$ is shown in Figure 27.

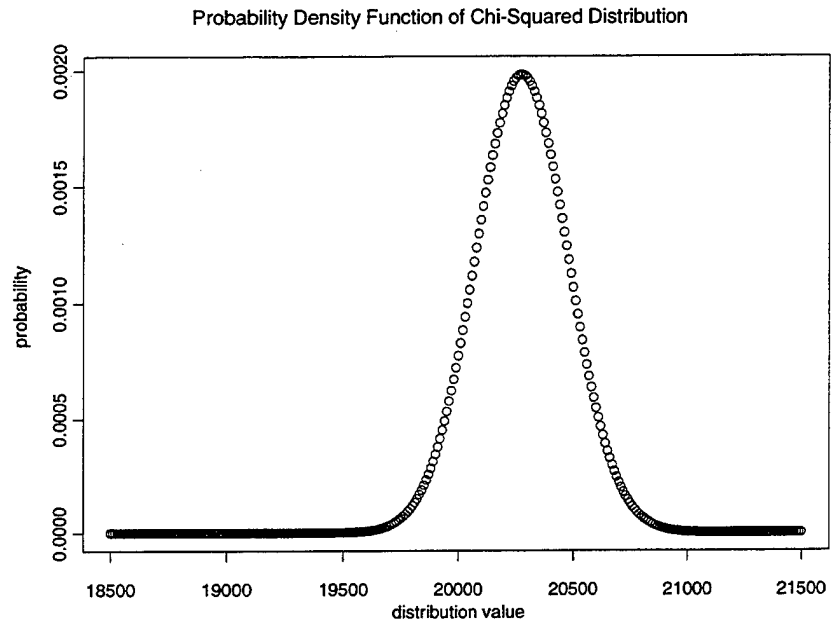


Figure 27. Probability Density Function for Chi-Squared Distribution. Chi-squared distribution of $2n\hat{\lambda}$ with 20277 degrees of freedom.

The maximum likelihood estimates and 95% credible interval for $\hat{\lambda}$ given a 3 second and 2 second booster track revisit rate are 929.25 and (908.31, 950.56) and 755 and (736.14, 774.22), respectively. The corresponding p-values from the Kolmogorov-Smirnov goodness of fit test are 0.4231 and 0.5578. The plots for these distributions are similar to Figure 27.

The reasons for a ballistic track initiation failure are exactly analogous for those described in the case of a CSS-2 missile. The reason for an increased percentage of failures for a M-9 missile, compared to a CSS-2, is differences in dynamic motion throughout the boost phase and at booster burnout.

2. Synchronous Viewing

At time $t = 50$ seconds, Figure 28 shows synchronous viewing using the closest and second closest sensors.

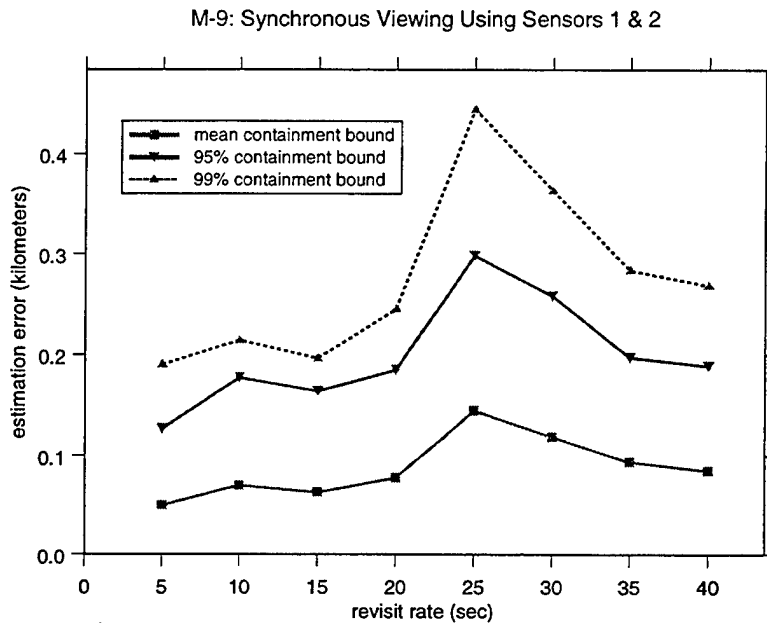


Figure 28. M-9: Synchronous Detection Using Sensors 1 and 2. Line plot of the revisit rate versus estimation error for a M-9 missile using a stereo symmetric tasking scheme for the closest and next closest satellite.

The shape of this plot is similar to the corresponding plot for the CSS-2 missile. However, each estimation error is smaller for the M-9 missile. Although a detailed statistical analysis was not conducted on the M-9 data, based on the similar difficulties encountered by the SBIRS Low model in fitting these observations to a gamma distribution, the observed data cannot be accurately modeled by a gamma distribution. It follows that no comparison could be made between the observed data and the chi-squared distribution since the observations could not even be modeled as the more general gamma distribution.

Figure 29 shows synchronous viewing using the closest and third closest sensors.

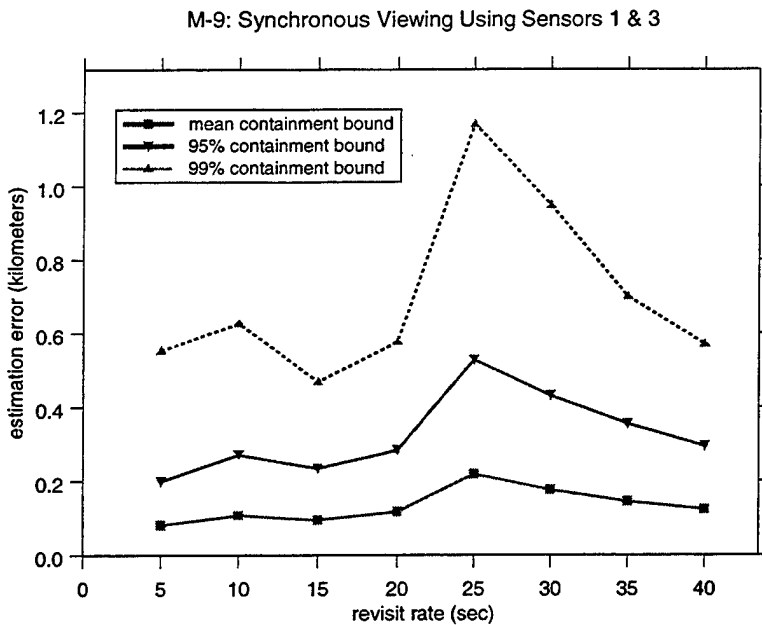


Figure 29. M-9: Synchronous Detection Using Sensors 1 and 3. Line plot of the revisit rate versus estimation error for a M-9 missile using a stereo symmetric tasking scheme for the closest and third closest satellite.

The estimation error for the mean containment bound is approximately constant over the range of revisit rates and is an "acceptable" accuracy. The large increase in the estimation error at a revisit rate of 25 seconds is due to the fact that the simulation computes its tracking statistics prior to making a detection. There is a large increase in the containment radius when going from the 95% containment bound to the 99% containment bound, especially at a revisit rate of 25 seconds. Based on this result, the probability density function may rise quicker than a normal distribution, but the tails are significantly longer. The cause of this increase is most likely associated with the increase in the sensor-to-object distance for sensor 3 compared to sensor 2 since the presence of longer tails is not present in the sensor 1 and 2 tasking scheme.

Figure 30 shows synchronous viewing using the second and third closest sensors.

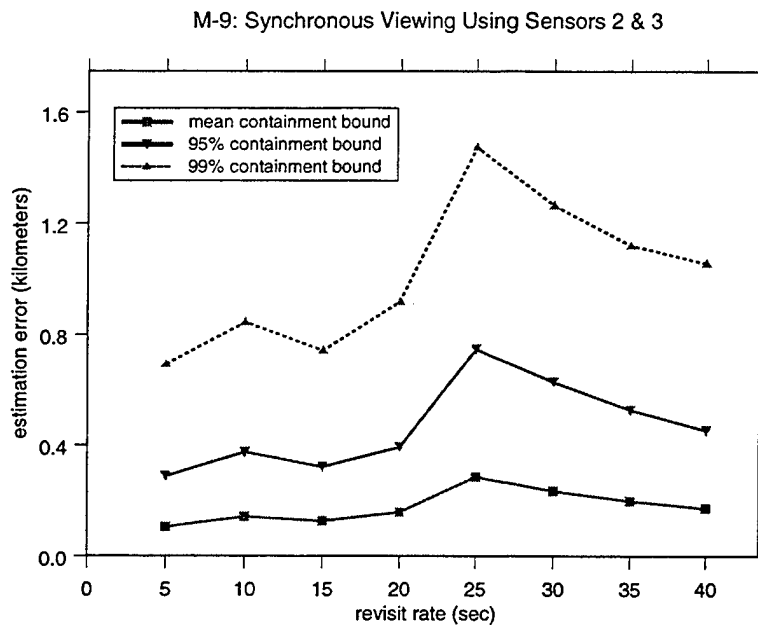


Figure 30. M-9: Synchronous Detection Using Sensors 2 and 3. Line plot of the revisit rate versus estimation error for a M-9 missile using a stereo symmetric tasking scheme for the second and third closest satellite.

The analysis of Figure 30 is similar to that of Figure 29, where the presence of longer tails is most likely associated with the increase in the sensor-to-object distance for sensor 3 compared to sensor 2.

Figure 31 shows the mean containment bound for each of the three sensor combinations.

M-9: Mean Containment Bound Using Syncrounous Viewing

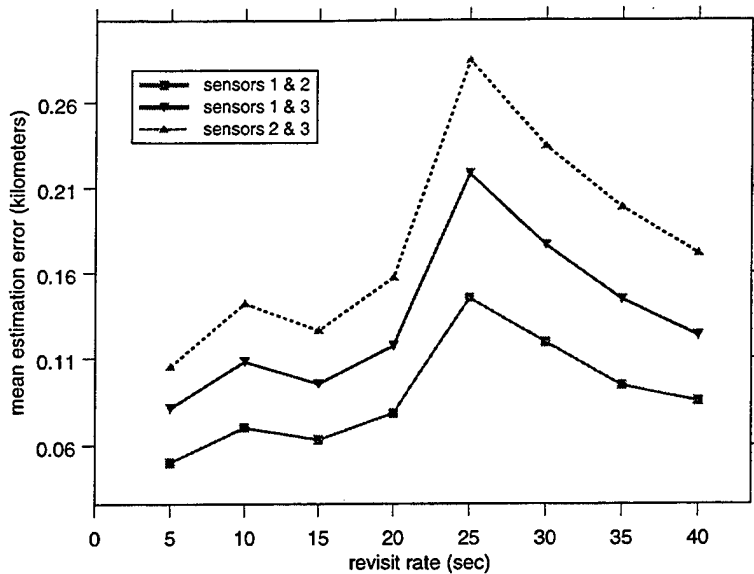


Figure 31. M-9: Mean Containment Bounds Using Synchronous Detection. Line plot of the revisit rate versus mean estimation error for a M-9 missile comparing the tracking performance for the three synchronous viewing tasking schemes.

The shape of the line plots for each of the three satellite tasking schemes is nearly identical. The mean estimation error increases when comparing the combination of sensors 1 and 2 to sensors 1 and 3 and then sensors 1 and 3 to sensors 2 and 3. This result is intuitive since the affect of bias errors increases with range, and the occurrences of a satellite being in the ballistic object's orbital plane does not affect one satellite more than another.

Figure 32 shows the 95% containment bound for each of three sensor combinations.

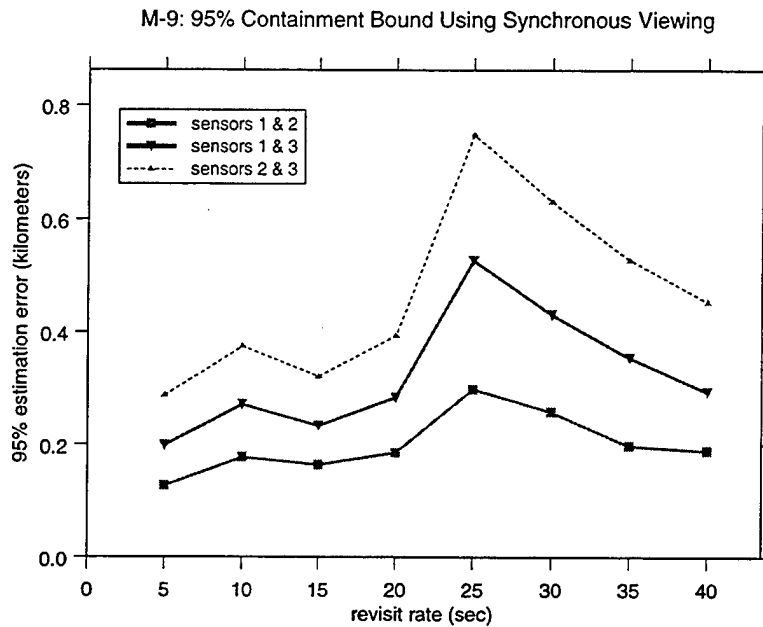


Figure 32. M-9: 95% Containment Bounds Using Synchronous Detection. Line plot of the revisit rate versus 95% estimation error for a M-9 missile comparing the tracking performance of the three synchronous viewing tasking schemes.

Analysis for Figure 32 is similar to that for Figure 31.

Figure 33 shows the 99% containment bound for each of the three sensor combinations.

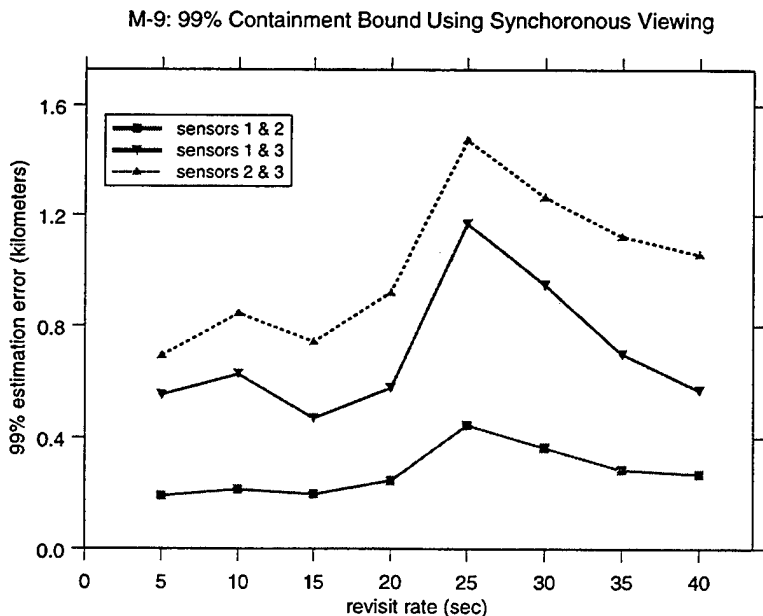


Figure 33. M-9: 99% Containment Bounds Using Synchronous Detection. Line plot of the revisit rate versus 99% estimation error for a M-9 missile comparing the tracking performance of the three synchronous viewing tasking schemes.

Analysis for Figure 33 is similar to that for Figure 31.

3. Mono Viewing

At time $t = 50$ seconds, Figure 34 shows mono viewing using the closest sensor.

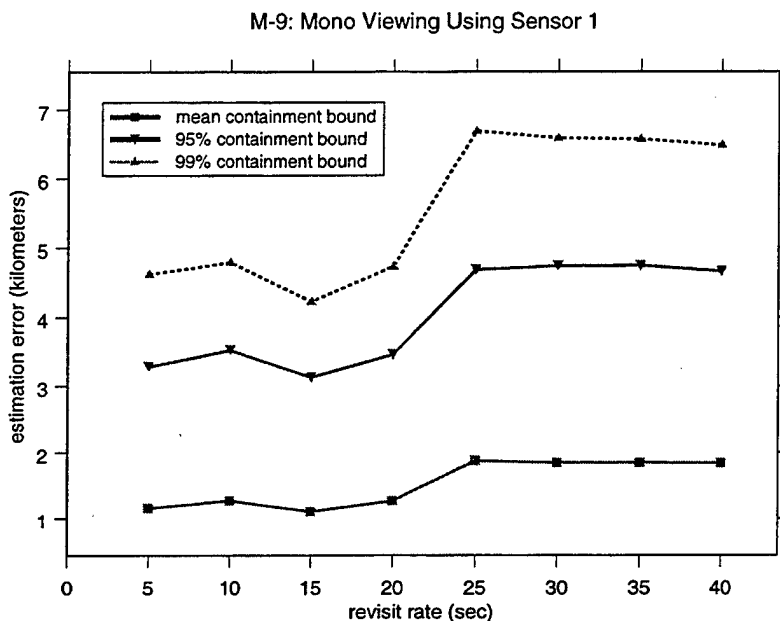


Figure 34. M-9: Mono Detection Using Sensor 1. Line plot of the revisit rate versus estimation error for a M-9 missile using a mono tasking scheme for the closest satellite.

The estimation error for the mean containment bound is approximately constant over the range of revisit rates and the accuracy is "unacceptable." The percentage increase in the estimation error is approximately 300% when comparing the mean containment bound to the 95% containment bound. The similarity in shape of the three containment bounds suggests that the flight dynamics of the M-9 missile does not present tracking difficulties for the SBIRS Low system.

Figure 35 shows mono viewing using the second closest sensor.

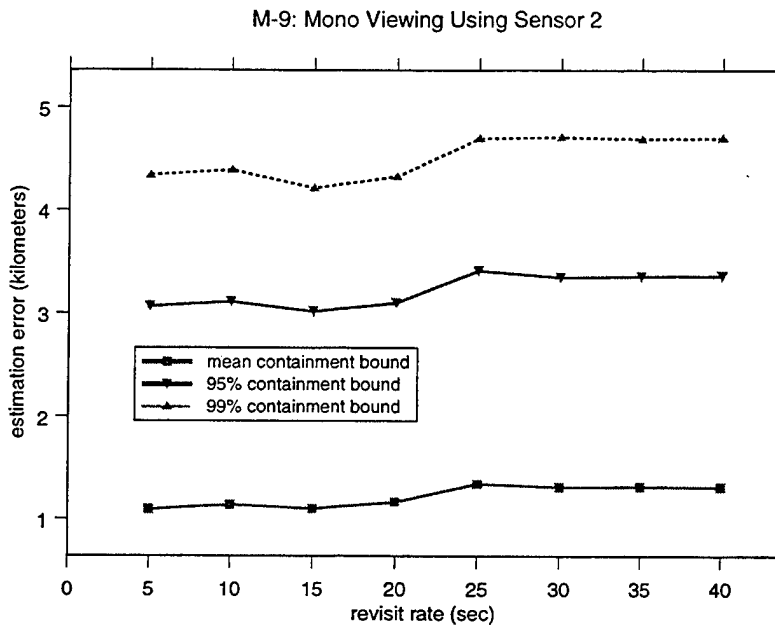


Figure 35. M-9: Mono Detection Using Sensor 2. Line plot of the revisit rate versus estimation error for a M-9 missile using a mono tasking scheme for the second closest satellite.

The estimation error for the mean containment bound is nearly constant over the range of revisit rates and the accuracy is "unacceptable." The analysis of Figure 35 is similar to that for Figure 34.

Figure 36 shows mono viewing using the third closest sensor.

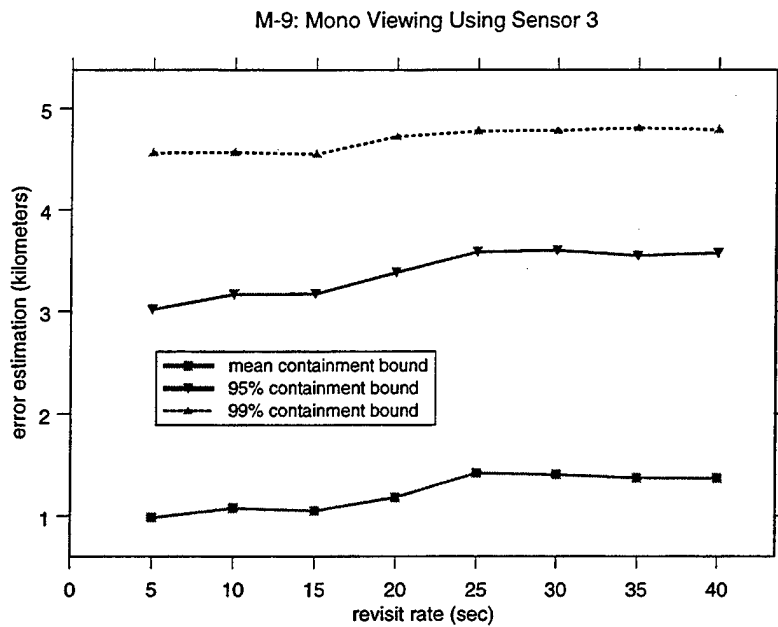


Figure 36. M-9: Mono Detection Using Sensor 3. Line plot of the revisit rate versus estimation error for a M-9 missile using a mono tasking scheme for the third closest satellite.

Analysis of Figure 36 is similar to that for Figure 34.

Figure 37 shows the mean containment bound for each of the three sensor combinations.

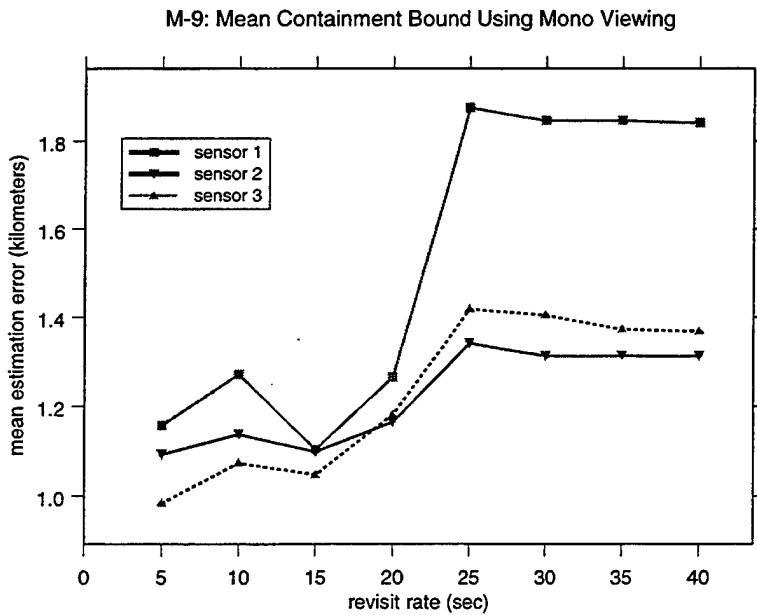


Figure 37. M-9: Mean Containment Bounds Using Mono Detection. Line plot of the revisit rate versus mean estimation error for a M-9 missile comparing the tracking performance of the three mono viewing tasking schemes.

From Figure 37, tracking accuracy plots are similarly shaped for sensors 2 and 3. However, the tracking accuracy for sensor 1 varies considerably, and over the entire range of revisit rates its tracking accuracy provides the worst performance. This result is counter-intuitive since the affect of sensor bias error increases with range. The analysis provided for Figure 17 is germane.

Figure 38 shows the 95% containment bound for each of the three sensor combinations.

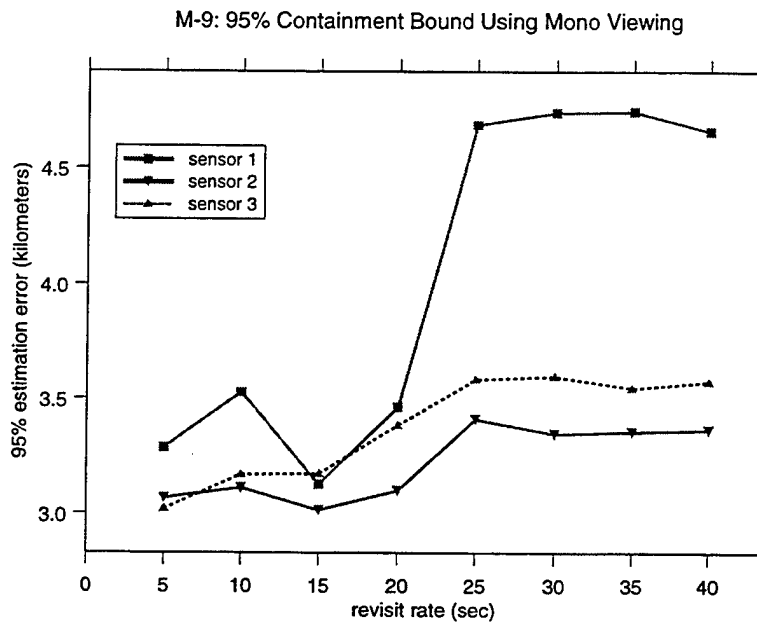


Figure 38. M-9: 95% Containment Bounds Using Mono Detection. Line plot of the revisit rate versus 95% estimation error for a M-9 missile comparing the tracking performance of the three mono viewing tasking schemes.

Analysis of Figure 38 is similar to that for Figure 37.

Figure 39 shows the 99% containment bound for each of the three sensor combinations.

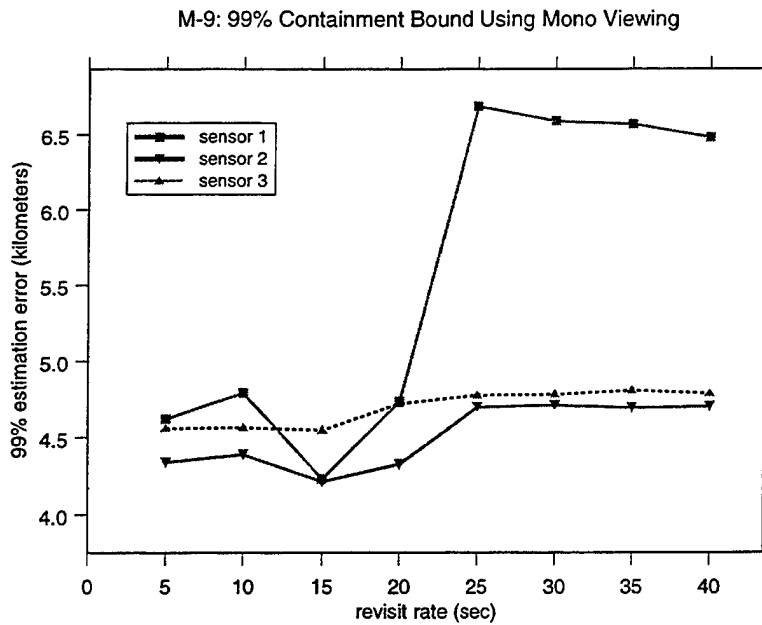


Figure 39. M-9: 99% Containment Bounds Using Mono Detection Line plot of the revisit rate versus 99% estimation error for a M-9 missile comparing the tracking performance of the three mono viewing tasking schemes.

Analysis of Figure 39 is similar to that for Figure 37.

E. COMPARISON OF CSS-2 AND M-9 MISSILE DATA

This section is organized by showing the mean containment bounds for the CSS-2 and M-9 using synchronous viewing and then mono viewing. Then, the 95% containment bounds are shown followed by the 99% containment bounds. From these figures, two significant results are: (1) mono viewing does not provide an "acceptable" level of tracking accuracy for all revisit rates for both missiles, and (2) the SBIRS Low system tracks the M-9 missile with greater accuracy than the CSS-2.

Figure 40 is plotted using the data shown in Figures 16 and 31.

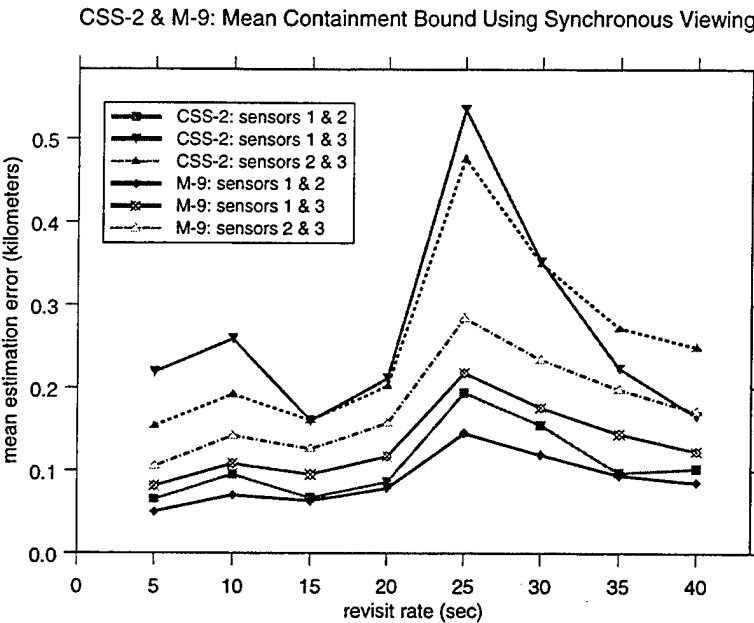


Figure 40. CSS-2 & M-9: Mean Containment Bounds Using Synchronous Detection. Line plot of the revisit rate versus mean estimation error comparing the tracking performance of the three synchronous viewing tasking schemes for the two types of missiles.

Over the entire range of revisit rates, the M-9 tracking accuracy was better than the CSS-2 tracking accuracy for corresponding sensor combinations. All configurations exhibited an increase in containment radius at a revisit rate of 25 seconds. Again, this increase is a result of the SBIRS Low model computing statistics prior to scheduling a detection, which results in the tracking data "aging" the longest for the eight tested revisit rates. The tracking accuracy is shown to improve as the revisit rate increases since the "aging" time is decreasing.

Figure 41 is plotted using the data shown in Figures 23 and 37.

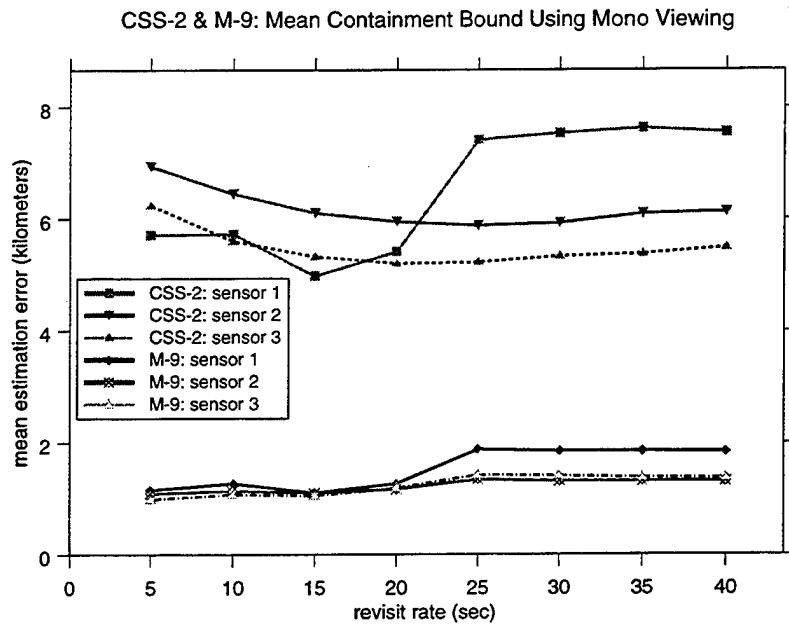


Figure 41. CSS-2 & M-9: Mean Containment Bounds Using Mono Detection. Line plot of the revisit rate versus mean estimation error comparing the tracking performance of the three mono viewing tasking schemes for the two types of missiles.

Again, the M-9 tracking accuracy is significantly better than that of the CSS-2. Additionally, in each case, sensor 1 provides the worst tracking accuracy for revisit rates greater than approximately 20 seconds.

Comparing the mono viewing shown in Figure 39 to the synchronous viewing shown in Figure 38, the mean estimation error increased by a factor of ten in the case of the M-9 and a factor of thirty in the case of the CSS-2.

Figure 42 is plotted using the data shown in Figures 18 and 32.

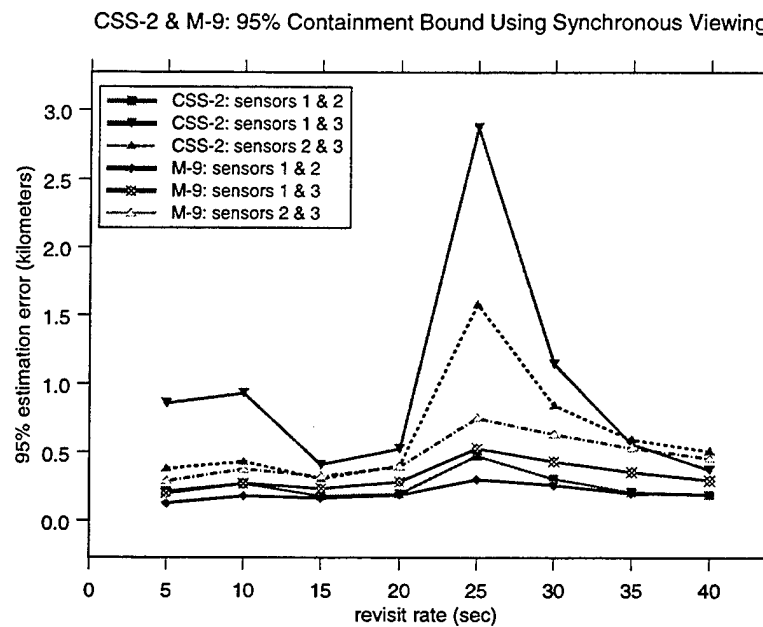


Figure 42. CSS-2 & M-9: 95% Containment Bounds Using Synchronous Detection. Line plot of the revisit rate versus 95% estimation error comparing the tracking performance of the three synchronous viewing tasking schemes for the two types of missiles.

Analysis of Figure 42 is similar to that of Figure 40.

Figure 43 is plotted using the data shown in Figures 24 and 38.

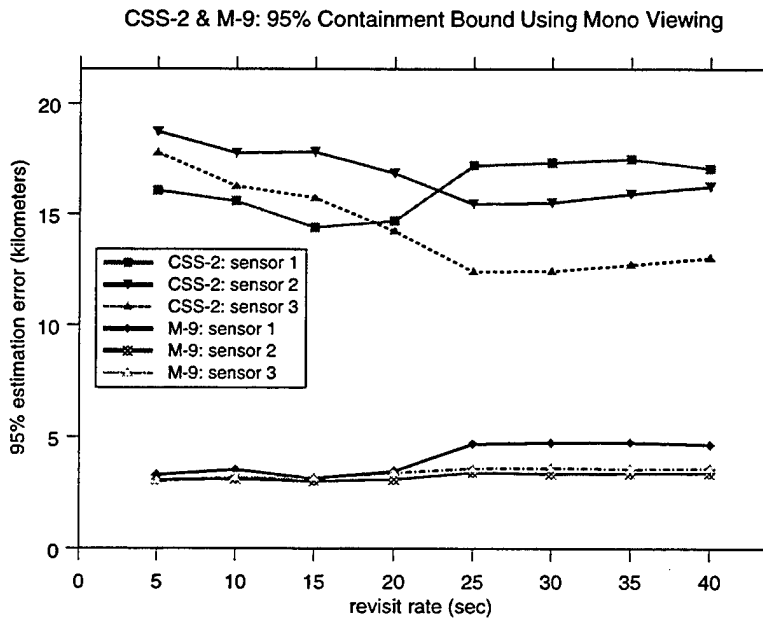


Figure 43. CSS-2 & M-9: 95% Containment Bounds Using Mono Detection. Line plot of the revisit rate versus 95% estimation error comparing the tracking performance of the three mono viewing tasking schemes for the two types of missiles.

Analysis of Figure 43 is similar to that of Figure 39.

Figure 44 is plotted using the data shown in Figures 19 and 33.

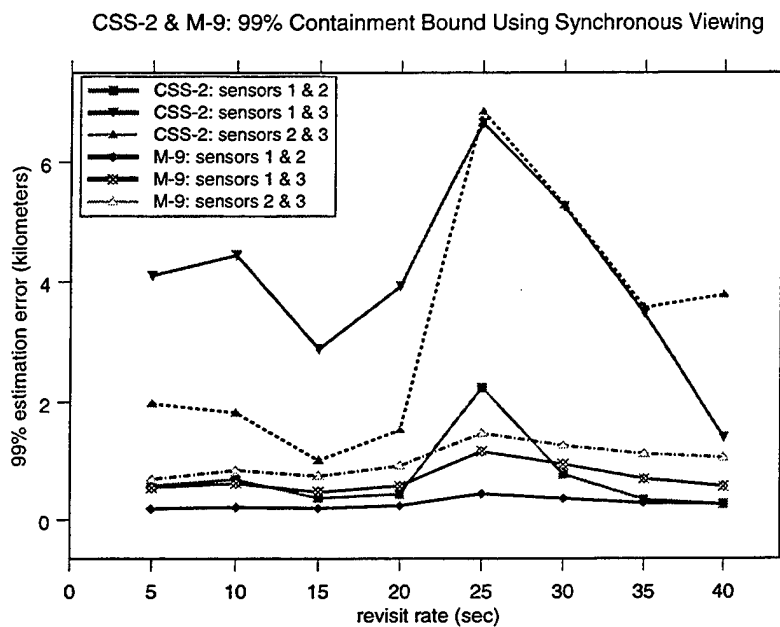


Figure 44. CSS-2 & M-9: 99% Containment Bounds Using Synchronous Detection. Line plot of the revisit rate versus 99% estimation error comparing the tracking performance of the three synchronous viewing tasking schemes for the two types of missiles.

Analysis of Figure 44 is similar to that of Figure 40.

Figure 45 is plotted using the data shown in Figures 25 and 39.

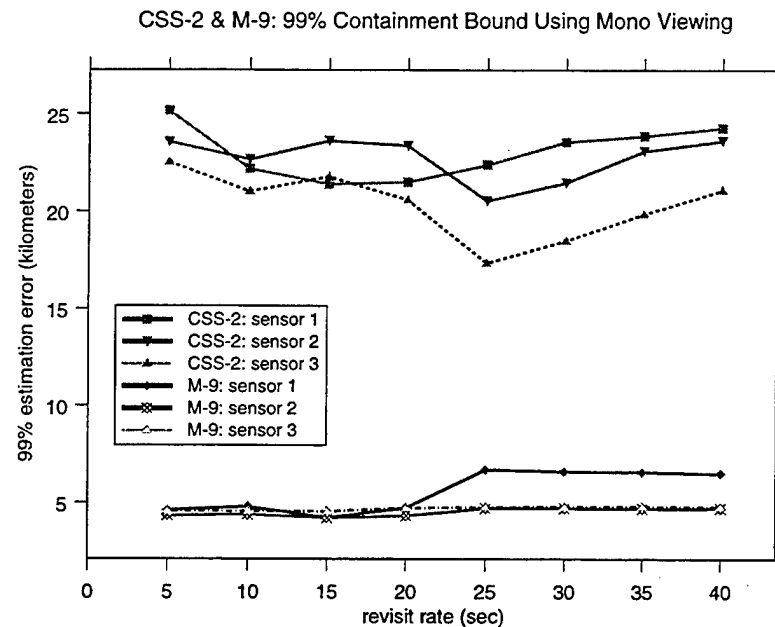


Figure 45. CSS-2 & M-9: 99% Containment Bounds Using Mono Detection. Line plot of the revisit rate versus 99% estimation error comparing the tracking performance of the three mono viewing tasking schemes for the two types of missiles.

Analysis of Figure 45 is similar to that of Figure 41.

THIS PAGE INTENTIONALLY LEFT BLANK

delay. In certain instances, track accuracy is an artifact of computing statistics first then performing missile detection. This result is most apparent with a revisit rate of 25 seconds. The large increase in estimation error occurs because, given a detection at time $t = 25$ seconds (after booster burnout), the track "ages" an additional 25 seconds prior to the computation of tracking statistics. This revisit rate has the longest time between detections when computing statistics at 50 seconds after booster burnout. By comparison, given a 40 second revisit rate with a detection at time $t = 40$ seconds, the track "ages" only ten seconds prior to the computation of tracking statistics.

Mono viewing alone does not provide the required tracking accuracy even in the single target tactical scenario. The mean containment bound for the CSS-2 and M-9 varied between 4.75 and 7.75 kilometers and 1.0 and 6.5 kilometers, respectively. Since the SBIRS Low system, in general, will be unable to classify a threat missile, the most conservative course of action in judging system performance is to assume the larger uncertainty. This mean containment bound is "unacceptable" for achieving critical requirements such as object resolution, object discrimination, and intercept support. However, mono viewing is acceptable for tasking schemes that incorporate stereo detections.

The SBIRS Low model has shown tracking accuracy is a function of missile classification. There is a large increase in positional uncertainty when going from a 95% to 99% containment radius for the CSS-2 missile, compared to the M-9 missile when using the tasking scheme of synchronous detections by sensors 1 and 3 and sensors 2 and 3. Thus, although a probability distribution was not fit to the data, it can be inferred that the probability density function must rise faster than a normal distribution but have significantly longer tails. Since the CSS-2 has a larger change in velocity at booster burnout (compared to the M-9), which affects the accuracy of the initialization of the Kepler orbit tracking algorithm,

Tracking accuracy is a function of track-to-sensor range. In certain synchronous revisit schemes for detecting a CSS-2 missile, sensors 2 and 3, the second-closest and third-closest sensors, provided better tracking accuracy compared to sensors 1 and 3, the closest and second-closest sensors. For example, see Figure 17, which shows the 99% containment bounds for each of the three sensor combinations used for synchronous viewing. However, it is not intuitive that tracking accuracy would improve as the track-to-sensor range increases because the affect of the sensor bias error increases with range. This decrease in tracking accuracy for the closest satellite

VI. CONCLUSION

The relatively large number of unknowns and absence of a "correct" answer with which to compare the model's output to makes validation of the SBIRS Low model impossible. However, as with any computer model, if the output is at least plausibly correct, insight into the applicable questions regarding performance of the system being analyzed is possible. When the output is not intuitively correct, analysis of the model itself must be made, or it may reveal hidden, important factors not anticipated by the analyst. From the 13,760,000 missiles tracked during the exploratory analysis, the SBIRS Low model output revealed both intuitively correct answers and unanticipated, but apparently correct results.

The results are listed in order of significance to actual system operation followed by a discussion on the importance of providing a benchmark/reference book of track accuracies for various sensor revisit schemes. The final paragraph discusses using the results of this exploratory model analysis in follow-on research projects.

The global scheduler must predict the result of each task prior to scheduling it. Figure 17 shows one aspect of the nontrivial difficulties associated with defining the best sensor. The closest sensor, in general, will have the highest signal-to-noise ratio but could provide the worst track positional data because it is in the object's orbital plane. Also, using the closest and second closest sensor to update a track may provide little reduction in positional uncertainty if their viewing geometry results in an extremely small scissors angle. Additionally, in a high-tasking scenario, the slew-settle-stare time for any given satellite may constrain feasible tasking schemes.

For the M-9 missile, where the launch point was randomly selected between N02 and N05, an unacceptably large number of events resulted in a failure to initiate a ballistic track. Thus, the SBIRS Low system had no capability to target the missile. Systematically increasing the revisit rate during the booster phase from every 5 seconds to every 3 seconds then to every 2 seconds did reduce the number of track failures, but not to an acceptable number. Events run with a CSS-2 missile and a booster phase revisit rate of 5 seconds between the above latitudes also resulted in ballistic track initiation failures, but the number of failures was acceptable.

If the system can anticipate an occurrence of a long period of time between observations on a given track, a stereo detection should be scheduled immediately prior to the start of the

is due to the fact that if a sensor is in the orbital plane of the missile, it is most likely to be the closest satellite.

The instantaneous track accuracy, for both synchronous and mono viewing for the CSS-2 and M-9 missiles, did not fit a gamma distribution. It was predicted that the ratio of the sum of the absolute value of the three-dimensional positional uncertainty and variance would be a gamma distribution. The SBIRS Low model attempted to fit the histogram of the mean containment bound to a gamma distribution and reported the estimated parameters in the output report. By fitting the gamma distribution, anticipated values for the mean and variance of instantaneous track accuracy could be compared to observed data. The reason the data did not fit a gamma distribution is that the individual gamma distributions in x, y, and z position errors have different scale parameters and hence are not closed under addition. Also, the probabilities for each gamma are not independent. Therefore, the convolution of the three distributions no longer resembles a chi-squared distribution or even a gamma distribution. Additional statistical analysis of the data revealed that the data could not be fit to the following distributions: exponential, Weibull, lognormal, normal, or Rayleigh.

The specific insights gained by the exploratory data analysis of the SBIRS Low model were only one goal of the project. Perhaps a more important goal was to provide a benchmark/reference book of track accuracies for various sensor revisit schemes. This reference book is contained in Appendices C and D and balances the requirements of running enough model events to detect significant trends with an acceptable incremental increase in the sensor revisit rate. The Monte Carlo methodology was computationally efficient and provided the desired level of accuracy. The necessary level of model fidelity was present for each component in the SBIRS Low system and underlying orbital mechanics. Because of these features, multiple acceptable revisit schemes were identified and provide a first step in solving the global scheduler problem.

The insight gained from this exploratory model analysis and development of data contained in Appendices C and D can be used in follow-on analysis. The fact that the data could not be fit to any well-known probability distribution is perhaps the most important topic for additional research. If the data is determined to be from a probability distribution, tracking accuracy and containment probability could be easily computed at any time for the launch scenario. Another topic requiring additional research is the minimization of the slew-settle-stare problem, which could be modeled as a traveling salesman problem, given certain viewing

geometry constraints. Utility theory and decision-making analysis could be used to assign a sensor to a track in an overload condition. Also, linear and/or non-linear programming could be used to analyze interceptor salvo doctrines. Finally, a discrete event simulation could be written to test end-to-end SBIRS Low system operation, from enemy missile launch to interceptor impact.

APPENDIX A: MONTE CARLO METHODOLOGY

When a model is not a high-resolution surrogate of the actual system, the meaning of its outputs must be provided by a larger context. Typically, this context must be an analytic strategy that justifies its use. The analytic strategy of Monte Carlo methods, that branch of experimental mathematics which is concerned with experiments on random numbers, is used in the SBIRS Low model. The idea behind the Monte Carlo approach is to replace theory by experiment whenever the former falters. [Ref. 28] For example the bias values assigned to all sensors are random numbers that amount to a random sample from the population of all possible error values. The conclusions from the simulation are valid if the random sample is representative of all observations which might have been made.

Despite the fact that the result is not absolutely certain, uncertainty can be managed to a point where it is negligible for all practical purposes. Additionally, Monte Carlo methods are one technique capable of providing a high degree of accuracy (covariance analysis, if it can be done, can generally provide accurate answers for probabilities between about 10% and 90%) necessary to assess capabilities on the tails of a distribution. [Ref. 29] The accuracy can be made arbitrarily small by taking a sufficiently large number of samples or at least suggest a distribution that can be used to analytically solve the problem.

The Monte Carlo approach provides a method of solving probability theory problems in situations where system performance is based upon the behavior and outcome of random processes. In the case of a probabilistic problem the simplest Monte Carlo approach is to observe random numbers, chosen in such a way that they directly simulate the physical random processes of the original problem, and to infer the desired solution from the behavior of these random numbers. In the case of the SBIRS Low model, tracking accuracy is the outcome of the random processes of satellite phasing, individual errors that affect the accuracy of a sensor's line of sight measurements, and missile launch location (only if the random launch mode is chosen).

There are various reasons for using Monte Carlo methods and the main one is based upon the inferential nature of Monte Carlo techniques. The Monte Carlo method in the SBIRS Low model is concerned with estimating the unknown numerical value of the positional uncertainty of a threat missile given some sensor revisit scheme, a quantity difficult to determine analytically. Thus, the positional uncertainty parameter is called an estimand. The available data, tracking accuracy at specified times in a missile's trajectory, will consist of a number of observed random

variables, constituting the sample. The number of observations in the sample is the sample size. The connection between the sample and the estimand is that the latter is a parameter of the probability distribution of the random variables constituting the former. For the SBIRS Low model, the predicted probability distribution of positional uncertainty is the generalized gamma.

Another feature of Monte Carlo calculations is that, if the calculations are repeated, then slightly different answers are given each time (provided that a different place in the random number sequence is used on each occasion). Thus, the Monte Carlo calculations simulate real life situations, where the repetition of a particular experiment of limited experimental accuracy or of finite statistics is liable to produce a somewhat different result from the previous measurement.

A procedural problem that arises in virtually every Monte Carlo simulation is present in the SBIRS Low model. The problem concerns the number of replications that must be performed in order to guarantee a specified bound on error. This number, called the sample size, depends on the tolerable error specification of the problem under study. There is no specified "real world" precision of the SBIRS Low system, however, it is computationally feasible to reduce the uncertainty of the Monte Carlo calculations to the order of five meters.

The Law of Large Numbers states that, as the sample size n increases, the error of approximation in estimating the mean, μ , by $\frac{X_1 + X_2 + \dots + X_n}{n}$, where X_i is a sequence of independent random variables have a common distribution, becomes vanishingly small. [Ref. 30] Additionally, in principle, the Central Limit Theorem provides a way of assessing the extent of that statistical error for large n . In practice, however, the Monte Carlo method relies on techniques that contradict both of these statistical laws. Since all numerical-valued samples generated in a Monte Carlo experiment arise from transforming numbers that a pseudorandom number generator produces, and since sequences of these numbers repeat themselves after a finite number of steps P , sampling without limit in a Monte Carlo experiment does not make statistical error vanish. Based on current implementation and foreseeable modifications, the random number generator in the SBIRS Low model essentially eliminates this consequence because, by design, its value of P is significantly greater than 1,000,000.

Improving computational efficiency is a prevalent theme in Monte Carlo methods because in general, there is a square law relationship between the error in an answer and the requisite number of observations. The estimated standard error is given by

$$\frac{\sigma}{\sqrt{n}}$$

where:

σ \equiv standard deviation

n \equiv sample size.

Hence, to reduce the error by a factor of ten requires a hundredfold increase in the number of observations. The sampling plan that induces the smallest variance per replication leads to the smallest sample size required to achieve a specified absolute error criterion. Thus, it is often beneficial to develop sampling plans that reduce variance to improve efficiency in Monte Carlo experiments. Procedures that improve the efficiency of Monte Carlo methods are known as variance reduction techniques. Examples of variance reduction techniques include importance sampling, stratified sampling, control variates, antithetic variates, regression methods, and use of orthonormal functions. [Ref. 31]

Variance reduction techniques in Monte Carlo methods distort the original problem in such a manner that the uncertainty in the answer is reduced for the same number of samples. Hence, the term variance-reducing method is a misnomer. In reality, the cost of implementing a sampling plan and the variance it induces collectively dictate its appeal relative to an alternative plan. To combat misplaced emphasis, this topic is better described as efficiency-improving techniques.

Every problem amenable to the Monte Carlo method comes with an explicit or implicit sampling plan usually dictated by the context in which the problem arises. If the cost of using this plan to achieve the desired statistical accuracy for the estimate of the parameter in question falls within the available computing budget, then no need exists to consider alternative plans. When the cost of the original sampling plan exceeds the available budget, then selecting an alternative sampling plan that meets the budget constraint is an essential first step in the application of the Monte Carlo method. It should be noted that although the sample size is

reduced, some amount of time-dependent computational savings is offset by an increase in computational complexity.

The SBIRS Low model does not utilize a variance reduction technique because the required sample size, 20,000 events, the use of random numbers to assign bias errors, establish satellite phasing, and establish missile launch location does not justify increasing the computational complexity.

APPENDIX B: SBIRS LOW MODEL INPUT AND OUTPUT FILES

A. SBIRS LOW MODEL INPUT FILE FORMAT

A description of each of the input parameters is listed below.

System: initializes the constellation from data contained in the specification file. The default file is gp27.specs, which specifies a constellation of nine rings with three satellites in each ring.

Events: specifies the number of events to be generated in the Monte Carlo simulation

Ack_Level: specifies the frequency at which the user is notified of the number of completed events

KBoost: specifies whether kinematic tracking is used during the boost phase. If set to “on”, kinematic tracking is used, in which case the choice of profile in the boost phase parameters only affects the model used to fly the booster. If “off” is selected, the choice of profile in the boost phase parameters also affects the tracking algorithm.

Profile: specifies the overall booster trajectory. Options are rigid wire, flexible wire, or stereo kinematic.

Type: specifies the particular missile by either the (code internal) missile index or by one of the following entries described in Chapter 5, section A.

Mode: specifies the random launch generation procedure. Options are random or fixed. If random is selected, launch latitude, longitude, and azimuths are selected randomly (according to a uniform distribution) within the user specified entries. If fixed is selected, launch and impact latitudes and longitudes are fixed at the user specified values and the launch azimuth is calculated by the computer using either a lofted or depressed angle, as specified in the code.

T_Window: specifies Tmin and Tmax in units of seconds. Launch times for individual events are selected randomly, according to a uniform distribution, within this interval. This parameter is primarily used to ensure a variable phasing of the satellite constellation.

Lat_Window: specifies Lat_min and Lat_max in units of degrees. Minimum and maximum launch latitude values for random launch mode. Values are chosen according to a uniform distribution over the surface area of the earth with positive values representing east latitudes and negative values representing west latitudes. If the fixed launch mode is selected, the launch point is specified by the Launch_Pt parameter.

Lon_Window: specifies Lon_min and Lon_max in units of degrees. Minimum and maximum launch longitude values for random launch mode. Values are chosen according to a uniform distribution over the surface area of the earth with positive values

representing north longitudes and negative values representing south longitudes. If the fixed launch mode is selected, the launch point is specified by the Launch_Pt parameter.

Az_Window: specifies Az_min and Az_max in units of degrees east of north. Minimum and maximum values for random launch mode. Values are chosen according to a uniform distribution with positive values representing degrees east of north and negative values representing degrees west of north. If the fixed mode is selected, the specified launch and target points determine this value.

Launch_Pt: specifies the latitude and longitude of the launch point in units of degrees when the user selects the fixed launch mode. Positive values represent east latitudes and north longitudes and negative values represent west latitudes and south longitudes. If the random launch mode is selected, the launch point is determined by the Lat_Window and Lon_Window parameters.

Target_Pt: specifies the latitude and longitude of the target point in units of degrees when the user selects the fixed launch mode. Positive values represent east latitudes and north longitudes and negative values represent west latitudes and south longitudes. If the random launch mode is selected, the target point is dependent upon the randomly chosen launch point and azimuth parameters.

DT: specifies delta_time, the revisit time (scan rate) in units of seconds for boost phase viewing. This parameter is the time between consecutive detection attempts on a given target by the acquisition sensor on a given satellite.

Viewers: specifies the number of satellites that will be used to build a track. Options are "all" or "2Best". If all is selected, the boost track is built from all sensors within line-of-sight of the missile. If 2Best is selected, the boost track is built from the two closest sensors, regardless of the scissors angle.

MaxViewers: sets the maximum number of sensors to view each ballistic event. This value must be set prior to any of the following ballistic phase parameters.

Sensor: specifies the timing of detection of the i-th sensor, with $1 \leq ID \leq \text{MaxViewers}$. The sensor ID number is followed by a list of (t_start, t_step) pairs specifying beginning at time t_start, the sensor make a detection attempt every t_step seconds. Sensors are ordered by range-to-target so that sensor ID = 1 is the closest sensor, sensor ID = 2 is the next closest sensor, etc.

T_Window: sets the internal time window, in units of seconds, used for identifying and ordering the sensors that can detect the target. The sensor ordering is with respect to range-to-target. The identification and ordering sensors is done only once every time window and that ordering is used for the entire sampling interval.

DT_Handover: specifies a notional uncertainty in the time of booster burnout. This value is used in estimating the initial state covariance matrix of the reentry vehicle. The default value is 1.

N_Bins: specifies/resets the number of bins for position error histograms. The default value is 80.

X_Max: sets the histogram upper edge. If this value is exceeded, a "++....++" is displayed in the applicable output field.

FitList: specifies whether or not the parameters α and λ for a Gamma distribution are calculated and displayed to the user.

HDump: specifies the data file to write the full output of the predict-ahead histogram contents. If this entry is not included in the input file, only the report described in section C is outputted.

CDump: same as HDump, but for cumulative probabilities.

NM_Cl: specifies the number and levels of confidence intervals that are computed for track containment probabilities. The confidence intervals are one-sided. This line should be entered only once since it simply sets a list of confidence levels which are used during final answer outputs.

N_Times: specifies the number of times to predict the confidence intervals specified in the previous entry.

Times: specifies the elapsed time and length of time for prediction of the defined confidence intervals. Note, there will be a total of N_Times individual entries for this field.

A representative input file is listed below. Additionally, some parameters described in the previous section are not shown because they are not applicable to the specified launch mode.

```
CONTROL
  System = gp27.specs
  Events = 20000
  Ack_Level = 500
  KBoost = On
END CONTROL

BOOSTER
  Profile = Flexible
  Type = M9
  Mode = Random
  Lat_Window = 42.0 45.0
  Lon_Window = 52.0 56.0
  Az_Window = -10.0 30.0
  T_Window = 0.0, 7200.0
  DT = 5.0
  Viewers = 2Best
END BOOSTER

BALLISTIC
  MaxViewers = 3
  Sensor=1, 0.0, 20.0
  Sensor=2, 0.0, 20.0
  Sensor=3, 400.0, 20.0
  T_Window = 60
  DT_Handover = 1
END BALLISTIC
```

```

OUTPUT
  X_Max = 8.0
  NM_Conf = 4, 0.80, 0.90, 0.95, 0.99
  N_Times = 3
  FitList = On
  HDump = plotm91220.out
  CDump = cdfm91220.out
  Times = 50.0, NH = 3, 0.0, 50.0, 100.0
  Times = 100.0, NH = 3, 0.0, 50.0, 100.0
  Times = 200.0, NH = 3, 0.0, 50.0, 100.0
END OUTPUT

```

B. SBIRS LOW MODEL OUTPUT FILE FORMAT

A representative output file is listed below. A general description of this output file was given in Chapter 5, section B.

Running From Input File M91220.dat

System Initializations File : gp27.specs

Run Control Boost Component Summary -----
 Flexible Profile, M9
 Launch Time Window: 0.00 To 7200.00 [sec]
 Random Launches
 Latitude Window: 42.00 To 45.00 [d]
 Longitude Window: 52.00 To 56.00 [d]
 Azimuth Window: -10.00 To 30.00 [d]
 Use Two Closest Viewers
 Revisit Time: 5.0 [s]
 Tracking Done With Kinematic (Polynomial) Fits

Run Control Ballistic Component Summary -----
 Maximum Number Of Viewers: 3
 Sensor Order Viewing Window: 10.0 [s]
 Notional Booster Burnout Time Uncertainty: 1.00 [s]
 Viewing Frequencies By Sensors:
 Sensing 1: (0.00,20.00)
 Sensing 2: (0.00,20.00)
 Sensing 3: (400.00,20.00)

Run Control Output Selection Summary -----

Generate State Predictions At 3 Slices
 3 Predicts At 50.0 [s], DTs: 0.0 50.0 100.0
 3 Predicts At 100.0 [s], DTs: 0.0 50.0 100.0
 3 Predicts At 200.0 [s], DTs: 0.0 50.0 100.0
 Compute Containment Radii For CLs: 0.8000 0.9000 0.9500 0.9900

Run_Control Results -----

20000: Number Of Event Attempts
 20000: Number Of Successful Events

104.850: Seconds In Boost Phase (5.243 msec/Event)
 539.170: Seconds In Ballistic Phase (26.958 msec/Event)
 3.800: Seconds In Output Phase (0.190 msec/Event)
 647.820: Seconds Total (32.391 msec/Event)
 0.249: Mean Initial Kepler Track Error [km]
 64.069: Mean Initial Kepler Speed Error [m/s]

Generate 3 Position Error Analysis Sets

State/Prediction Statistics, Ballistic Track Time 50.0 Seconds After BBO

20000 Simulated Events

Mean Detections Per Track: 7.00

DT [s]	Counts	<Delta X> [km]	Upper Bounds [km]			
			R[0.800]	R[0.900]	R[0.950]	R[0.990]
0.00	20000	0.078 +- 0.047	0.1181	0.1628	0.1852	0.2451
50.00	20000	0.185 +- 0.110	0.2664	0.3265	0.3873	0.5432
100.00	20000	0.296 +- 0.174	0.4101	0.5096	0.6072	0.8577

P(x) = Gamma(x;Alpha,Lambda) Fits, Data Through 50.0 [s]

DT[s]	Alpha +- Error	Lambda +- Error	Corrl.	Score	(mu,sigma)
0.0	1.270 +- 0.022	16.248 +- 0.240	0.818	98.08	(0.08,0.07)
50.0	2.620 +- 0.024	12.943 +- 0.135	0.891	180.64	(0.20,0.13)
100.0	2.633 +- 0.024	8.308 +- 0.083	0.879	126.54	(0.32,0.20)

State/Prediction Statistics, Ballistic Track Time 100.0 Seconds After BBO

20000 Simulated Events

Mean Detections Per Track: 11.00

DT [s]	Counts	<Delta X> [km]	Upper Bounds [km]			
			R[0.800]	R[0.900]	R[0.950]	R[0.990]
0.00	20000	0.078 +- 0.045	0.1219	0.1652	0.1868	0.2522
50.00	20000	0.136 +- 0.079	0.1952	0.2580	0.2947	0.3955
100.00	20000	0.195 +- 0.114	0.2823	0.3588	0.4227	0.5745

P(x) = Gamma(x;Alpha,Lambda) Fits, Data Through 100.0 [s]

DT[s]	Alpha +- Error	Lambda +- Error	Corrl.	Score	(mu,sigma)
0.0	1.510 +- 0.031	19.040 +- 0.339	0.906	149.26	(0.08,0.06)
50.0	3.072 +- 0.033	21.627 +- 0.260	0.948	9.00	(0.14,0.08)
100.0	3.030 +- 0.027	15.281 +- 0.153	0.921	5.67	(0.20,0.11)

State/Prediction Statistics, Ballistic Track Time 200.0 Seconds After BBO

20000 Simulated Events

Mean Detections Per Track: 21.00

DT [s]	Counts	<Delta X> [km]	Upper Bounds [km]			
			R[0.800]	R[0.900]	R[0.950]	R[0.990]
0.00	20000	0.055 +- 0.032	0.0883	0.0994	0.1478	0.1909

50.00	20000	0.077	+-	0.045	0.1203	0.1643	0.1863	0.2490
100.00	20000	0.099	+-	0.058	0.1601	0.1894	0.2243	0.2949

$P(x) = \text{Gamma}(x; \text{Alpha}, \text{Lambda})$ Fits, Data Through 200.0 [s]

DT[s]	Alpha	+- Error	Lambda	+- Error	Corrl.	Score	(mu, sigma)
0.0	...	Fits Failed	...				
50.0	...	Fits Failed	...				
100.0	3.326	+- 0.051	30.424	+- 0.480	0.974	51.26	(0.11, 0.06)

APPENDIX C: CSS-2 MISSILE DATA

The tables do not contain the values for the Gamma distribution parameters, $\hat{\alpha}$ and $\hat{\lambda}$, fit by the SBIRS Low model because the observed data cannot be fit to a gamma distribution.

A. BALLISTIC TRACK INITIATION FAILURE

Table 2 shows the fraction of ballistic track initiation failures with the launch latitude randomly selected between N02 and N05.

CSS-2 Ballistic Track Initiation Failures

Booster Track Revisit Rate (sec)	Ballistic Track Revisit Rate (sec)	Fraction of Failures
5	5	0.00005
5	10	0.00015
5	15	0.00040
5	20	0.00020
5	25	0.00025
5	30	0.00030
5	35	0.00035
5	40	0.00025

Table 2. CSS-2: Ballistic Track Initiation Failure.

B. SYNCHRONOUS STEREO VIEWING

At time $t = 50$ seconds, the data shown in Table 3, Table 4, and Table 5 was generated for the instantaneous positional accuracy using the stated sensor combination.

Sensors 1 and 2

Revisit Rate	ΔX	95% C.I.	99% C.I.
5	0.065 ± 0.121	0.2143	0.5827
10	0.095 ± 0.156	0.2686	0.6885
15	0.067 ± 0.072	0.1791	0.3731
20	0.086 ± 0.087	0.1964	0.4392
25	0.194 ± 0.325	0.4720	2.2400
30	0.155 ± 0.512	0.3023	0.7773
35	0.097 ± 0.083	0.2058	0.3439
40	0.102 ± 0.483	0.1869	0.2653

Table 3. CSS-2: Synchronous Detection Using Sensors 1 and 2.

Sensors 1 and 3

Revisit Rate	ΔX	95% C.I.	99% C.I.
5	0.219 ± 0.655	0.8560	4.1000
10	0.259 ± 0.708	0.9293	4.4400
15	0.160 ± 0.436	0.4066	2.8833
20	0.211 ± 0.576	0.5248	3.9231
25	0.535 ± 1.149	2.8714	6.6545
30	0.352 ± 0.856	1.1435	5.2455
35	0.223 ± 0.533	0.5600	3.4714
40	0.166 ± 0.431	0.3712	1.4000

Table 4. CSS-2: Synchronous Detection Using Sensors 1 and 3.

Sensors 2 and 3

Revisit Rate	ΔX	95% C.I.	99% C.I.
5	0.154 ± 0.589	0.3771	1.9750
10	0.192 ± 0.583	0.4298	1.8143
15	0.161 ± 0.541	0.3036	1.0091
20	0.202 ± 0.612	0.3987	1.5300
25	0.476 ± 1.117	1.5778	6.8500
30	0.350 ± 0.941	0.8402	5.2667
35	0.272 ± 0.778	0.5903	3.5667
40	0.249 ± 0.778	0.5045	3.7750

Table 5. CSS-2: Synchronous Detection Using Sensors 2 and 3.

C. MONO VIEWING

At time $t = 50$ seconds, the data shown in Table 6, Table 7, and Table 8 was generated for the instantaneous positional accuracy using the stated sensor combination.

Sensor 1

Revisit Rate	ΔX	95% C.I.	99% C.I.
5	5.710 ± 5.498	16.0667	25.1652
10	5.722 ± 5.023	15.5753	22.1739
15	4.973 ± 4.804	14.4000	21.3882
20	5.409 ± 4.771	14.6804	21.5000
25	7.409 ± 4.715	17.1942	22.3704
30	7.527 ± 4.843	17.3217	23.5429
35	7.622 ± 4.934	17.4769	23.8667
40	7.543 ± 4.918	17.0565	24.2824

Table 6. CSS-2: Mono Detection Using Sensor 1.

Sensor 2

Revisit Rate	ΔX	95% C.I.	99% C.I.
5	6.941 ± 5.729	18.7220	23.5579
10	6.447 ± 5.400	17.7560	22.6556
15	6.099 ± 5.403	17.8133	23.6258
20	5.943 ± 5.191	16.8427	23.3571
25	5.876 ± 4.613	15.4517	20.5290
30	5.922 ± 4.678	15.5054	21.4533
35	6.087 ± 4.876	15.9086	23.0875
40	6.127 ± 4.938	16.2338	23.6143

Table 7. CSS-2: Mono Detection Using Sensor 2.

Sensor 3

Revisit Rate	ΔX	95% C.I.	99% C.I.
5	6.236 ± 5.686	17.7691	22.5158
10	5.599 ± 5.155	16.2575	21.0133
15	5.319 ± 5.102	15.7294	21.7667
20	5.195 ± 4.689	14.2211	20.5838
25	5.218 ± 3.978	12.4035	17.3286
30	5.325 ± 4.031	12.4142	18.4714
35	5.369 ± 4.188	12.6931	19.8500
40	5.485 ± 4.339	13.0115	21.0750

Table 8. CSS-2: Mono Detection Using Sensor 3.

D. SEQUENTIAL MONO VIEWING

At time $t = 50$ seconds the data shown in Table 9, Table 10, Table 11, Table 12, Table 13, and Table 14 was generated for the instantaneous positional accuracy using the stated sensor combination.

Sensor 1 Handover to Sensor 2 at Time $t = 75$ seconds

Revisit Rate	ΔX	95% C.I.	99% C.I.
5	5.664 ± 5.388	15.7073	24.8571
10	5.750 ± 4.948	15.4722	21.7333
15	4.931 ± 4.830	14.5347	21.6000
20	5.432 ± 4.729	14.7053	21.3391
25	7.480 ± 4.770	17.1955	22.6815
30	7.538 ± 4.880	17.3824	23.4462
35	7.499 ± 4.876	17.3545	23.7895
40	7.563 ± 4.977	17.4313	24.7304

Table 9. CSS-2 Sequential Mono Viewing: Sensor 1 Handover to Sensor 2 at Time $t = 75$ seconds.

Sensor 1 Handover to Sensor 2 at Time $t = 150$ seconds

Revisit Rate	ΔX	95% C.I.	99% C.I.
5	5.664 ± 5.388	15.7073	24.8571
10	5.799 ± 5.035	15.7708	21.9810
15	4.931 ± 4.830	14.5347	21.6000
20	5.427 ± 4.729	14.7009	21.2571
25	7.480 ± 4.770	17.1955	22.6815
30	7.462 ± 4.795	17.2754	22.9103
35	7.499 ± 4.876	17.3545	23.7895
40	7.563 ± 4.977	17.4313	24.7304

Table 10. CSS-2 Sequential Mono Viewing: Sensor 1 Handover to Sensor 2 at Time $t = 150$ seconds.

Sensor 1 Handover to Sensor 3 at Time t = 75 seconds

Revisit Rate	ΔX	95% C.I.	99% C.I.
5	5.632 ± 5.367	15.7679	24.3765
10	5.723 ± 5.014	15.6667	22.2000
15	4.980 ± 4.828	14.5558	21.4222
20	5.460 ± 4.775	14.7040	21.4667
25	7.455 ± 4.700	16.9287	22.6182
30	7.561 ± 4.931	17.4813	23.3760
35	7.518 ± 4.927	17.1778	24.2222
40	7.576 ± 4.955	17.3851	24.1455

Table 11. CSS-2 Sequential Mono Viewing: Sensor 1 Handover to Sensor 3 at Time t = 75 seconds.

Sensor 1 Handover to Sensor 3 at Time t = 150 seconds

Revisit Rate	ΔX	95% C.I.	99% C.I.
5	5.683 ± 5.386	15.8462	24.4250
10	5.767 ± 5.021	15.8521	22.0000
15	5.005 ± 4.906	14.7673	21.7524
20	5.456 ± 4.721	14.6721	21.0667
25	7.494 ± 4.753	17.1678	22.6621
30	7.488 ± 4.815	17.3000	23.1000
35	7.456 ± 4.855	17.1463	23.5000
40	7.605 ± 4.960	17.2400	24.7000

Table 12. CSS-2 Sequential Mono Viewing: Sensor 1 Handover to Sensor 3 at Time t = 150 seconds.

Sensor 2 Handover to Sensor 3 at Time t = 75 seconds

Revisit Rate	ΔX	95% C.I.	99% C.I.
5	6.976 ± 5.729	18.7882	23.5529
10	6.506 ± 5.461	18.0710	22.6824
15	6.192 ± 5.539	18.1519	23.7677
20	6.011 ± 5.177	17.0833	23.1704
25	5.916 ± 4.679	15.6178	20.8000
30	5.983 ± 4.767	15.8457	22.0824
35	6.084 ± 4.907	16.2000	23.1500
40	6.203 ± 4.942	16.3536	23.0080

Table 13. CSS-2 Sequential Mono Viewing: Sensor 2 Handover to Sensor 3 at Time t = 75 seconds.

Sensor 2 Handover to Sensor 3 at Time t = 150 seconds

Revisit Rate	ΔX	95% C.I.	99% C.I.
5	6.976 ± 5.733	18.8747	23.5222
10	6.527 ± 5.465	18.0240	22.8154
15	6.152 ± 5.482	17.9830	23.9048
20	5.989 ± 5.184	16.9531	23.4162
25	5.933 ± 4.639	15.4488	20.7143
30	5.959 ± 4.763	15.8409	21.7333
35	5.947 ± 4.786	15.7487	22.6750
40	6.117 ± 4.894	16.1412	23.0667

Table 14. CSS-2 Sequential Mono Viewing: Sensor 2 Handover to Sensor 3 at Time t = 150 seconds.

E. ASYNCHRONOUS VIEWING

At time t = 50 seconds, the data shown in Tables 15 to 32 was generated for the instantaneous positional accuracy using the stated sensor combination.

Sensor 1 has a constant revisit rate of every 5 seconds and sensor 2 has a variable revisit rate given in the "Revisit Rate" column

Revisit Rate	ΔX	95% C.I.	99% C.I.
5	0.065 ± 0.121	0.2143	0.5827
10	0.137 ± 0.392	0.4112	2.6696
15	0.112 ± 0.314	0.3358	2.0957
20	0.174 ± 0.512	0.5108	3.3286
25	0.639 ± 1.462	3.8829	7.4333
30	0.411 ± 1.083	2.7382	5.8250
35	0.257 ± 0.742	0.9603	4.4955
40	0.177 ± 0.526	0.4945	3.4350

Table 15. CSS-2 Asynchronous Viewing: Sensor 1 and Sensor 2.

Sensor 1 has a constant revisit rate of every 10 seconds and sensor 2 has a variable revisit rate given in the "Revisit Rate" column

Revisit Rate	ΔX	95% C.I.	99% C.I.
5	0.062 ± 0.088	0.1633	0.4539
10	0.095 ± 0.156	0.2686	0.6885
15	0.078 ± 0.111	0.1963	0.5217
20	0.104 ± 0.199	0.2604	0.8575
25	0.330 ± 0.852	1.2565	5.1375
30	0.202 ± 0.526	0.5350	3.4833
35	0.144 ± 0.348	0.3362	2.4542
40	0.116 ± 0.371	0.2538	0.9405

Table 16. CSS-2 Asynchronous Viewing: Sensor 1 and Sensor 2.

Sensor 1 has a constant revisit rate of every 15 seconds and sensor 2 has a variable revisit rate given in the "Revisit Rate" column

Revisit Rate	ΔX	95% C.I.	99% C.I.
5	0.056 ± 0.084	0.1432	0.3589
10	0.080 ± 0.108	0.1967	0.4913
15	0.067 ± 0.072	0.1791	0.3731
20	0.086 ± 0.117	0.1971	0.5975
25	0.262 ± 0.669	0.8269	4.1708
30	0.163 ± 0.399	0.3958	2.8895
35	0.114 ± 0.233	0.2600	1.0353
40	0.087 ± 0.117	0.1955	0.5976

Table 17. CSS-2 Asynchronous Viewing: Sensor 1 and Sensor 2.

Sensor 1 has a constant revisit rate of every 20 seconds and sensor 2 has a variable revisit rate given in the "Revisit Rate" column

Revisit Rate	ΔX	95% C.I.	99% C.I.
5	0.062 ± 0.076	01648.	0.3761
10	0.079 ± 0.073	0.1937	0.3940
15	0.069 ± 0.061	0.1779	0.2855
20	0.086 ± 0.087	0.1964	0.4392
25	0.207 ± 0.483	0.5029	3.2900
30	0.137 ± 0.261	0.2961	1.1647
35	0.103 ± 0.127	0.2334	0.6324
40	0.096 ± 0.341	0.1952	0.4048

Table 18. CSS-2 Asynchronous Viewing: Sensor 1 and Sensor 2.

Sensor 1 has a constant revisit rate of every 25 seconds and sensor 2 has a variable revisit rate given in the "Revisit Rate" column

Revisit Rate	ΔX	95% C.I.	99% C.I.
5	0.112 ± 0.204	0.3489	0.8280
10	0.111 ± 0.158	0.2626	0.5710
15	0.108 ± 0.193	0.2326	0.5419
20	0.112 ± 0.127	0.2538	0.4940
25	0.194 ± 0.325	0.4720	2.2400
30	0.239 ± 0.973	0.3899	4.1750
35	0.223 ± 1.003	0.2986	4.6400
40	0.289 ± 1.265	0.2970	7.6857

Table 19. CSS-2 Asynchronous Viewing: Sensor 1 and Sensor 2.

Sensor 1 has a constant revisit rate of every 30 seconds and sensor 2 has a variable revisit rate given in the "Revisit Rate" column

Revisit Rate	ΔX	95% C.I.	99% C.I.
5	0.079 ± 0.098	0.1950	0.4642
10	0.091 ± 0.095	0.1965	0.3989
15	0.085 ± 0.090	0.1925	0.3667
20	0.096 ± 0.098	0.1984	0.3578
25	0.276 ± 1.061	0.4847	4.8000
30	0.097 ± 0.083	0.2058	0.3439
35	0.124 ± 0.429	0.2480	0.4434
40	0.199 ± 1.006	0.2096	4.8600

Table 20. CSS-2 Asynchronous Viewing: Sensor 1 and Sensor 2.

Sensor 2 has a constant revisit rate of every 5 seconds and sensor 3 has a variable revisit rate given in the "Revisit Rate" column

Revisit Rate	ΔX	95% C.I.	99% C.I.
5	0.154 ± 0.589	0.3771	1.9750
10	0.280 ± 1.003	0.7488	5.5000
15	0.233 ± 0.875	0.5409	4.6000
20	0.386 ± 1.318	1.3829	7.8667
25	1.029 ± 2.251	5.4360	8.0000+
30	0.718 ± 1.893	3.6724	8.0000+
35	0.512 ± 1.544	2.5444	8.0000+
40	0.411 ± 1.415	1.5325	8.0000+

Table 21. CSS-2 Asynchronous Viewing: Sensor 2 and Sensor 3.

Sensor 2 has a constant revisit rate of every 10 seconds and sensor 3 has a variable revisit rate given in the "Revisit Rate" column

Revisit Rate	ΔX	95% C.I.	99% C.I.
5	0.148 ± 0.504	0.3409	1.0222
10	0.192 ± 0.583	0.4298	1.8143
15	0.180 ± 0.605	0.3830	1.4778
20	0.231 ± 0.745	0.4906	3.2750
25	0.619 ± 1.717	2.8622	8.0000+
30	0.421 ± 1.282	1.4114	7.2500
35	0.308 ± 0.998	0.7467	5.7000
40	0.278 ± 0.943	0.5981	5.1200

Table 22. CSS-2 Asynchronous Viewing: Sensor 2 and Sensor 3.

Sensor 2 has a constant revisit rate of every 15 seconds and sensor 3 has a variable revisit rate given in the "Revisit Rate" column

Revisit Rate	ΔX	95% C.I.	99% C.I.
5	0.142 ± 0.524	0.2798	0.8750
10	0.181 ± 0.594	0.3535	1.7000
15	0.161 ± 0.541	0.3036	1.0091
20	0.213 ± 0.734	0.3955	2.8000
25	0.540 ± 1.585	2.2233	8.0000+
30	0.394 ± 1.301	1.0354	7.5333
35	0.311 ± 1.093	0.6397	6.5250
40	0.257 ± 0.913	0.5136	4.9600

Table 23. CSS-2 Asynchronous Viewing: Sensor 2 and Sensor 3.

Sensor 2 has a constant revisit rate of every 20 seconds and sensor 3 has a variable revisit rate given in the "Revisit Rate" column

Revisit Rate	ΔX	95% C.I.	99% C.I.
5	0.153 ± 0.503	0.3025	1.3900
10	0.186 ± 0.562	0.3703	1.5714
15	0.183 ± 0.595	0.3537	1.5200
20	0.202 ± 0.612	0.3987	1.5300
25	0.456 ± 1.278	1.5475	7.3200
30	0.345 ± 1.064	0.8396	5.9000
35	0.282 ± 0.917	0.5792	4.9333
40	0.242 ± 0.786	0.4765	3.5000

Table 24. CSS-2 Asynchronous Viewing: Sensor 2 and Sensor 3.

Sensor 2 has a constant revisit rate of every 25 seconds and sensor 3 has a variable revisit rate given in the "Revisit Rate" column

Revisit Rate	ΔX	95% C.I.	99% C.I.
5	0.275 ± 0.797	0.6536	4.0200
10	0.266 ± 0.707	0.5824	3.3889
15	0.249 ± 0.715	0.5405	2.2143
20	0.266 ± 0.664	0.5708	2.4667
25	0.476 ± 1.117	1.5778	6.8500
30	0.374 ± 0.917	0.8937	5.2000
35	0.337 ± 0.903	0.7750	5.1286
40	0.326 ± 0.912	0.6945	4.8500

Table 25. CSS-2 Asynchronous Viewing: Sensor 2 and Sensor 3.

Sensor 2 has a constant revisit rate of every 30 seconds and sensor 3 has a variable revisit rate given in the "Revisit Rate" column

Revisit Rate	ΔX	95% C.I.	99% C.I.
5	0.211 ± 0.643	0.4561	2.8875
10	0.229 ± 0.654	0.4604	2.4000
15	0.206 ± 0.552	0.4253	1.7286
20	0.238 ± 0.667	0.4781	2.0500
25	0.436 ± 1.079	1.3045	6.3667
30	0.350 ± 0.941	0.8402	5.2667
35	0.299 ± 0.855	0.6541	4.0500
40	0.285 ± 0.854	0.5821	4.3250

Table 26. CSS-2 Asynchronous Viewing: Sensor 2 and Sensor 3.

Sensor 3 has a constant revisit rate of every 5 seconds and sensor 2 has a variable revisit rate given in the "Revisit Rate" column

Revisit Rate	ΔX	95% C.I.	99% C.I.
5	0.154 ± 0.589	0.3771	1.9750
10	0.148 ± 0.504	0.3409	1.0222
15	0.142 ± 0.524	0.2798	0.8750
20	0.153 ± 0.503	0.3025	1.3900
25	0.275 ± 0.797	0.6536	4.0200
30	0.211 ± 0.643	0.4561	2.8875
35	0.181 ± 0.625	0.3639	1.7600
40	0.161 ± 0.549	0.2951	1.5286

Table 27. CSS-2 Asynchronous Viewing: Sensor 3 and Sensor 2.

Sensor 3 has a constant revisit rate of every 10 seconds and sensor 2 has a variable revisit rate given in the "Revisit Rate" column

Revisit Rate	ΔX	95% C.I.	99% C.I.
5	0.280 ± 1.003	0.7488	5.5000
10	0.192 ± 0.583	0.4298	1.8143
15	0.181 ± 0.594	0.3535	1.7000
20	0.186 ± 0.562	0.3703	1.5714
25	0.266 ± 0.707	0.5824	3.3889
30	0.229 ± 0.654	0.4604	2.4000
35	0.205 ± 0.630	0.3873	2.0000
40	0.192 ± 0.605	0.3739	1.6857

Table 28. CSS-2 Asynchronous Viewing: Sensor 3 and Sensor 2.

Sensor 3 has a constant revisit rate of every 15 seconds and sensor 2 has a variable revisit rate given in the "Revisit Rate" column

Revisit Rate	ΔX	95% C.I.	99% C.I.
5	0.233 ± 0.875	0.5409	4.6000
10	0.180 ± 0.605	0.3830	1.4778
15	0.161 ± 0.541	0.3036	1.0091
20	0.183 ± 0.595	0.3537	1.5200
25	0.249 ± 0.715	0.5405	2.2143
30	0.206 ± 0.552	0.4253	1.7286
35	0.190 ± 0.584	0.3758	1.2667
40	0.178 ± 0.542	0.3509	1.2857

Table 29. CSS-2 Asynchronous Viewing: Sensor 3 and Sensor 2.

Sensor 3 has a constant revisit rate of every 20 seconds and sensor 2 has a variable revisit rate given in the "Revisit Rate" column

Revisit Rate	ΔX	95% C.I.	99% C.I.
5	0.386 ± 1.318	1.3829	7.8667
10	0.231 ± 0.745	0.4906	3.2750
15	0.213 ± 0.734	0.3955	2.8000
20	0.202 ± 0.612	0.3987	1.5300
25	0.266 ± 0.664	0.5708	2.4667
30	0.238 ± 0.667	0.4781	2.0500
35	0.227 ± 0.673	0.4292	2.4375
40	0.213 ± 0.655	0.4192	1.7500

Table 30. CSS-2 Asynchronous Viewing: Sensor 3 and Sensor 2.

Sensor 3 has a constant revisit rate of every 25 seconds and sensor 2 has a variable revisit rate given in the "Revisit Rate" column

Revisit Rate	ΔX	95% C.I.	99% C.I.
5	1.029 ± 2.251	5.4360	8.0000+
10	0.619 ± 1.717	2.8622	8.0000+
15	0.540 ± 1.585	2.2233	8.0000+
20	0.456 ± 1.278	1.5475	7.3200
25	0.476 ± 1.117	1.5778	6.8500
30	0.436 ± 1.079	1.3045	6.3667
35	0.448 ± 1.229	1.2862	7.3286
40	0.477 ± 1.359	1.4854	8.0000+

Table 31. CSS-2 Asynchronous Viewing: Sensor 3 and Sensor 2.

Sensor 3 has a constant revisit rate of every 30 seconds and sensor 2 has a variable revisit rate given in the "Revisit Rate" column

Revisit Rate	ΔX	95% C.I.	99% C.I.
5	0.718 ± 1.893	3.6724	8.0000+
10	0.421 ± 1.282	1.4114	7.2500
15	0.394 ± 1.301	1.0354	7.5333
20	0.345 ± 1.064	0.8396	5.9000
25	0.374 ± 0.917	0.8937	5.2000
30	0.350 ± 0.941	0.8402	5.2667
35	0.330 ± 0.935	0.7632	4.8250
40	0.358 ± 1.099	0.8371	6.6333

Table 32. CSS-2 Asynchronous Viewing: Sensor 3 and Sensor 2.

F. DELAYED VIEWING

At time $t = 50$ seconds, the data shown in Tables 33 to Table 38 was generated for the instantaneous positional accuracy using the stated sensor combination.

Sensor 1 and 2 delay turning on for 5 seconds after booster burnout

Revisit Rate	ΔX	95% C.I.	99% C.I.
5	0.084 ± 0.192	0.3333	0.8104
10	0.082 ± 0.138	0.2569	0.6196
15	0.140 ± 0.249	0.4035	1.6333
20	0.074 ± 0.073	0.1897	0.3892
25	0.181 ± 0.477	0.4268	1.9727
30	0.113 ± 0.133	0.2769	0.5694
35	0.098 ± 0.338	0.1945	0.3404
40	0.069 ± 0.052	0.1745	0.1994

Table 33. CSS-2 Delayed Viewing: Sensor 1 and Sensor 2.

Sensor 1 and 2 delay turning on for 10 seconds after booster burnout

Revisit Rate	ΔX	95% C.I.	99% C.I.
5	0.102 ± 0.233	0.3698	1.4667
10	0.140 ± 0.278	0.4713	1.7778
15	0.121 ± 0.203	0.3626	1.0231
20	0.248 ± 0.501	0.7511	2.7692
25	0.139 ± 0.202	0.3750	0.9194
30	0.108 ± 0.267	0.2533	0.5477
35	0.075 ± 0.078	0.1849	0.2890
40	5.289 ± 2.699	8.0000+	8.0000+

Table 34. CSS-2 Delayed Viewing: Sensor 1 and Sensor 2.

Sensor 1 and 2 delay turning on for 15 seconds after booster burnout

Revisit Rate	ΔX	95% C.I.	99% C.I.
5	0.134 ± 0.299	0.5168	1.8053
10	0.113 ± 0.213	0.3873	1.2190
15	0.101 ± 0.159	0.3000	0.8413
20	0.186 ± 0.324	0.5287	2.0361
25	0.125 ± 0.248	0.3599	0.8043
30	0.086 ± 0.092	0.2019	0.4821
35	3.453 ± 2.594	7.5811	8.0000+
40	3.442 ± 2.598	7.5914	8.0000+

Table 35. CSS-2 Delayed Viewing: Sensor 1 and Sensor 2.

Sensor 1 and 2 delay turning on for 20 seconds after booster burnout

Revisit Rate	ΔX	95% C.I.	99% C.I.
5	0.190 ± 0.418	0.9586	2.2483
10	0.234 ± 0.482	1.1030	2.5700
15	0.321 ± 0.619	1.4446	3.6286
20	0.148 ± 0.239	0.4362	1.4438
25	0.102 ± 0.134	0.2978	0.7125
30	2.206 ± 2.114	6.3299	7.2763
35	2.206 ± 2.114	6.3299	7.2763
40	2.221 ± 2.113	6.3227	7.2692

Table 36. CSS-2 Delayed Viewing: Sensor 1 and Sensor 2.

Sensor 1 and 2 delay turning on for 25 seconds after booster burnout

Revisit Rate	ΔX	95% C.I.	99% C.I.
5	0.253 ± 0.495	1.1926	2.7212
10	0.162 ± 0.310	0.6642	1.6714
15	0.218 ± 0.417	0.8849	2.3053
20	0.118 ± 0.168	0.3681	1.0034
25	1.363 ± 1.560	5.0290	5.9560
30	1.365 ± 1.568	5.0487	5.9808
35	1.377 ± 1.571	5.0570	5.9553
40	1.376 ± 1.570	5.0548	5.9425

Table 37. CSS-2 Delayed Viewing: Sensor 1 and Sensor 2.

Sensor 1 and 2 delay turning on for 30 seconds after booster burnout

Revisit Rate	ΔX	95% C.I.	99% C.I.
5	0.298 ± 0.511	1.4137	2.5556
10	0.358 ± 0.611	1.6425	3.1522
15	0.149 ± 0.233	0.5402	1.2000
20	0.819 ± 1.119	3.5600	4.7642
25	0.824 ± 1.130	3.5625	4.7690
30	0.827 ± 1.153	3.6386	4.8325
35	0.825 ± 1.130	3.5352	4.7532
40	0.825 ± 1.130	3.5352	4.7532

Table 38. CSS-2 Delayed Viewing: Sensor 1 and Sensor 2.

G. STAGGERED VIEWING

At time $t = 50$ seconds, the data shown in Table 39, Table 40, Table 41, Table 42, and Table 43 was generated for the instantaneous positional accuracy using the stated sensor combination.

Sensor 1 and 2 delay turning for 5 seconds after booster burnout, sensor 1 has a constant revisit rate of every 5 seconds, and sensor 2 has a variable revisit rate given in the "Revisit Rate" column

Revisit Rate	ΔX	95% C.I.	99% C.I.
5	0.084 ± 0.192	0.3333	0.8104
10	0.111 ± 0.290	0.3790	2.0323
15	0.315 ± 0.824	1.8710	4.5771
20	0.140 ± 0.387	0.4536	2.5724
25	0.514 ± 1.207	3.0957	6.2250
30	0.313 ± 0.831	1.8391	4.7192
35	0.205 ± 0.578	0.6667	3.5733
40	0.145 ± 0.399	0.4502	2.6667

Table 39. CSS-2 Staggered Viewing: Sensor 1 and Sensor 2.

Sensor 1 and 2 delay turning for 10 seconds after booster burnout, sensor 1 has a constant revisit rate of every 5 seconds, and sensor 2 has a variable revisit rate given in the "Revisit Rate" column

Revisit Rate	ΔX	95% C.I.	99% C.I.
5	0.102 ± 0.233	0.3698	1.4667
10	0.220 ± 0.560	1.0644	3.3083
15	0.241 ± 0.617	1.2578	3.5933
20	0.610 ± 1.262	3.1200	6.5167
25	0.372 ± 0.897	2.1836	4.9300
30	0.239 ± 0.622	1.2057	3.6514
35	0.160 ± 0.412	0.5857	2.6519
40	4.161 ± 3.890	8.0000+	8.0000+

Table 40. CSS-2 Staggered Viewing: Sensor 1 and Sensor 2.

Sensor 1 and 2 delay turning for 15 seconds after booster burnout, sensor 1 has a constant revisit rate of every 5 seconds, and sensor 2 has a variable revisit rate given in the "Revisit Rate" column

Revisit Rate	ΔX	95% C.I.	99% C.I.
5	0.134 ± 0.299	0.5168	1.8053
10	0.163 ± 0.385	0.7523	2.3406
15	0.174 ± 0.419	0.7977	2.5118
20	0.433 ± 0.932	2.3297	4.9500
25	0.269 ± 0.642	1.5223	3.6118
30	0.178 ± 0.427	0.8145	2.6167
35	3.082 ± 3.194	8.0000+	8.0000+
40	3.107 ± 3.197	8.0000+	8.0000+

Table 41. CSS-2 Staggered Viewing: Sensor 1 and Sensor 2.

Sensor 1 and 2 delay turning for 20 seconds after booster burnout, sensor 1 has a constant revisit rate of every 5 seconds, and sensor 2 has a variable revisit rate given in the "Revisit Rate" column

Revisit Rate	ΔX	95% C.I.	99% C.I.
5	0.190 ± 0.418	0.9586	2.2483
10	0.328 ± 0.659	1.7064	3.4029
15	0.506 ± 0.887	2.3248	4.3160
20	0.309 ± 0.659	1.6022	3.5643
25	0.198 ± 0.441	1.0436	2.5455
30	2.102 ± 2.422	7.0359	8.0000+
35	2.102 ± 2.422	7.0359	8.0000+
40	2.124 ± 2.432	7.1000	8.0000+

Table 42. CSS-2 Staggered Viewing: Sensor 1 and Sensor 2.

Sensor 1 and 2 delay turning for 25 seconds after booster burnout, sensor 1 has a constant revisit rate of every 5 seconds, and sensor 2 has a variable revisit rate given in the "Revisit Rate" column

Revisit Rate	ΔX	95% C.I.	99% C.I.
5	0.253 ± 0.495	1.1926	2.7212
10	0.243 ± 0.491	1.2462	2.6583
15	0.364 ± 0.659	1.7585	3.2385
20	0.230 ± 0.470	1.1675	2.5744
25	1.322 ± 1.691	4.7658	7.2733
30	1.337 ± 1.713	4.7862	7.4400
35	1.346 ± 1.719	4.8205	7.4300
40	1.346 ± 1.721	4.8284	7.4526

Table 43. CSS-2 Staggered Viewing: Sensor 1 and Sensor 2.

Sensor 1 and 2 delay turning for 30 seconds after booster burnout, sensor 1 has a constant revisit rate of every 5 seconds, and sensor 2 has a variable revisit rate given in the "Revisit Rate" column

Revisit Rate	ΔX	95% C.I.	99% C.I.
5	0.298 ± 0.511	1.4137	2.5556
10	0.392 ± 0.621	1.7915	2.7828
15	0.255 ± 0.467	1.2547	2.4698
20	0.818 ± 1.141	3.0460	5.0769
25	0.827 ± 1.141	3.1288	4.9136
30	0.843 ± 1.189	3.1263	5.0300
35	0.832 ± 1.162	3.0865	4.8800
40	0.830 ± 1.160	3.0875	4.8556

Table 44. CSS-2 Staggered Viewing: Sensor 1 and Sensor 2.

H. LATITUDE SHIFT

At time $t = 50$ seconds, the data shown in Table 45, Table 46, Table 47, and Table 48 was generated for the instantaneous positional accuracy using sensors 1 and 2 at the stated latitude.

Sensors 1 and 2 at Latitude N02

Revisit Rate	ΔX	95% C.I.	99% C.I.
5	0.270 ± 0.726	1.4874	3.8715
10	0.334 ± 0.811	1.7018	4.6129
15	0.221 ± 0.580	0.5952	3.6231
20	0.264 ± 0.642	0.6820	4.0006
25	0.650 ± 1.250	3.2268	6.4339
30	0.420 ± 1.047	1.5627	5.4020
35	0.273 ± 0.612	0.6724	3.7509
40	0.231 ± 0.814	0.5121	2.8025

Table 45. CSS-2 Latitude Shift to N02: Sensor 1 and Sensor 2.

Sensors 1 and 2 at Latitude N20

Revisit Rate	ΔX	95% C.I.	99% C.I.
5	0.130 ± 0.352	0.4286	2.0605
10	0.166 ± 0.388	0.4723	2.2267
15	0.115 ± 0.266	0.2692	1.5871
20	0.143 ± 0.314	0.3237	1.8629
25	0.335 ± 0.619	1.1444	3.4500
30	0.241 ± 0.597	0.5586	2.6737
35	0.157 ± 0.301	0.3496	1.6800
40	0.150 ± 0.529	0.2847	0.7778

Table 46. CSS-2 Latitude Shift to N20: Sensor 1 and Sensor 2.

Sensors 1 and 2 at Latitude N60

Revisit Rate	ΔX	95% C.I.	99% C.I.
5	0.085 ± 0.315	0.2434	0.8100
10	0.118 ± 0.443	0.2614	1.0923
15	0.082 ± 0.235	0.1852	0.4593
20	0.103 ± 0.281	0.1981	0.6450
25	0.218 ± 0.612	0.4325	1.9833
30	0.173 ± 0.595	0.2924	1.3067
35	0.113 ± 0.248	0.2178	0.5220
40	0.120 ± 0.620	0.1947	0.4542

Table 47. CSS-2 Latitude Shift to N60: Sensor 1 and Sensor 2.

Sensors 1 and 2 at Latitude N80

Revisit Rate	ΔX	95% C.I.	99% C.I.
5	0.096 ± 0.252	0.1998	0.6048
10	0.137 ± 0.305	0.2787	0.8187
15	0.106 ± 0.158	0.2056	0.5246
20	0.141 ± 0.249	0.2789	0.7583
25	0.285 ± 0.582	0.5106	2.5800
30	0.277 ± 1.036	0.4303	3.7000
35	0.177 ± 0.305	0.3368	1.0789
40	0.191 ± 0.811	0.2945	1.1333

Table 48. CSS-2 Latitude Shift to N80: Sensor 1 and Sensor 2.

APPENDIX D: M-9 MISSILE DATA

The tables do not contain the values for the Gamma distribution parameters, $\hat{\alpha}$ and $\hat{\lambda}$, fit by the SBIRS Low model because the observed data cannot be fit to a gamma distribution.

A. BALLISTIC TRACK INITIATION FAILURE

Table 49 shows the fraction of ballistic track initiation failures with the launch latitude randomly selected between N02 and N05 and the booster track revisit varied from 5 to 3 then 2 seconds.

M-9 Ballistic Track Initiation Failures

Booster Track Revisit Rate (sec)			Ballistic Track Revisit Rate (sec)	Fraction of Failures		
5	3	2	5	0.0645	0.0492	0.0386
5	3	2	10	0.0648	0.0453	0.0366
5	3	2	15	0.0624	0.0456	0.0360
5	3	2	20	0.0629	0.0490	0.0393
5	3	2	25	0.0629	0.0463	0.0382
5	3	2	30	0.0634	0.0450	0.0385
5	3	2	35	0.0630	0.0478	0.0384
5	3	2	40	0.0632	0.0435	0.0364

Table 49. M-9: Ballistic Track Initiation Failure.

B. SYNCHRONOUS STEREO VIEWING

At time $t = 50$ seconds, the data shown in Table 50, Table 51, and Table 52 was generated for the instantaneous positional accuracy using the stated sensor combination.

Sensors 1 and 2

Revisit Rate	ΔX	95% C.I.	99% C.I.
5	0.050 ± 0.037	0.1269	0.1903
10	0.070 ± 0.045	0.1774	0.2140
15	0.063 ± 0.036	0.1641	0.1964
20	0.078 ± 0.047	0.1852	0.2451
25	0.145 ± 0.094	0.2983	0.4444
30	0.119 ± 0.118	0.2580	0.3637
35	0.094 ± 0.051	0.1974	0.2835
40	0.085 ± 0.117	0.1888	0.2685

Table 50. M-9: Synchronous Detection Using Sensors 1 and 2.

Sensors 1 and 3

Revisit Rate	ΔX	95% C.I.	99% C.I.
5	0.081 ± 0.109	0.1989	0.5524
10	0.108 ± 0.121	0.2711	0.6268
15	0.095 ± 0.098	0.2333	0.4687
20	0.117 ± 0.112	0.2831	0.5767
25	0.218 ± 0.211	0.5270	1.1676
30	0.176 ± 0.183	0.4308	0.9469
35	0.144 ± 0.137	0.3538	0.6988
40	0.123 ± 0.128	0.2938	0.5695

Table 51. M-9: Synchronous Detection Using Sensors 1 and 3.

Sensors 2 and 3

Revisit Rate	ΔX	95% C.I.	99% C.I.
5	0.105 ± 0.127	0.2870	0.6931
10	0.142 ± 0.152	0.3744	0.8444
15	0.126 ± 0.136	0.3209	0.7429
20	0.157 ± 0.167	0.3928	0.9190
25	0.284 ± 0.263	0.7473	1.4727
30	0.234 ± 0.231	0.6302	1.2636
35	0.198 ± 0.206	0.5279	1.1205
40	0.171 ± 0.192	0.4534	1.0551

Table 52. M-9: Synchronous Detection Using Sensors 2 and 3.

C. MONO VIEWING

At time $t = 50$ seconds, the data shown in Table 53, Table 54, and Table 55 was generated for the instantaneous positional accuracy using the stated sensor combination.

Sensor 1

Revisit Rate	ΔX	95% C.I.	99% C.I.
5	1.157 ± 1.059	3.2844	4.6186
10	1.271 ± 1.119	3.5250	4.7894
15	1.103 ± 0.988	3.1266	4.2282
20	1.264 ± 1.095	3.4601	4.7286
25	1.875 ± 1.508	4.6848	6.6867
30	1.846 ± 1.505	4.7386	6.5873
35	1.846 ± 1.490	4.7435	6.5684
40	1.841 ± 1.480	4.6586	6.4778

Table 53. M-9: Mono Detection Using Sensor 1.

Sensor 2

Revisit Rate	ΔX	95% C.I.	99% C.I.
5	1.092 ± 0.990	3.0661	4.3375
10	1.137 ± 0.998	3.1098	4.3883
15	1.098 ± 0.962	3.0138	4.2112
20	1.164 ± 0.982	3.0977	4.3241
25	1.341 ± 1.052	3.4094	4.6962
30	1.312 ± 1.042	3.3452	4.7091
35	1.313 ± 1.050	3.3538	4.6913
40	1.312 ± 1.045	3.3623	4.7000

Table 54. M-9: Mono Detection Using Sensor 2.

Sensor 3

Revisit Rate	ΔX	95% C.I.	99% C.I.
5	0.983 ± 1.003	3.0178	4.5570
10	1.073 ± 1.022	3.1675	4.5631
15	1.047 ± 1.017	3.1708	4.5443
20	1.180 ± 1.071	3.3814	4.7187
25	1.418 ± 1.098	3.5817	4.7739
30	1.404 ± 1.106	3.5952	4.7779
35	1.372 ± 1.088	3.5445	4.8051
40	1.368 ± 1.104	3.5719	4.7852

Table 55. M-9: Mono Detection Using Sensor 3.

D. SEQUENTIAL MONO VIEWING

At time $t = 50$ seconds, the data shown in Table 56, Table 57, Table 58, Table 59, Table 60, and Table 61 was generated for the instantaneous positional accuracy using the stated sensor combination.

Sensor 1 Handover to Sensor 2 at Time $t = 75$ seconds

Revisit Rate	ΔX	95% C.I.	99% C.I.
5	1.166 ± 1.078	3.3327	4.7135
10	1.264 ± 1.112	3.4809	4.8719
15	1.102 ± 1.004	3.1305	4.4000
20	1.273 ± 1.093	3.4615	4.7404
25	1.869 ± 1.514	4.7333	6.6759
30	1.866 ± 1.523	4.7686	6.7771
35	1.867 ± 1.509	4.6983	6.7211
40	1.841 ± 1.511	4.7675	6.6390

Table 56. M-9 Sequential Mono Viewing: Sensor 1 Handover to Sensor 2 at Time $t = 75$ seconds.

Sensor 1 Handover to Sensor 2 at Time $t = 150$ seconds

Revisit Rate	ΔX	95% C.I.	99% C.I.
5	1.166 ± 1.078	3.3327	4.7135
10	1.266 ± 1.109	3.4890	4.8047
15	1.102 ± 1.004	3.1305	4.4000
20	1.273 ± 1.093	3.4615	4.7404
25	1.869 ± 1.514	4.7333	6.6759
30	1.872 ± 1.509	4.7065	6.6800
35	1.867 ± 1.509	4.6983	6.7211
40	1.841 ± 1.511	4.7675	6.6390

Table 57. M-9 Sequential Mono Viewing: Sensor 1 Handover to Sensor 2 at Time $t = 150$ seconds.

Sensor 1 Handover to Sensor 3 at Time t = 75 seconds

Revisit Rate	ΔX	95% C.I.	99% C.I.
5	1.183 \pm 1.085	3.3757	4.7115
10	1.268 \pm 1.113	3.5033	4.8395
15	1.104 \pm 0.997	3.1119	4.3584
20	1.271 \pm 1.097	3.4675	4.7339
25	1.867 \pm 1.513	4.4732	6.7000
30	1.848 \pm 1.484	4.7067	6.6535
35	1.871 \pm 1.514	4.7775	6.6810
40	1.824 \pm 1.484	4.7150	6.6030

Table 58. M-9 Sequential Mono Viewing: Sensor 1 Handover to Sensor 3 at Time t = 75 seconds.

Sensor 1 Handover to Sensor 3 at Time t = 150 seconds

Revisit Rate	ΔX	95% C.I.	99% C.I.
5	1.159 \pm 1.062	3.2896	4.6071
10	1.258 \pm 1.105	3.4900	4.8371
15	1.091 \pm 0.991	3.1126	4.3433
20	1.284 \pm 1.100	3.4667	4.7788
25	1.878 \pm 1.524	4.7748	6.7013
30	1.859 \pm 1.502	4.7057	6.6718
35	1.852 \pm 1.516	4.7957	6.7526
40	1.837 \pm 1.502	4.7492	6.6217

Table 59. M-9 Sequential Mono Viewing: Sensor 1 Handover to Sensor 3 at Time t = 150 seconds.

Sensor 2 Handover to Sensor 3 at Time t = 75 seconds

Revisit Rate	ΔX	95% C.I.	99% C.I.
5	1.109 \pm 1.005	3.0859	4.3891
10	1.133 \pm 1.002	3.1090	4.3735
15	1.094 \pm 0.958	3.0090	4.1550
20	1.161 \pm 0.987	3.1212	4.3220
25	1.333 \pm 1.041	3.3647	4.6694
30	1.330 \pm 1.064	3.4037	4.7862
35	1.303 \pm 1.033	3.3467	4.6509
40	1.309 \pm 1.048	3.3374	4.7125

Table 60. M-9 Sequential Mono Viewing: Sensor 2 Handover to Sensor 3 at Time t = 75 seconds.

Sensor 2 Handover to Sensor 3 at Time t = 150 seconds

Revisit Rate	ΔX	95% C.I.	99% C.I.
5	1.095 ± 0.979	3.0302	4.2754
10	1.116 ± 0.985	3.0858	4.3278
15	1.100 ± 0.967	3.0463	4.2359
20	1.167 ± 0.992	3.1315	4.3429
25	1.338 ± 1.062	3.4266	4.7649
30	1.332 ± 1.059	3.4134	4.7521
35	1.298 ± 1.033	3.3265	4.6733
40	1.295 ± 1.027	3.2785	4.5558

Table 61. M-9 Sequential Mono Viewing: Sensor 1 Handover to Sensor 3 at Time t = 150 seconds.

E. ASYNCHRONOUS VIEWING

At time t = 50 seconds, the data shown in Tables 62 to 79 was generated for the instantaneous positional accuracy using the stated sensor combination.

Sensor 1 has a constant revisit rate of every 5 seconds and sensor 2 has a variable revisit rate given in the "Revisit Rate" column

Revisit Rate	ΔX	95% C.I.	99% C.I.
5	0.050 ± 0.037	0.1269	0.1903
10	0.067 ± 0.062	0.1769	0.2521
15	0.061 ± 0.054	0.1649	0.1988
20	0.074 ± 0.071	0.1867	0.2820
25	0.142 ± 0.174	0.3726	0.9302
30	0.110 ± 0.131	0.2776	0.6026
35	0.089 ± 0.097	0.2136	0.3568
40	0.075 ± 0.067	0.1888	0.2828

Table 62. M-9 Asynchronous Viewing: Sensor 1 and Sensor 2.

Sensor 1 has a constant revisit rate of every 10 seconds and sensor 2 has a variable revisit rate given in the "Revisit Rate" column

Revisit Rate	ΔX	95% C.I.	99% C.I.
5	0.058 ± 0.042	0.1519	0.1959
10	0.070 ± 0.045	0.1774	0.2140
15	0.067 ± 0.046	0.1719	0.1994
20	0.076 ± 0.052	0.1856	0.2580
25	0.128 ± 0.126	0.2976	0.5194
30	0.103 ± 0.085	0.2461	0.3604
35	0.088 ± 0.066	0.1963	0.2905
40	0.080 ± 0.088	0.1879	0.2674

Table 63. M-9 Asynchronous Viewing: Sensor 1 and Sensor 2.

Sensor 1 has a constant revisit rate of every 15 seconds and sensor 2 has a variable revisit rate given in the "Revisit Rate" column

Revisit Rate	ΔX	95% C.I.	99% C.I.
5	0.054 ± 0.035	0.1358	0.1902
10	0.068 ± 0.046	0.1749	0.2144
15	0.063 ± 0.036	0.1641	0.1964
20	0.072 ± 0.047	0.1807	0.2316
25	0.121 ± 0.105	0.2916	0.4448
30	0.100 ± 0.077	0.2417	0.3456
35	0.084 ± 0.056	0.1937	0.2798
40	0.075 ± 0.047	0.1842	0.2469

Table 64. M-9 Asynchronous Viewing: Sensor 1 and Sensor 2.

Sensor 1 has a constant revisit rate of every 20 seconds and sensor 2 has a variable revisit rate given in the "Revisit Rate" column

Revisit Rate	ΔX	95% C.I.	99% C.I.
5	0.061 ± 0.038	0.1600	0.1964
10	0.073 ± 0.044	0.1797	0.2222
15	0.068 ± 0.042	0.1737	0.1994
20	0.078 ± 0.047	0.1852	0.2451
25	0.124 ± 0.092	0.2880	0.3994
30	0.102 ± 0.066	0.2406	0.3177
35	0.089 ± 0.055	0.1956	0.2829
40	0.083 ± 0.090	0.1884	0.2643

Table 65. M-9 Asynchronous Viewing: Sensor 1 and Sensor 2.

Sensor 1 has a constant revisit rate of every 25 seconds and sensor 2 has a variable revisit rate given in the "Revisit Rate" column

Revisit Rate	ΔX	95% C.I.	99% C.I.
5	0.093 \pm 0.075	0.2217	0.3540
10	0.100 \pm 0.067	0.2178	0.3323
15	0.097 \pm 0.064	0.2110	0.3114
20	0.104 \pm 0.062	0.2211	0.3193
25	0.145 \pm 0.094	0.2983	0.4444
30	0.145 \pm 0.236	0.2835	0.7118
35	0.136 \pm 0.240	0.2653	0.8900
40	0.145 \pm 0.298	0.2718	1.7478

Table 66. M-9 Asynchronous Viewing: Sensor 1 and Sensor 2.

Sensor 1 has a constant revisit rate of every 30 seconds and sensor 2 has a variable revisit rate given in the "Revisit Rate" column

Revisit Rate	ΔX	95% C.I.	99% C.I.
5	0.077 \pm 0.056	0.1887	0.2802
10	0.088 \pm 0.057	0.1934	0.2793
15	0.083 \pm 0.048	0.1896	0.2666
20	0.092 \pm 0.052	0.1955	0.2840
25	0.149 \pm 0.208	0.2969	0.7100
30	0.119 \pm 0.118	0.2580	0.3637
35	0.105 \pm 0.114	0.2072	0.2958
40	0.117 \pm 0.246	0.1997	0.8684

Table 67. M-9 Asynchronous Viewing: Sensor 1 and Sensor 2.

Sensor 2 has a constant revisit rate of every 5 seconds and sensor 3 has a variable revisit rate given in the "Revisit Rate" column

Revisit Rate	ΔX	95% C.I.	99% C.I.
5	0.105 \pm 0.127	0.2870	0.6931
10	0.141 \pm 0.170	0.4146	0.9140
15	0.131 \pm 0.164	0.3783	0.8676
20	0.157 \pm 0.198	0.4791	1.0808
25	0.283 \pm 0.333	0.9242	1.7327
30	0.230 \pm 0.277	0.7562	1.4674
35	0.197 \pm 0.248	0.6555	1.2836
40	0.170 \pm 0.214	0.5356	1.1527

Table 68. M-9 Asynchronous Viewing: Sensor 2 and Sensor 3.

Sensor 2 has a constant revisit rate of every 10 seconds and sensor 3 has a variable revisit rate given in the "Revisit Rate" column

Revisit Rate	ΔX	95% C.I.	99% C.I.
5	0.116 ± 0.122	0.2915	0.6438
10	0.142 ± 0.152	0.3744	0.8444
15	0.133 ± 0.146	0.3510	0.7915
20	0.152 ± 0.165	0.3929	0.9184
25	0.254 ± 0.278	0.7549	1.4851
30	0.213 ± 0.238	0.6293	1.3071
35	0.186 ± 0.208	0.5176	1.1437
40	0.164 ± 0.194	0.4443	1.0657

Table 69. M-9 Asynchronous Viewing: Sensor 2 and Sensor 3.

Sensor 2 has a constant revisit rate of every 15 seconds and sensor 3 has a variable revisit rate given in the "Revisit Rate" column

Revisit Rate	ΔX	95% C.I.	99% C.I.
5	0.112 ± 0.118	0.2874	0.6446
10	0.135 ± 0.138	0.3533	0.7521
15	0.126 ± 0.136	0.3209	0.7429
20	0.147 ± 0.157	0.3870	0.8358
25	0.242 ± 0.267	0.7288	1.3863
30	0.204 ± 0.227	0.5908	1.2132
35	0.175 ± 0.199	0.4871	1.0797
40	0.157 ± 0.176	0.4209	0.9414

Table 70. M-9 Asynchronous Viewing: Sensor 2 and Sensor 3.

Sensor 2 has a constant revisit rate of every 20 seconds and sensor 3 has a variable revisit rate given in the "Revisit Rate" column

Revisit Rate	ΔX	95% C.I.	99% C.I.
5	0.124 ± 0.133	0.3148	0.7407
10	0.143 ± 0.144	0.3669	0.7980
15	0.136 ± 0.140	0.3383	0.7737
20	0.157 ± 0.167	0.3928	0.9190
25	0.247 ± 0.255	0.7074	1.3556
30	0.209 ± 0.228	0.5746	1.1787
35	0.181 ± 0.194	0.4838	1.0548
40	0.164 ± 0.181	0.4212	0.9958

Table 71. M-9 Asynchronous Viewing: Sensor 2 and Sensor 3.

Sensor 2 has a constant revisit rate of every 25 seconds and sensor 3 has a variable revisit rate given in the "Revisit Rate" column

Revisit Rate	ΔX	95% C.I.	99% C.I.
5	0.183 ± 0.198	0.5048	1.0681
10	0.194 ± 0.188	0.4861	1.0435
15	0.184 ± 0.179	0.4617	0.9840
20	0.202 ± 0.193	0.4998	1.0842
25	0.284 ± 0.263	0.7473	1.4727
30	0.249 ± 0.240	0.6306	1.3024
35	0.234 ± 0.239	0.6108	1.2681
40	0.222 ± 0.249	0.5827	1.3063

Table 72. M-9 Asynchronous Viewing: Sensor 2 and Sensor 3.

Sensor 2 has a constant revisit rate of every 30 seconds and sensor 3 has a variable revisit rate given in the "Revisit Rate" column

Revisit Rate	ΔX	95% C.I.	99% C.I.
5	0.158 ± 0.174	0.4210	0.9310
10	0.171 ± 0.166	0.4216	0.9167
15	0.166 ± 0.165	0.4104	0.9025
20	0.183 ± 0.183	0.4586	1.0178
25	0.269 ± 0.264	0.7383	1.4405
30	0.234 ± 0.231	0.6302	1.2636
35	0.213 ± 0.219	0.5643	1.2057
40	0.198 ± 0.221	0.5133	1.1719

Table 73. M-9 Asynchronous Viewing: Sensor 2 and Sensor 3.

Sensor 3 has a constant revisit rate of every 5 seconds and sensor 2 has a variable revisit rate given in the "Revisit Rate" column

Revisit Rate	ΔX	95% C.I.	99% C.I.
5	0.105 ± 0.127	0.2870	0.6931
10	0.116 ± 0.122	0.2915	0.6438
15	0.112 ± 0.118	0.2874	0.6446
20	0.124 ± 0.133	0.3148	0.7407
25	0.183 ± 0.198	0.5048	1.0681
30	0.158 ± 0.174	0.4210	0.9310
35	0.140 ± 0.150	0.3680	0.8089
40	0.132 ± 0.151	0.3463	0.8474

Table 74. M-9 Asynchronous Viewing: Sensor 3 and Sensor 2.

Sensor 3 has a constant revisit rate of every 10 seconds and sensor 2 has a variable revisit rate given in the "Revisit Rate" column

Revisit Rate	ΔX	95% C.I.	99% C.I.
5	0.141 ± 0.170	0.4146	0.9140
10	0.142 ± 0.152	0.3744	0.8444
15	0.135 ± 0.138	0.3533	0.7521
20	0.143 ± 0.144	0.3669	0.7980
25	0.194 ± 0.188	0.4861	1.0435
30	0.171 ± 0.166	0.4216	0.9167
35	0.158 ± 0.159	0.3928	0.9050
40	0.153 ± 0.165	0.3971	0.9250

Table 75. M-9 Asynchronous Viewing: Sensor 3 and Sensor 2.

Sensor 3 has a constant revisit rate of every 15 seconds and sensor 2 has a variable revisit rate given in the "Revisit Rate" column

Revisit Rate	ΔX	95% C.I.	99% C.I.
5	0.131 ± 0.164	0.3783	0.8676
10	0.133 ± 0.146	0.3510	0.7915
15	0.126 ± 0.136	0.3209	0.7429
20	0.136 ± 0.140	0.3383	0.7737
25	0.184 ± 0.179	0.4617	0.9840
30	0.166 ± 0.165	0.4104	0.9025
35	0.152 ± 0.160	0.3798	0.8981
40	0.143 ± 0.156	0.3669	0.8294

Table 76. M-9 Asynchronous Viewing: Sensor 3 and Sensor 2.

Sensor 3 has a constant revisit rate of every 20 seconds and sensor 2 has a variable revisit rate given in the "Revisit Rate" column

Revisit Rate	ΔX	95% C.I.	99% C.I.
5	0.157 ± 0.198	0.4791	1.0808
10	0.152 ± 0.165	0.3929	0.9184
15	0.147 ± 0.157	0.3870	0.8358
20	0.157 ± 0.167	0.3928	0.9190
25	0.202 ± 0.193	0.4998	1.0842
30	0.183 ± 0.183	0.4586	1.0178
35	0.169 ± 0.170	0.4253	0.9327
40	0.161 ± 0.172	0.4119	0.9642

Table 77. M-9 Asynchronous Viewing: Sensor 3 and Sensor 2.

Sensor 3 has a constant revisit rate of every 25 seconds and sensor 2 has a variable revisit rate given in the "Revisit Rate" column

Revisit Rate	ΔX	95% C.I.	99% C.I.
5	0.283 \pm 0.333	0.9242	1.7327
10	0.254 \pm 0.278	0.7549	1.4851
15	0.242 \pm 0.267	0.7288	1.3863
20	0.247 \pm 0.255	0.7074	1.3556
25	0.284 \pm 0.263	0.7473	1.4727
30	0.269 \pm 0.264	0.7383	1.4405
35	0.265 \pm 0.274	0.7593	1.4878
40	0.258 \pm 0.277	0.7542	1.4885

Table 78. M-9 Asynchronous Viewing: Sensor 3 and Sensor 2.

Sensor 3 has a constant revisit rate of every 30 seconds and sensor 2 has a variable revisit rate given in the "Revisit Rate" column

Revisit Rate	ΔX	95% C.I.	99% C.I.
5	0.230 \pm 0.277	0.7562	1.4674
10	0.213 \pm 0.238	0.6293	1.3071
15	0.204 \pm 0.227	0.5908	1.2132
20	0.209 \pm 0.228	0.5746	1.1787
25	0.249 \pm 0.240	0.6306	1.3024
30	0.234 \pm 0.231	0.6302	1.2636
35	0.221 \pm 0.234	0.5988	1.3000
40	0.219 \pm 0.239	0.6167	1.3195

Table 79. M-9 Asynchronous Viewing: Sensor 3 and Sensor 2.

F. DELAYED VIEWING

At time $t = 50$ seconds, the data shown in Tables 80 to 85 was generated for the instantaneous positional accuracy using the stated sensor combination.

Sensor 1 and 2 delay turning on for 5 seconds after booster burnout

Revisit Rate	ΔX	95% C.I.	99% C.I.
5	0.053 ± 0.047	0.1367	0.1941
10	0.060 ± 0.039	0.1587	0.1956
15	0.098 ± 0.065	0.2010	0.2979
20	0.067 ± 0.038	0.1710	0.1979
25	0.127 ± 0.102	0.2747	0.3925
30	0.099 ± 0.056	0.2058	0.2912
35	0.085 ± 0.078	0.1902	0.2721
40	0.071 ± 0.039	0.1779	0.1999

Table 80. M-9 Delayed Viewing: Sensor 1 and Sensor 2.

Sensor 1 and 2 delay turning on for 10 seconds after booster burnout

Revisit Rate	ΔX	95% C.I.	99% C.I.
5	0.056 ± 0.047	0.1503	0.1981
10	0.080 ± 0.058	0.1879	0.2782
15	0.084 ± 0.056	0.1902	0.2769
20	0.139 ± 0.098	0.2902	0.4720
25	0.106 ± 0.065	0.2281	0.3120
30	0.087 ± 0.062	0.1909	0.2707
35	0.072 ± 0.040	0.1781	0.1995
40	0.771 ± 0.563	1.8584	2.9684

Table 81. M-9 Delayed Viewing: Sensor 1 and Sensor 2.

Sensor 1 and 2 delay turning on for 15 seconds after booster burnout

Revisit Rate	ΔX	95% C.I.	99% C.I.
5	0.061 ± 0.057	0.1626	0.2868
10	0.066 ± 0.048	0.1712	0.2149
15	0.069 ± 0.045	0.1750	0.2023
20	0.114 ± 0.075	0.2496	0.3690
25	0.089 ± 0.060	0.1936	0.2833
30	0.072 ± 0.040	0.1778	0.1988
35	0.500 ± 0.340	1.1720	1.7465
40	0.501 ± 0.343	1.1534	1.7587

Table 82. M-9 Delayed Viewing: Sensor 1 and Sensor 2.

Sensor 1 and 2 delay turning on for 20 seconds after booster burnout

Revisit Rate	ΔX	95% C.I.	99% C.I.
5	0.067 ± 0.063	0.1758	0.3741
10	0.094 ± 0.076	0.1975	0.4500
15	0.126 ± 0.096	0.2767	0.5481
20	0.092 ± 0.060	0.1955	0.2935
25	0.073 ± 0.043	0.1791	0.2123
30	0.342 ± 0.259	0.7929	1.3600
35	0.342 ± 0.259	0.7929	1.3600
40	0.343 ± 0.261	0.7849	1.3617

Table 83. M-9 Delayed Viewing: Sensor 1 and Sensor 2.

Sensor 1 and 2 delay turning on for 25 seconds after booster burnout

Revisit Rate	ΔX	95% C.I.	99% C.I.
5	0.071 ± 0.070	0.1836	0.4205
10	0.073 ± 0.057	0.1815	0.3229
15	0.098 ± 0.073	0.1989	0.4253
20	0.073 ± 0.044	0.1800	0.2318
25	0.241 ± 0.176	0.5436	1.0190
30	0.242 ± 0.180	0.5497	1.0481
35	0.242 ± 0.179	0.5411	1.0114
40	0.242 ± 0.179	0.5411	1.0114

Table 84. M-9 Delayed Viewing: Sensor 1 and Sensor 2.

Sensor 1 and 2 delay turning on for 30 seconds after booster burnout

Revisit Rate	ΔX	95% C.I.	99% C.I.
5	0.072 ± 0.065	0.1867	0.3944
10	0.099 ± 0.077	0.2074	0.4679
15	0.074 ± 0.051	0.1826	0.2857
20	0.178 ± 0.176	0.3894	0.7787
25	0.179 ± 0.164	0.3982	0.8020
30	0.178 ± 0.159	0.3933	0.8264
35	0.178 ± 0.164	0.3922	0.8068
40	0.178 ± 0.164	0.3922	0.8068

Table 85. M-9 Delayed Viewing: Sensor 1 and Sensor 2.

G. STAGGERED VIEWING

At time $t = 50$ seconds, the data shown in Tables 86 to 91 was generated for the instantaneous positional accuracy using the stated sensor combination.

Sensor 1 and 2 delay turning for 5 seconds after booster burnout, sensor 1 has a constant revisit rate of every 5 seconds, and sensor 2 has a variable revisit rate given in the "Revisit Rate" column

Revisit Rate	ΔX	95% C.I.	99% C.I.
5	0.053 \pm 0.047	0.1367	0.1941
10	0.060 \pm 0.056	0.1631	0.2055
15	0.095 \pm 0.107	0.2345	0.4984
20	0.066 \pm 0.065	0.1751	0.2526
25	0.123 \pm 0.144	0.3030	0.7600
30	0.095 \pm 0.107	0.2360	0.4833
35	0.079 \pm 0.074	0.1918	0.2966
40	0.069 \pm 0.059	0.1792	0.2557

Table 86. M-9 Staggered Viewing: Sensor 1 and Sensor 2.

Sensor 1 and 2 delay turning for 10 seconds after booster burnout, sensor 1 has a constant revisit rate of every 5 seconds, and sensor 2 has a variable revisit rate given in the "Revisit Rate" column

Revisit Rate	ΔX	95% C.I.	99% C.I.
5	0.056 \pm 0.047	0.1503	0.1981
10	0.077 \pm 0.079	0.1894	0.3616
15	0.082 \pm 0.084	0.1939	0.3939
20	0.138 \pm 0.160	0.3638	0.8650
25	0.105 \pm 0.120	0.2655	0.6000
30	0.082 \pm 0.080	0.1942	0.3652
35	0.071 \pm 0.062	0.1807	0.2726
40	0.768 \pm 0.719	2.1400	3.3560

Table 87. M-9 Staggered Viewing: Sensor 1 and Sensor 2.

Sensor 1 and 2 delay turning for 15 seconds after booster burnout, sensor 1 has a constant revisit rate of every 5 seconds, and sensor 2 has a variable revisit rate given in the "Revisit Rate" column

Revisit Rate	ΔX	95% C.I.	99% C.I.
5	0.061 \pm 0.057	0.1626	0.2868
10	0.067 \pm 0.063	0.1759	0.2957
15	0.071 \pm 0.067	0.1809	0.3258
20	0.112 \pm 0.122	0.2869	0.6655
25	0.087 \pm 0.086	0.1980	0.4470
30	0.072 \pm 0.064	0.1831	0.2920
35	0.542 \pm 0.555	1.6676	2.6378
40	0.544 \pm 0.554	1.6778	2.6080

Table 88. M-9 Staggered Viewing: Sensor 1 and Sensor 2.

Sensor 1 and 2 delay turning for 20 seconds after booster burnout, sensor 1 has a constant revisit rate of every 5 seconds, and sensor 2 has a variable revisit rate given in the "Revisit Rate" column

Revisit Rate	ΔX	95% C.I.	99% C.I.
5	0.067 \pm 0.063	0.1758	0.3741
10	0.089 \pm 0.091	0.2043	0.5301
15	0.120 \pm 0.130	0.3041	0.7000
20	0.091 \pm 0.089	0.2072	0.5028
25	0.075 \pm 0.067	0.1861	0.3554
30	0.374 \pm 0.403	1.1978	1.9511
35	0.374 \pm 0.403	1.1978	1.9511
40	0.375 \pm 0.408	1.1955	1.9792

Table 89. M-9 Staggered Viewing: Sensor 1 and Sensor 2.

Sensor 1 and 2 delay turning for 25 seconds after booster burnout, sensor 1 has a constant revisit rate of every 5 seconds, and sensor 2 has a variable revisit rate given in the "Revisit Rate" column

Revisit Rate	ΔX	95% C.I.	99% C.I.
5	0.071 \pm 0.070	0.1836	0.4205
10	0.075 \pm 0.068	0.1870	0.3986
15	0.095 \pm 0.091	0.2354	0.5107
20	0.077 \pm 0.068	0.1883	0.3828
25	0.247 \pm 0.268	0.7934	1.3403
30	0.246 \pm 0.266	0.7847	1.3323
35	0.249 \pm 0.272	0.8145	1.3431
40	0.248 \pm 0.270	0.8061	1.3322

Table 90. M-9 Staggered Viewing: Sensor 1 and Sensor 2.

Sensor 1 and 2 delay turning for 30 seconds after booster burnout, sensor 1 has a constant revisit rate of every 5 seconds, and sensor 2 has a variable revisit rate given in the "Revisit Rate" column

Revisit Rate	ΔX	95% C.I.	99% C.I.
5	0.072 \pm 0.065	0.1867	0.3944
10	0.094 \pm 0.088	0.2393	0.5059
15	0.076 \pm 0.066	0.1894	0.3822
20	0.165 \pm 0.180	0.4870	0.9265
25	0.167 \pm 0.188	0.4956	0.9242
30	0.165 \pm 0.191	0.4946	0.9107
35	0.168 \pm 0.183	0.5124	0.9384
40	0.168 \pm 0.183	0.5124	0.9384

Table 91. M-9 Staggered Viewing: Sensor 1 and Sensor 2.

H. LATITUDE SHIFT

At time $t = 50$ seconds, data shown in Table 92, Table 93, Table 94, and Table 95 was generated for the instantaneous positional accuracy using sensors 1 and 2 at the stated latitude.

Sensors 1 and 2 at Latitude N02

Revisit Rate	ΔX	95% C.I.	99% C.I.
5	0.089 ± 0.134	0.2367	0.3733
10	0.123 ± 0.177	0.2979	0.4862
15	0.107 ± 0.098	0.2752	0.3982
20	0.132 ± 0.125	0.3258	0.4976
25	0.242 ± 0.238	0.5858	0.8930
30	0.204 ± 0.279	0.4796	0.7603
35	0.160 ± 0.163	0.3881	0.5960
40	0.146 ± 0.244	0.3478	0.5531

Table 92. M-9 Latitude Shift to N02: Sensor 1 and Sensor 2.

Sensors 1 and 2 at Latitude N20

Revisit Rate	ΔX	95% C.I.	99% C.I.
5	0.072 ± 0.075	0.1874	0.2916
10	0.101 ± 0.089	0.2444	0.3834
15	0.088 ± 0.070	0.1983	0.3015
20	0.109 ± 0.089	0.2614	0.3861
25	0.200 ± 0.156	0.4576	0.7360
30	0.165 ± 0.170	0.3753	0.5920
35	0.131 ± 0.094	0.2955	0.4529
40	0.119 ± 0.169	0.2703	0.3964

Table 93. M-9 Latitude Shift to N20: Sensor 1 and Sensor 2.

Sensors 1 and 2 at Latitude N60

Revisit Rate	ΔX	95% C.I.	99% C.I.
5	0.051 ± 0.032	0.1205	0.1866
10	0.072 ± 0.041	0.1779	0.2000
15	0.065 ± 0.035	0.1656	0.1960
20	0.080 ± 0.043	0.1857	0.2410
25	0.145 ± 0.077	0.2917	0.3934
30	0.122 ± 0.117	0.2587	0.3537
35	0.098 ± 0.052	0.1973	0.2838
40	0.087 ± 0.110	0.1889	0.2682

Table 94. M-9 Latitude Shift to N60: Sensor 1 and Sensor 2.

Sensors 1 and 2 at Latitude N80

Revisit Rate	ΔX	95% C.I.	99% C.I.
5	0.085 ± 0.066	0.1926	0.3257
10	0.120 ± 0.088	0.2654	0.4301
15	0.106 ± 0.078	0.2308	0.3958
20	0.132 ± 0.101	0.2819	0.5058
25	0.244 ± 0.180	0.4885	1.0000
30	0.204 ± 0.216	0.3997	1.0385
35	0.163 ± 0.125	0.3364	0.6932
40	0.152 ± 0.223	0.2944	0.8326

Table 95. M-9 Latitude Shift to N80: Sensor 1 and Sensor 2.

LIST OF REFERENCES

1. U.S. Air Force. Space Based InfraRed System: Providing the Essential High Ground Advantage of Space Based IR Surveillance to the Warfighter of the 21st Century. Los Angeles, CA.: Department of the Air Force, 1998.
2. U.S. Air Force. Space Based InfraRed System: Providing the Essential High Ground Advantage of Space Based IR Surveillance to the Warfighter of the 21st Century. Los Angeles, CA.: Department of the Air Force, 1998.
3. U.S. Air Force. Space Based InfraRed System: Providing the Essential High Ground Advantage of Space Based IR Surveillance to the Warfighter of the 21st Century. Los Angeles, CA.: Department of the Air Force, 1998.
4. Martz, Bob. "Scheduler Logic for FDS & Objective System," Interoffice Correspondence, The Aerospace Corporation, 1997.
5. Gottschalk, Thomas D. "SBIRS-Low Tasking Algorithms," Interoffice Correspondence, The Aerospace Corporation, 1999.
6. Gottschalk, Thomas D. "SBIRS-Low Tasking Algorithms," Interoffice Correspondence, The Aerospace Corporation, 1999.
7. Gottschalk, Thomas D. "The Case for Scalable, Appropriate-Fidelity Simulations," Interoffice Correspondence, The Aerospace Corporation, 1999.
8. Gottschalk, Thomas D. "SBIRS-Low Tasking Algorithms," Interoffice Correspondence, The Aerospace Corporation, 1999.
9. Gottschalk, Thomas D. "The Case for Scalable, Appropriate-Fidelity Simulations," Interoffice Correspondence, The Aerospace Corporation, 1999.
10. Martz, Bob. "Scheduler Logic for FDS & Objective System," Interoffice Correspondence, The Aerospace Corporation, 1997.
11. Martz, Bob. "Scheduler Logic for FDS & Objective System," Interoffice Correspondence, The Aerospace Corporation, 1997.
12. Martz, Bob. "Scheduler Logic for FDS & Objective System," Interoffice Correspondence, The Aerospace Corporation, 1997.
13. Martz, Bob. "Scheduler Logic for FDS & Objective System," Interoffice Correspondence, The Aerospace Corporation, 1997.
14. Bankes, Steve. "Reasoning About Complex and Uncertain Systems with Computational Experiments," Naval Postgraduate School Operations Research Department Seminar, 10 December 1998.
15. Bankes, Steve. "Exploratory Modeling For Policy Analysis." Operations Research, Vol. 41, No. 3, May-June 1993, pp. 435-449.

16. Bankes, Steve. "Reasoning About Complex and Uncertain systems with Computational Experiments," Naval Postgraduate School Operations Research Department Seminar, 10 December 1998.
17. U.S. Air Force. Space Based InfraRed System: Providing the Essential High Ground Advantage of Space Based IR Surveillance to the Warfighter of the 21st Century. Los Angeles, CA.: Department of the Air Force, 1998.
18. Gottschalk, Thomas D. "Detecting Theater Targets With SBIRS Low." Interoffice Correspondence, The Aerospace Corporation, 1998.
19. Hoult, Charles P. "SBIRS Low TT&C Operator's Auto Agent Notes." Interoffice Correspondence, The Aerospace Corporation, 1999.
20. Bate, Roger R., Mueller, Donald D., and White, Jerry E. Fundamentals of Astrodynamics. New York: Dover Publishing, Inc., 1971.
21. Bate, Roger R., Mueller, Donald D., and White, Jerry E. Fundamentals of Astrodynamics. New York: Dover Publishing, Inc., 1971.
22. Bate, Roger R., Mueller, Donald D., and White, Jerry E. Fundamentals of Astrodynamics. New York: Dover Publishing, Inc., 1971.
23. Bate, Roger R., Mueller, Donald D., and White, Jerry E. Fundamentals of Astrodynamics. New York: Dover Publishing, Inc., 1971.
24. Press, William H., Flannery, Brian P., Teukolsky, Saul A., and Vetterling, William T. Numerical Recipes in C. New York: Cambridge University Press, 1988.
25. Lennox, Duncan. Jane's Strategic Weapon Systems. Coulsdon, Surrey, U.K.: Jane's Information Group, Limited, 1997.
26. Box, George E.P. and Tiao, George C. Bayesian Inference in Statistical Analysis. Menlo Park, CA: Addison-Wesley Publishing Company, 1973.
27. Mood, Alexander M., Graybill, Franklin A., and Boes, Duane C. Introduction to the Theory of Statistics. New York: McGraw-Hill Book Company, 1974.
28. Hammersley, J.M. and Handscomb, D.C. Monte Carlo Methods. New York: Chapman & Hall, 1992.
29. Fishman, George S. Monte Carlo Concepts, Algorithms, and Applications. New York: Springer-Verlag, 1996.
30. Ross, Sheldon M. Introduction to Probability Models. New York: Academic Press, 1997.
31. Fishman, George S. Monte Carlo Concepts, Algorithms, and Applications. New York: Springer-Verlag, 1996.

BIBLIOGRAPHY

Barlow, R.J. Statistics. New York: John Wiley & Sons, Inc., 1989.

Bazaraa, Mokhtar S., Sherali, Hanif D., and Shetty, C.M. Nonlinear Programming Theory and Algorithms. New York: John Wiley & Sons, Inc., 1993.

Box, George E. P., Hunter, William G., and Hunter, J. Stuart. Statistics for Experimenters. New York: John Wiley & Sons, 1978.

Gottschalk, Thomas D. "Containment Error Estimation," Interoffice Correspondence, The Aerospace Corporation, 1999.

Gottschalk, Thomas D. "Tracking Primer," Interoffice Correspondence, The Aerospace Corporation, 1999.

Hoult, Charles P. "Global Scheduler," Interoffice Correspondence, The Aerospace Corporation, 1999.

Lyons, Louis. Statistics for Nuclear and Particle Physicists. New York: Cambridge University Press, 1989.

THIS PAGE INTENTIONALLY LEFT BLANK

INITIAL DISTRIBUTION LIST

1. Defense Technical Information Center 2
8725 John J. Kingman Rd., STE 0944
Ft. Belvoir, VA 22060-6218
2. Dudley Knox Library 2
Naval Postgraduate School
411 Dyer Rd.
Monterey, CA 93943-5101
3. Dr. Thomas W. Lucas 1
Operations Research Department
Naval Postgraduate School
Monterey, CA 93943
4. Dr. Robert R. Read 1
Operations Research Department
Naval Postgraduate School
Monterey, CA 93943
4. Dr. Thomas D. Gottschalk 1
California Institute of Technology
Mail Code 158-79
Pasadena, CA 91125
5. Aerospace Corporation 1
P.O. Box 92957
Los Angeles, CA 90009-2957
Attn: Charles P. Hoult
6. CDR Jim O'Brien USN 2
CNO-N632D
2000 Navy Pentagon
Washington, DC 20350-2000
7. LCDR Brian Morgan 1
44633 Smith Nursery Rd.
Hollywood, MD 20636
8. LCDR Dave Jazdyk 1
Unit 45002 Box 398
APO AP 96337-5002